THERMODYNAMIC STUDIES IN LIQUID Fe-V-O AND Fe-Cr-O SYSTEMS USING ELECTROCHEMICAL CELLS

THERMODYNAMIC STUDIES IN LIQUID Fe-V-O AND Fe-Cr-O SYSTEMS USING ELECTROCHEMICAL CELLS

By

PRASAD APTE, B.Tech.

A Thesis

Submitted to the School of Graduate Studies

in Partial Fulfilment of the Requirements

for the Degree

Doctor of Philosophy

McMaster University

January, 1977

DOCTOR OF PHILOSOPHY (1977)
(Metallurgy & Materials Science)

McMASTER UNIVERSITY
Hamilton, Ontario

TITLE: Thermodynamic Studies in Liquid Fe-V-O and Fe-Cr-O Systems Using Electrochemical Cells

AUTHOR: Prasad Apte, B.Tech. (I.I.T., Bombay)

SUPERVISOR: Professor D.A.R. Kay

NUMBER OF PAGES: (xv) 184

Abstract

A high temperature oxygen concentration cell

$$Mo_{(s)}, Cr\text{-}Cr_2O_{3(s)} \mid \begin{matrix}\text{calcia stabilized}\\ \text{zirconia}\\ \text{solid electrolyte}\end{matrix} \mid Fe\text{-}M\text{-}O_{(\ell)}, \begin{matrix}Mo/ZrO_2\\ \text{Cermet}\end{matrix}{}_{(s)}$$

has been employed to study the deoxidation thermodynamics of liquid Fe-V-O and Fe-Cr-O systems in the temperature range 1550-1600°C. A new cell design and a cermet contact to the liquid metal have been developed to continuously monitor the oxygen activity of liquid iron alloys, during oxidation and reduction and the exact oxygen potentials where two deoxidation products coexist have been determined. Thus a chronopotentiometric technique has been successfully applied to deoxidation studies at steelmaking temperatures. Using this technique deoxidation products can be obtained, in a controlled manner, from a known stage of oxidation.

The deoxidation products in the Fe-V-O system and their ranges of stability at 1600°C are:

oxide	stability range
FeV_2O_3	wt%V < 0.17
V_2O_3	0.17 to 1% V
VO	wt%V > 1%V

The standard free energy changes for the reactions

$$Fe_{(\ell)} + \underline{O}_{1w/o} + V_2O_{3(s)} \rightleftarrows FeV_2O_{4(s)}$$

and $$2VO_{(s)} + \underline{O}_{1w/o} \rightleftarrows V_2O_{3(s)}$$

have been determined in the temperature range 1550° to 1600°C. The standard heat of formation of 'VO' calculated from the present data by Third Law analysis is -80,900 ± 300 cals/mole. These data for the transition from FeV_2O_4 to V_2O_3 are in good agreement with results reported in the literature. The data for the transition from V_2O_3 to VO and the stability of VO as a deoxidation product have been carefully characterized for the first time and discrepancies reported in the literature in the deoxidation thermodynamics of the Fe-V-O system have been resolved.

In the Fe-Cr-O system, chromic oxide (Cr_2O_3) was not found to be a stable deoxidation product. This is contrary to recent reports in the literature. Thus other results based on the assumption that Cr_2O_3 is a stable deoxidation product need to be reinterpreted. The formation of the following deoxidation products in the Fe-Cr-O system is proposed:

oxide	stability range
chromite	wt%Cr < 0.3
distorted spinel	0.3% to 1.8% Cr
Cr_3O_4	wt%Cr > 1.8%

The formation of Cr_3O_4 and the exact composition of the distorted spinel needs to be confirmed by precise X-ray diffraction and spectrochemical analysis.

The deoxidation products were examined by scanning electron microscopy and appeared to form agglomerates of small crystallites.

The successful extension of chronopotentiometry to steelmaking systems has facilitated the study of complex deoxidation systems which cannot be studied easily by equilibration techniques. The significance of the determinations of the stability ranges of deoxidation products and their form to steelmaking processes have been indicated.

Acknowledgements

The author wishes to express his sincere gratitude to Dr. D.A.R. Kay for his guidance and encouragement during the course of this study. Grateful acknowledgements are also due to the members of the technical staff and graduate students of the Metallurgy Department for their help in the solution of various problems. Special thanks are due to Dr. D. Ghosh and Mr. C. Stournaras for their valuable assistance in the study and to Ms. V. Komczynski for her accurate and rapid typing of the thesis. Finally, the author wishes to express his gratitude to the National Research Council of Canada for a postgraduate scholarship.

TABLE OF CONTENTS

LIST OF TABLES

LIST OF ILLUSTRATIONS

LIST OF SYMBOLS

s, ℓ, g	(subscripts) indicate the physical state of the material - solid, liquid and gas respectively
ΔG^{o}	change in the Gibbs standard free energy
ΔH^{o}	change in the standard enthalpy
T	absolute temperature in degrees Kelvin
K	equilibrium constant for a reaction as written
K'	quasi-deoxidation constant (obtained by replacing activities by concentration in K)
-1w/o	standard state of 1 wt% of the element in solution in iron
h_i	Henrian activity of component i
a_i	Raoultion activity of component i
E, EMF	electromotive force of an electrochemical cell
γ_i^{o}	activity coefficient of solute i at infinite dilution
M	atomic weight
F	Faraday, 96494 coul./mole
t_i	transport number of species i
σ_i	conductivity of species i
μ_i	chemical potential of component i
n,Z	number of electrons involved in the cell reaction
P_i,	partial pressure of gaseous species i
Q_i	activation energy for electrical conduction by charge carrier i
$\oplus$	p-type charge carriers
$\ominus$	n-type charge carriers

ΔH^{o}_{298}	standard heat of formation
R	gas constant 1.987 cal/mole-deg.
gef_T	Gibbs energy function, $(G^{o}-H^{o}_{298})/T$

CHAPTER 1

INTRODUCTION

1.1 Deoxidation in Steelmaking

In conventional steelmaking processes, impurities like carbon, silicon, manganese and phosphorous, invariably present in blast furnace pig iron,are removed by oxidation. The oxide products thus formed are insoluble in the melt and are removed from the molten iron either as gaseous products or by assimilation in the slag. During steelmaking, liquid iron gets super-saturated with oxygen. On teeming into ingots the excess oxygen reacts with carbon dissolved in the iron forming carbon monoxide which tends to escape when the refined steel is allowed to solidify, often with enough force to throw out most of the metal poured in the ingot.

Successful casting practice is attained by employing deoxidizing elements in two ways.

1. Allowing the oxygen to escape as a gas (CO) at a controlled rate during solidification as in rimming and semi-killed steel. In this case the carbon dissolved in the steel acts as the deoxidizing element. The reaction may be expressed as

$$\underline{C}_{1w/o} + \underline{O}_{1w/o} \rightarrow CO_{(g)} \qquad 1.1$$

where '$\underline{\ }_{1w/o}$' refers to the standard state of 1 wt% of the element in solution in iron. The extent to which the reaction will proceed is controlled by

the equilibrium constant

$$K_1 = P_{CO}/h_C h_O \qquad 1.2$$

where P_{CO} is the partial pressure of the CO gas and h_C and h_O are Henrian activities of carbon and oxygen in the iron.

2. Combining the oxygen into non-metallic compounds thereby preventing any gas formation during solidification. This is referred to as 'killing' the steel and is done chemically by adding elements that are strong oxide formers (deoxidizers). The deoxidation reaction and the corresponding equilibrium constant may be expressed as

$$2\underline{M}_{1w/o} + x\underline{O}_{1w/o} \rightleftarrows M_2O_{x(s)} \qquad 1.3$$

$$K_2 = a_{M_2O_x}/h_M^2 h_O^x \qquad 1.4$$

where 'h' once again refers to the Henrian activity of the component.

In the first case the rimming action and its control depends on the amount of carbon and oxygen in solution in the melt. In the second case the amount of deoxidizer added depends once again on the oxygen content of the melt. Proper control of deoxidation processes is possible only when the behaviour of both oxygen and the deoxidizer in liquid iron and the thermodynamics of the deoxidation reactions are known.

The elements used most commonly for deoxidation of the second type are aluminium and silicon. Many different deoxidation products are formed when these elements are used, depending on the concentrations of both these elements as well as of oxygen. These oxides are varied in composition, structure and properties. The type of deoxidation product formed can be critical, both in its removal from the liquid steel and in its behaviour in

hot rolling and in other mechanical forming processes. Therefore it is necessary to determine the types of deoxidation products formed and the conditions for their stability.

One typical case is that of elements which form two or more deoxidation products. Apart from pure oxides of the metal formed following reaction 1.3, the oxides generally form a spinel with the oxide of iron following a reaction of the type

$$Fe(\ell) + 2\underline{M}_{1w/o} + (x+1)\underline{O}_{1w/o} \rightleftarrows FeM_2O_{x+1(s)} \qquad 1.5$$

and with an equilibrium constant K given by

$$K_5 = a_{FeM_2O_{x+1}}/h_M^2 h_O^{x+1} \qquad 1.6$$

It is common practice to use a 'quasi-deoxidation constant' in place of the equilibrium constant of equation 1.6. The quasi-deoxidation constant K' is given by the relation

$$K' = [\%M]^2[\%O]^{x+1} \qquad 1.6a$$

and is calculated from the concentrations of the deoxidant and oxygen in solution in iron.

In order to obtain a clean steel, oxides have to be removed by floatation from molten steel and this depends on their physical properties like interfacial energy, density, morphology,etc. Generally the spinel is formed at higher oxygen activities and lower concentrations of the deoxidant than the simple oxide and is more difficult to remove from the melt.

In steelmaking practice deoxidation by aluminium and silicon is followed by alloying. Both these processes are carried out in a ladle which

is exposed to air. A number of common alloying elements like vanadium, chromium, titanium and niobium can form stable oxides with the oxygen dissolved in iron. Oxidation of these elements makes it difficult to produce steel to meet the composition specifications.

Oxidation losses are unavoidable since the molten steel is exposed to air during alloying and ingot teeming. Therefore a certain amount of these elements in excess of the desired residual concentration has to be added to the melt. Most of the alloying elements used in steel are very expensive and an understanding of the thermodynamics of deoxidation of steel by these elements is essential for good quality control of the steel.

In the case of high strength low alloy (HSLA) steels which contain small quantities - less than one percent each - of these alloying elements, deoxidation control is very critical.

Vanadium is used in HSLA steels (up to 0.3%) and in tool and die steels. Chromium is used extensively in making stainless steels and other low and high alloy steels. In the case of both vanadium and chromium the interest in deoxidation thermodyanamics arises out of the need for precise composition control and minimization of oxidation losses. Further, the entrapped deoxidation products of these elements affect the mechanical properties and corrosion resistance of steels containing chromium and vanadium. Hence it is necessary to determine the nature and the properties of the deoxidation products formed by these elements.

1.2 Determination of Deoxidation Thermodynamics

The study of the thermodynamic behaviour of oxygen and deoxidizers in liquid iron forms the scope of deoxidation thermodynamics. Investigations

are generally carried out to determine data of the following types:

1. The activities of oxygen and deoxidant in liquid iron.

2. The interaction parameters between oxygen and the deoxidizer.

3. The number and the type of deoxidation products formed when any particular element is added to liquid iron.

4. The ranges of activities of oxygen and the deoxidizer in which the various deoxidation products are stable and the transition points where one deoxidation product transforms to another.

5. The free energies of formation of the various deoxidation products.

This data can then be used to determine the quantities and the sequence of additions to be made to steel during deoxidation and alloying.

Deoxidation thermodynamics have been generally determined by equilibrating iron melts containing the deoxidant with any one of the possible deoxidation products, under controlled atmospheres. The melts were cooled after equilibration and analyzed for oxygen and the deoxidant. The measured concentrations were used to determine the "quasi-deoxidation constant-K" using relations similar to equation 1.6a. The true equilibrium constants of the type given in equations 1.4 and 1.6 could also be calculated by using solution thermodynamics. This technique will be reviewed in Chapter 2.

With the development of solid oxide electrolytes the general trend in studies of deoxidation thermodynamics has been to use oxygen concentration cells employing solid electrolytes. These cells can be represented as:

$$\text{Pt}, \mu_{O_2}^{I} \mid \text{solid oxide electrolyte} \mid \mu_{O_2}^{II}, \text{Pt} \qquad 1.7$$

and can be used to measure the chemical potential of oxygen - μ_{O_2} - at one electrode with respect to a reference potential maintained at the other electrode. The various criteria for the successful applications of such cells are discussed in Chapter 2.

The cell used in the present work is a modification of the cell represented in the expression (1.7) which enables the continuous monitoring of the oxygen activity in liquid iron. The cell may be represented as:

$$\text{Mo}, \underset{\text{reference electrode}}{\text{Cr}/\text{Cr}_2\text{O}_{3(s)}} \mid \underset{\text{solid electrolyte}}{\text{calcia stabilized zirconia}} \mid \underset{\text{Unknown electrode}}{\text{Fe-M-O}_{(\ell)}}, \underset{\text{Cermet}}{\text{Mo-ZrO2}} \qquad 1.8$$

Using this cell it is possible to measure the oxygen activity in iron during the formation and transformation of deoxidation products as the melt is continually oxidized or reduced. The technique has the advantage that it simulated reoxidation under steelmaking conditions in the sense that the steel is continuously oxidized and the deoxidation products are allowed to form with few external constraints.

Chronopotentiometric techniques are commonly used at low temperatures but their successful application is extremely difficult at steelmaking temperatures and has not been reported in the literature. Successful employment of the cell at high temperatures (1600^{o}C) offers the possibility of making oxygen potential measurements in deoxidation systems and of obtaining deoxidation products in a controlled manner from a known stage of oxidation.

In the Fe-V-O system, the formation of three deoxidation products - FeV_2O_4, V_2O_3 and VO - have been reported in a number of investigations.

While the thermodynamics of FeV_2O_4 and V_2O_3 have been well documented, there is no general agreement in the literature on similar data for VO. The vanadium concentration at which the stable deoxidation product transforms from V_2O_3 to VO, as reported in the literature, ranges from 0.9 to 12%. Further, the thermodynamic data for this transformation reaction have not been carefully characterized.

In the Fe-Cr-O system there is little agreement about the type of deoxidation products formed and their ranges of stability. Most of the data reported in the literature assume that Cr_2O_3 is formed as a deoxidation product, and there is little agreement about the chromium content (reported values range from 3% to 7% Cr) and the Henrian activity of oxygen (ranging from 0.3 to 0.017) required to form Cr_2O_3.

Some other reports in the literature suggest that Cr_2O_3 is not formed as a deoxidation product. At present, all analyses of the solution thermodynamics of the Fe-Cr-O system are based on the assumption that Cr_2O_3 is formed at steelmaking temperatures, and hence the resolution of this discrepancy is crucial. Since deoxidation products could not be obtained from a known stage of oxidation in any of the determinations reported in the literature, the present technique offers the best possibility of determining if Cr_2O_3 is formed under steelmaking conditions.

This technique has been used to characterize the deoxidation thermodynamics of the Fe-V-O and Fe-Cr-O systems. The determinations have been analyzed to resolve the controversies in the literature. Further, since the nature of the deoxidation products affects their removal from liquid steel and their behaviour in processing of steel, the present technique has been coupled with X-ray diffraction and electron optical methods to make some preliminary observations on the morphology of deoxidation products in steel.

CHAPTER 2

LITERATURE REVIEW

2.1 Introduction

This chapter reviews the work reported in the literature related to this investigation. The chapter has been divided into three main sections:

1. The first section deal with studies of the deoxidation thermodynamics of the Fe-V-O system. Determinations of the activity of oxygen in equilibrium with different deoxidation products and the determination of the free energies of formation of those products have been reviewed.

2. The second section deals with the Fe-Cr-O system. Since there have been a number of studies on this system and the agreement between the results is rather poor, the salient features of the various studies have been included. Further, due to uncertainties in the types of chromium oxide that are formed, even theoretical predictions about such oxides have been included.

Since both V and Cr form chemical compounds with oxygen they also affect the behaviour of oxygen in solution in iron. A number of studies of the effect of these elements on the activity of oxygen in iron have been reported and there are a number of excellent reviews of these studies.[1,2,3] Since this type of determination is not a major objective of this work, these studies have not been included in this literature review.

3. The final section deals with the applications of solid electrolytes

in the determination of deoxidation thermodynamics. A brief look at the theory of solid electrolytes and the characterization of calcia stabilized zirconia has been included for the sake of completeness. This section also includes studies related to this investigation that have employed solid electrolytes.

2.2 Deoxidation Equilibria in Fe-M-O Systems

Most elements used in deoxidizing steel form more than one deoxidation product. The stability of the products is determined by the temperature and the amount of deoxidizer in the melt. In some systems at least one of the products is a spinel of the type FeM_2O_{x+1} while the remaining products are oxides of the element 'M'. Where the deoxidizer has more than one valency, different oxides could form depending on the physical stability of these oxide phases.

The reaction for the formation of a spinel may be expressed as:

$$Fe_{(\ell)} + 2\underline{M}_{1w/o} + (x+1)\,\underline{O}_{1w/o} \rightleftarrows FeM_2O_{x+1(s)} \qquad 2.1$$

with an equilibrium constant 'K' given by

$$K_1 = \frac{1}{h_M^2 \cdot h_0^{(x+1)}} \qquad 2.2$$

where 'h' stands for the Henrian activities and the activities of the liquid iron and the spinel are taken as unity. Equation 2.2 can also be written as:

$$\log h_M = -\frac{1}{2} \log K_1 - \frac{x+1}{2} \log h_0 \qquad 2.3$$

Similarly for the formation of a pure oxide M_yO_x the corresponding relations may be written as:

$$y\underline{M}_{1w/o} + x\,\underline{O}_{1w/o} \rightleftarrows M_yO_{x(s)} \qquad 2.4$$

$$K_4 = \frac{1}{h_M^y \cdot h_O^x} \qquad 2.5$$

and $$\log h_M = -\frac{1}{y} \log K_4 - \frac{x}{y} \log h_O \qquad 2.6$$

A plot of $\log h_O$ against $\log h_M$ yields linear relationships with slopes of $-\frac{2}{x+1}$ and $-\frac{y}{x}$ for melts in equilibrium with the spinel and the oxide respectively (Fig. 2.1).

The intersection of these lines represents values of h_M and h_O in equilibrium with both the products. Following the phase rule, this point has only one degree of freedom and hence the values of h_O and h_M are unique at any fixed temperature. During oxidation or reduction of a melt, this point represents the oxygen activity at which the deoxidation products will transform from one to the other. The oxygen activity in the melt will remain a constant for the time taken for the transformation. Further, one such invariant point exists for every two deoxidation products at a fixed temperature.

2.3 Methods of Determining the Univariant Point

Several methods can be used to determine the transition points where deoxidation products transform. However, they can be classified into two basic categories: 1. indirect and 2. direct.

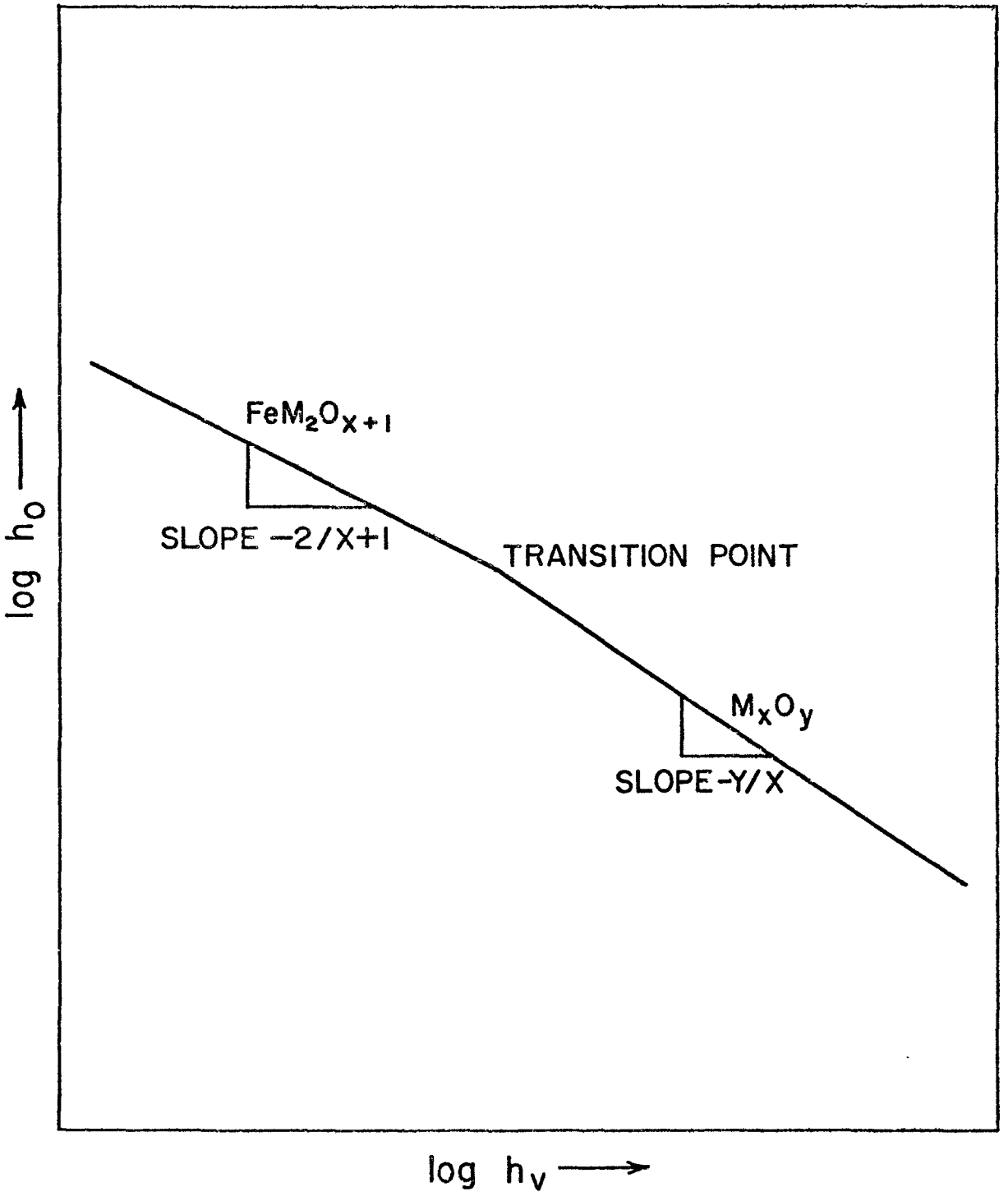

Fig. 2.1 Schematic deoxidation diagram for the system Fe-M-O

2.3.1 The Indirect Method

Three main techniques are used in this method.

a) Equilibrating an iron melt saturated with oxygen, with a known amount of deoxidant in solution in iron, under an inert atmosphere.

b) Equilibrating an iron melt containing the deoxidant in solution with a preferred deoxidation product under an inert atmosphere.

c) Equilibrating the melt with an oxidizing gas mixture - either CO/CO_2 or H_2/H_2O - at steelmaking temperatures.

In all three techniques, the melt is quenched and analyzed for 'M' the deoxidant and for the deoxidation product. The concentration of oxygen is determined by chemical analysis and converted to activity by using solution thermodynamics. The activity of oxygen can be measured during the experiment with a solid electrolyte probe or calculated from the partial pressure of oxygen in the gas phase using the relation

$$\frac{1}{2} O_{2(g)} \rightleftarrows \underline{O}_{1w/o} \qquad 2.7$$

for which $K_7 = \dfrac{h_O}{pO_2^{\frac{1}{2}}}$

The transition points are obtained by plotting log h_O against log h_M for equilibrium with each deoxidation product, to obtain lines given by equations 2.3 and 2.6 and extrapolating the lines to the point of intersection.

2.3.2 The Direct Method

This method comprises the monitoring of the oxygen activity, by a solid electrolyte galvanic cell, while the melt is being oxidized or reduced.

As an example, the reaction at a transition point may be expressed as:

$$M_2O_{x(s)} + \underline{O}_{1w/o} + Fe_{(\ell)} \rightleftarrows FeM_2O_{x+1(s)} \qquad 2.9$$

If the deoxidation products do not form a solid solution then their activities may be taken as unity and the equilibrium constant K_8 written as:

$$K_8 = \frac{1}{h_0} \qquad 2.10$$

Hence the transition point is represented by a constant oxygen activity during oxidation or reduction when two deoxidation products are in equilibrium with the melt simultaneously.

In certain systems the deoxidation products are well known. In such a case, two deoxidation products can be carefully synthesized and characterized and simultaneously equilibrated with the melt. The equilibrium oxygen activity represents the corresponding univariant point.

(A) The Iron Vanadium-Oxygen System

2.4 Introduction

Vanadium is used as an alloying element in tool and die steels and also in high strength low alloy steels. However, it is a mild deoxidizer and has been used as a deoxidant in continuous casting.

A number of investigations in the deoxidation thermodynamics of the Fe-V-O system have been reported. These have been reviewed quite extensively by Turkdogan,[1] Bodsworth and Bell,[2] and Jacquemont et al.[3]

The reactions for the deoxidation of iron by vanadium and the corresponding equilibrium constants 'K' can be written as

$$Fe_{(\ell)} + 4\underline{O}_{1w/o} + 2\underline{V}_{1w/o} \rightleftarrows FeV_2O_{4(s)} \qquad 2.11$$

with $$K_{11} = \frac{1}{h_V^2 h_O^4} \qquad 2.12$$

or $$2\underline{V}_{1w/o} + 3\underline{O}_{1w/o} \rightleftarrows V_2O_{3(s)} \qquad 2.13$$

with $$K_{13} = \frac{1}{h_V^2 h_O^3} \qquad 2.14$$

or $$\underline{V}_{1w/o} + \underline{O}_{1w/o} \rightleftarrows VO_{(s)} \qquad 2.15$$

with $$K_{15} = \frac{1}{h_V h_O} \qquad 2.16$$

where the activities of iron and the deoxidation product are taken as unity. However, in studies of deoxidation thermodynamics the equilibrium constant is generally reported for the reverse reactions and is thus the reciprocal of the values given by equations 2.12, 2.14, and 2.16. The experimental determinations of these reaction equilibria, their associated free energy changes and the free energies of formation of the deoxidation products - FeV_2O_4, V_2O_3 and VO will be considered in the following sections. Further, the experimental determinations of the equilibrium constants and the free energies of solution of vanadium and oxygen in iron:

$$V_{(s)} \rightleftarrows \underline{V}_{1w/o} \qquad 2.17$$

and $$\tfrac{1}{2}O_{2(g)} \rightleftarrows \underline{O}_{1w/o} \qquad 2.7$$

will also be reviewed.

2.5 Equilibrium Studies in the Fe-V-O System

Chipman and Dastur[4] have studied the reaction of H_2/H_2O gas mixtures with vanadium dissolved in liquid iron at 1600°C. The melt was oxidized till an oxide film appeared on the surface, allowed to equilibrate and then quenched. The oxide products were identified by X-ray diffraction as FeV_2O_4 and V_2O_3, depending on the vanadium content of the melt. Based on these observations they wrote the reactions as:

$$FeV_2O_{4(s)} + 4H_{2(g)} \rightleftarrows 2V_{-1w/o} + Fe_{(\ell)} + 4H_2O_{(g)} \qquad 2.19$$

$$\text{with} \quad K_{19} = h_V^2 \left(\frac{P_{H_2O}}{P_{H_2}}\right)^4 \qquad 2.20$$

$$\text{and} \quad V_2O_{3(s)} + 3H_{2(g)} \rightleftarrows 2V_{-1w/o} + 3H_2O_{(g)} \qquad 2.21$$

$$\text{for which} \quad K_{21} = h_V^2 \left(\frac{P_{H_2O}}{P_{H_2}}\right)^3 \qquad 2.22$$

They plotted log $\frac{P_{H_2O}}{P_{H_2}}$ against log %V and determined the transition point to be at 0.17% V. They noticed a deviation from linearity, for equilibrium with V_2O_3, at high V contents, but since they could not identify any other oxide, the deviation was attributed to either experimental inaccuracy or to solutions of vanadium in iron not obeying Henry's law at high vanadium contents. Their results have been summarized in Table 2.1.

Karasev[5] et al. have studied the Fe-V-O system by a similar technique and reported that FeV_2O_4 was the stable phase up to 0.2% V and V_2O_3 above 0.2. A plot of log h_V against log $\frac{P_{H_2O}}{P_{H_2}}$ yielded a slope of unity at vanadium concentrations greater than 0.3%. Hence they concluded that the stable phase was VO

above 0.3% V and that they could not identify it by X-ray diffraction as it decomposed to V_2O_3 and V during quenching.

Narita and Koyama[6] have reported a similar study at 1600°C, 1650°C and 1700°C. In addition to X-ray diffraction, they also used electron diffraction at high temperatures and room temperature for identification of the oxide. They identified FeV_2O_4 to be the stable phase up to 0.15% V and V_2O_3 above 0.15% V. However, in a later study, Narita et al.[7] have reported the formation of VO as the stable phase above 4% V.

Kojima et al.[8] studied this system by adding vanadium to an iron melt saturated with oxygen under an inert atmosphere. The melt was allowed to equilibrate at 1600°C and quenched by immersing an iron rod. The inclusions were examined by electron microprobe analysis and X-ray diffraction. They have identified FeV_2O_4 as the stable equilibrium phase up to 0.2% V, V_2O_3 between 0.2 and 0.9% V and VO between 0.9 and 4% V.

Turkdogan[1] has analyzed the results of Suzuki et al.[48] to obtain the values of the equilibrium constant for reactions 2.11 and 2.13 at 1600°C. Suzuki et al. equilibrated Fe-V melts, containing up to 5% V with a CO/CO_2 gas mixture to determine the solution thermodynamics of oxygen and vanadium in iron. Turkdogan has combined their data with that of Dastur and Chipman[4] to determine the stable deoxidation products at 1600°C. He reports the stable oxide as being FeV_2O_4 in melts with vanadium up to 0.1% and V_2O_3 above this composition.

In all these determinations, the activity of oxygen and vanadium where the deoxidation products transform has to be determined by plotting log h_O or log P_{H_2O}/P_{H_2} against log h_V, and extrapolating the lines from the

Table 2.1

Equilibrium in the Fe-V-O System

Source	Deoxidation Product	Stability Domain %V	- log K_T	$1/K_{1873}$	Reaction
Chipman & Dastur	FeV_2O_4	<0.15	-	7.2×10^{-8}	2.11
	V_2O_3	0.15 - 1.5	-42800/T + 17.10	1.8×10^{-6}	2.13
Karasev et al.	FeV_2O_4	<0.2	-50720/T + 21.90	6.6×10^{-8}	2.11
	V_2O_3	0.2 - 0.3	-41900/T + 18.12	5.6×10^{-5}	2.13
	V_2O_2(VO)	0.3 - 2.0	-25640/T + 10.48	6.5×10^{-3}	2.15
Narita & Koyama	FeV_2O_4	<0.15	-44704/T + 16.508	4.4×10^{-8}	2.11
	V_2O_3	0.15-5.0	-42300/T + 16.615	1.1×10^{-6}	2.13
Narita et al.	VO	4 - 10.0	-15530/T + 6.67	2.4×10^{-2}	2.15
Kay & Kontopoulos	FeV_2O_4	<0.2	-48320/T + 18.7	8.2×10^{-8}	2.11
	V_2O_3	0.2 - 10	-43430/T + 17.6	2.7×10^{-6}	2.13
Turkdogan	FeV_2O_4	<0.1		8.3×10^{-8}	2.11
	V_2O_3	0.3 - 10		3.5×10^{-6}	2.13

.....

Source	Deoxidation Product	Stability Domain %V	- log K_T	$1/K_{1873}$	Reaction
Kojima et al.	FeV_2O_4	<0.2		9.2×10^{-8}	2.11
	V_2O_3	0.2 - 0.9		2.5×10^{-6}	2.13
	VO	0.9 - 4		1.3×10^{-2}	2.15

$$Fe_{(\ell)} + 2\underline{V}_{1w/o} + 4\underline{O}_{1w/o} \rightleftarrows FeV_2O_{4(s)} \qquad (2.11)$$

$$2\underline{V}_{1w/o} + 3\underline{O}_{1w/o} \rightleftarrows V_2O_{3(s)} \qquad (2.13)$$

$$\underline{V}_{1w/o} + \underline{O}_{1w/o} \rightleftarrows VO_{(s)} \qquad (2.15)$$

regimes of each deoxidation product to the point of intersection.

Determinations using solid electrolyte galvanic cells have been reviewed in section 2.17. They are also summarized in Table 2.1, along with the results of other investigations.

Finally, Sticher and Schmalzried[20] used the data from various sources to draw phase stability diagrams of log P_{O_2} against mole fraction of vanadium at 1227°C. Pelton[21] has developed a computer programme to draw similar diagrams at any desired temperature.

2.6 Free Energies of Formation of the Deoxidation Products

2.6.1 Iron Vanadite FeV_2O_4

Chipman and Dastur[4] have determined the standard free energy change for the reaction

$$Fe_{(\ell)} + 2\underline{V}_{1w/o} + 4\underline{O}_{1w/o} \rightleftarrows FeV_2O_{4(s)} \qquad 2.11$$

at 1600°C, by combining the free energy change for reaction 2.19 with that for the reaction

$$H_{2(g)} + \underline{O}_{1w/o} \rightleftarrows H_2O_{(g)} \qquad 2.23$$

A similar method has been used by Karasev[5] and Narita et al.[6] Kontopoulos and Kay[12] have also studied reaction 2.11 using a solid electrolyte galvanic cell technique described in section 2.17.

Jacob and Alcock[55] using a technique described in section 2.17 have determined the oxygen potentials in the system Fe + V_2O_3 + FeV_2O_4 in the temperature range 750°C - 1600°C. They have also treated the thermodynamics of spinel formation theoretically in terms of the site preference energy.[9] Their results are summarized in Table 2.2.

Table 2.2

Standard Free Energy Change for Selected Reactions for FeV_2O_4

Source	Reaction	Temperature (Range) ^oK	$\Delta G^o(T_i)$ cals/mole	ΔG^o_{1873} cals/mole
Dastur & Chipman	$Fe_{(\ell)} + 2\underline{V} + 4\underline{O} \rightleftarrows FeV_2O_4$	1873		-61200
Karasev et al.		1868 - 1968	-232050 + 100T	-61530
Narita & Koyama		1873 - 1973	-204520 + 75.5T	-63000
Kay and Kontopoulos		1823 - 1973	-221060 + 85.6T	-60720
Turkdogan		1873		-60670
Kojima et al.		1873		-60300
Jacob & Alcock	$Fe_{(s,\ell)} + \frac{1}{2}O_{2(g)} + V_2O_{3(s)} \rightleftarrows FeV_2O_{4(s)}$	1023 - 1809	-69000 + 14.9T±300	
		1809 - 1973	-72,300 + 16.73T±300	-40980
Kunnmann et al.		1073 - 1380	(1073) -51200±250 (1380) -46,700±250	-39,473 (Extrapolated)
Wakihara & Katsura		1500°K	(1500°) -45,500±200	40100 (Extrapolated)

*Error values reported where available.

Kunnmann et al.[10] placed a sample of well characterized FeV_2O_4 in a silica boat at temperatures of up to 1100°C and increased the CO/CO_2 ratio of the equilibrating gas mixture until the reduction product was formed. Successive bracketing of the CO/CO_2 ratios enabled the determination of the exact equilibrium ratio of CO/CO_2 for the reaction:

$$CO_{(g)} + FeV_2O_{4(s)} \rightleftarrows Fe_{(s)} + V_2O_{3(s)} + CO_{2(g)} \qquad 2.24$$

They combined their data for reaction 2.24 with the free energy of formation of V_2O_3 to obtain the ΔG^o for the reaction:

$$FeV_2O_{4(s)} \rightleftarrows Fe_{(s)} + V_2O_{3(s)} + \frac{1}{2} O_{2(g)} \qquad 2.25$$

which is the same as that studied by Jacob and Alcock.

Wakihara and Katsura[11] have determined the standard free energy change for reaction 2.25 at 1227°C (1500°K) by a thermogravimetric method. A pellet of an oxide mixture of FeO and V_2O_3 was suspended in a vertical tube quenching furnace by a platinum wire and the weight changes were recorded as a function of the oxygen partial pressure. Their values are reasonably consistent with those of Kunnmann as can be seen from Table 2.2 and Fig. 2.3.

2.6.2 Vanadium Oxides (V_2O_3 and VO)

Chipman and Dastur[4] have also determined the standard free energy change for the reaction

$$2V_{\text{—1w/o}} + 3O_{\text{—1w/o}} \rightleftarrows V_2O_{3(s)} \qquad 2.13$$

at 1600°C by combining the free energy changes for reactions 2.21 and 2.23.

They have also given an expression for $\Delta G^{o}_{13}(T)$ by combining their data at 1600°C with ΔH^{o}_{f} (298°K), $\Delta C_p(T)$, and the free energy for solution of oxygen in iron. Kay and Kontopolous[12] have also determined this value with a galvanic cell technique described in section 2.17. The value for ΔG^{o}_{13} can be similarly obtained from the data of Karasev,[5] Narita,[6] Turkdogan[1] and Kojima et al.[8]

There have been a number of determinations of the free energy change for the reaction:

$$2V_{(s)} + \frac{3}{2}O_{2(g)} \rightleftarrows V_2O_{3(s)} \qquad 2.26$$

Kobayashi[13] has determined the equilibrium for reaction 2.26 by equilibrating pure (97%)V with a H_2/H_2O atmosphere in the temperature range 550°C to 1100°C. The reactions may be expressed as

$$V_2O_{3(s)} + H_{2(g)} \rightleftarrows 2VO_{(s)} + H_2O_{(g)} \qquad 2.27$$

and

$$VO_{(s)} + H_{2(g)} \rightleftarrows V_{(s)} + H_2O_{(g)} \qquad 2.28$$

Allen et al.[14] have corrected Kobayashi's result for the entropy terms and by combining them with the free energy of formation of H_2O determined the free energy changes for the reactions

$$2V_2O_{3(s)} \rightleftarrows 4VO_{(s)} + O_{2(g)} \quad (550^{o}C - 1100^{o}C) \qquad 2.29$$

and

$$2VO_{(s)} \rightleftarrows 2V_{(s)} + O_{2(g)} \quad (625^{o}C - 1527^{o}C) \qquad 2.30$$

The results of Kobayashi and Allen have been summarized in table 2.3.

Table 2.3

Standard Free Energy Change for Selected Reactions for V_2O_3

Source	Reaction	Temperature (Range) ^oK	$\Delta G^o(T_i)$ cals/mole	ΔG^o_{1873} cals/mole
Chipman		1873	-195810 + 78.23T	-49300
Karasev et al.		1868 - 1968	-191700 + 82.9T	-36450
Narita & Koyama		1873 - 1973	-193520 + 76.0T	-51060
Kay & Kontopoulos	$2V_{\text{lw/o}} + 3O_{\text{lw/o}} \rightleftarrows V_2O_{3(s)}$	1823 - 1973	-198700 + 80.5T	-47720
Turkdogan		1873		-46750
Kojima et al.		1873		-48000
Kobayashi	$2VO_{(s)} + H_2O_{(g)} \rightleftarrows V_2O_{3(s)} + H_{2(g)}$	823 - 1385	-29600 + 8.0T	
Allen et al.	$2VO_{(s)} + \frac{1}{2}O_{2(g)} \rightleftarrows V_2O_{3(s)}$	823 - 1385	-87650 + 20.25T	
Mah & Kelly		298 - 1700	(1700^o) -190,600	

.....

Source	Reaction	Temperature (Range) ^{o}K	$\Delta G^{o}(T_i)$ cals/mole	ΔG^{o}_{1873} cals/mole
Kontopoulos	$2V_{(s)} + \frac{3}{2}O_{2(g)} \rightleftarrows V_2O_{3(s)}$	1200 - 1700	(1700^{o}) -188400	
Barin & Knacke		298 - 2000	(1900^{o}) -182330	
Wicks & Block		298 - 1800	(1800^{o}) -191100	

Table 2.4

Standard Free Energy Change for Selected Reactions for VO

Source	Reaction	Temperature (Range) ^{o}K	$\Delta G^{o}(T_i)$ cals/mole	
Narita & Koyama	$\underline{V}_{1w/o} + \underline{O}_{1w/o} \rightleftarrows VO_{(s)}$	$1873^{o} - 1973^{o}$	-13900	(1873^{o})
Kojima et al.		1873^{o}	-16160	(1873^{o})
Kontopoulos	$V_{(s)} + \frac{1}{2}O_{2(g)} \rightleftarrows VO_{(s)}$	$1200^{o} - 1700^{o}$	-63900	(1700)
			-65700	(1600)
Mah & Kelly*		$298^{o} - 1700^{o}$	-70900	(1700)
			-69100	(1600)
Wicks & Block*		$298^{o} - 1700^{o}$	-63900	(1700)
Barin & Knacke		$298^{o} - 1973^{o}$	-65700	(1900)

*Compilations

Table 2.5

Thermodynamic Data for VO and V_2O_3

Source	VO $\Delta H_f^o(298)_{kcal/mole}$	V_2O_3 $\Delta H_f^o(298)_{kcal/mole}$
Allen et al.	-105.5±5	-299.4±7
Brewer	-98±5	-296.1±6
Rossini	-100	-290
Mah & Kelley	-103.2±0.3	-291.3±0.4
Charlu & Kleppa		-291.0±0.9
Wicks & Block	-98,000	-296,000

Heats of formation of both VO and V_2O_3 have been determined by bomb calorimetry by a number of workers[14-17] at 298°K. These values have been reported in Table 2.5. Mah and Kelley[17] have used high temperature entropy and heat content data to obtain heats and free energies of formation at temperatures up to 2000°K.

Kontopolous[78] has used the solid electrolyte technique (sec. 2.17) to determine the free energies of formation of V_2O_3 and VO in the temperature range 1000°C-1400°C.

Charlu and Kleppa[18] have used a high temperature combustion microcalorimeter to determine the enthalpy of formation of V_2O_3 by oxidizing at 910°K. This was then used to calculate ΔH_f^o for V_2O_3 at 298°K.

Barin and Knacke[22] and Wicks and Block[44] have used the values of ΔH_{298}^o of Allen at al.[14] and calculated the free energy increments of the compounds as well as the elements vanadium and oxygen up to 2000°K. The standard free energy data for VO and V_2O_3 calculated from the values of Barin and Knacke and from Wicks and Block in the temperature range of interest are shown in Table 2.3 and 2.4 along with the data from experimental determinations.

2.7 Free Energy of Solution of Oxygen and Vanadium in Iron

2.7.1 Oxygen:

The free energy change 'ΔG_7^o' for the reaction

$$\frac{1}{2}\,O_{2(g)} \rightleftarrows \underline{O}_{1w/o} \qquad 2.7$$

can be determined by equilibrating solid or molten iron with a gas mixture

of H_2/H_2O. The equilibrium may be expressed as

$$H_{2(g)} + \underline{O}_{1w/o} \rightleftarrows H_2O_{(g)} \qquad 2.23$$

with an equilibrium constant 'K_{23}' given by

$$K_{23} = \frac{P_{H_2O}}{P_{H_2}\, h_O} = \frac{P_{H_2O}}{P_{H_2} \cdot f_O[\%O]} \qquad 2.30$$

This data combined with the standard free energy of formation of H_2O gives the free energy change for reaction 2.7. Olette[3] has reviewed a number of determinations of reaction 2.23 and the presently accepted values are by Chipman and Floridis.[19]

$$\log f_O = -0.20[\%O] \qquad 2.31$$

The values of K_{23} obtained at 1550°C and 1600°C were 4.68 and 3.65 respectively. Combination with earlier data of Dastur and Chipman[4] gives the following temperature dependence of K_{23} and ΔG^o_{23}

$$\log K_{23} = \frac{7050}{T} - 3.20 \qquad 2.32$$

and $$\Delta G^o_{23} = -32{,}200 + 14.63T \text{ cals} \qquad 2.33$$

Combining this with the free energy formation of $H_2O_{(g)}$

$$H_{2(g)} + \frac{1}{2}O_{2(g)} \rightleftarrows H_2O_{(g)} \qquad 2.34$$

for which $\Delta G^o_{34} = -60{,}200 + 13.94T$ cals 2.35

the free energy change for reaction 2.7 is given by

$$\Delta G^o_7 = -28{,}000 - 0.69T \text{ cals} \qquad 2.36$$

2.7.2 Vanadium:

Dastur and Chipman[4] have calculated the standard free energy change for the reaction

$$V_{(s)} \rightleftarrows \underline{V}_{1w/o} \qquad 2.37$$

by combining the standard free energy changes for the reactions

$$2V_{(s)} + 3\underline{O}_{1w/o} \rightleftarrows V_2O_{3(s)}, \quad \Delta G^o_{38} = -203,700 + 56.0T \text{ cals} \qquad 2.38$$

$$2\underline{V}_{1w/o} + 3\underline{O}_{1w/o} \rightleftarrows V_2O_{3(s)} \qquad 2.13$$

The value obtained for ΔG^o_{37} at 1600°C is -24,700 cals. They compared this to the theoretical value by calculating the value of ΔG^o_{37}, assuming that iron and vanadium form an ideal solution. The discrepancy was attributed to deviation from Raoults law and was used to calculate the value of γ^o at 1600°C. The value of γ^o reported in their work is 0.12.

To apply this result to other temperatures a regular solution model was employed and the resultant equation was expressed as

$$\Delta G^o_{37}(T) = -3,900 - 11.1T \text{ cals} \qquad 2.39$$

Fruehan[84] has determined the value of γ^o for vanadium from his study of the Fe-V-O system using a solid electrolyte galvanic cell. The value of γ^o obtained from his data is 0.10. This value is in good agreement with that of Dastur and Chipman and the variation in ΔG^o_{37} is about 300 cals/mole at 1600°C.

(B) The Iron-Chromium-Oxygen System

2.8 Introduction

Chromium is used extensively in low and high alloy steels and especially stainless steels. Numerous investigations of the Fe-Cr-O system have been reported in the literature and these have been reviewed extensively by Jacquemont et al.,[3] Turkdogan[1] and Chipman.[23] Once again, the determinations of the solution thermodynamics of oxygen and chromium in iron have not been reviewed and only the salient features of the determinations pertinent to this work will be discussed.

The deoxidation reactions of iron by chromium, and the corresponding equilibrium constants 'K' have been reported as:

$$Fe_{(\ell)} + 4\underline{O}_{1w/o} + 2\underline{Cr}_{1w/o} \rightleftarrows FeCr_2O_{4(s)} \qquad 2.40$$

$$K_{40} = \frac{1}{h_O^4 h_{Cr}^2} \qquad 2.41$$

$$2\underline{Cr}_{1w/o} + 3\underline{O}_{1w/o} \rightleftarrows Cr_2O_{3(s)} \qquad 2.42$$

$$K_{42} = \frac{1}{h_{Cr}^2 h_O^3} \qquad 2.43$$

$$3\underline{Cr}_{1w/o} + 4\underline{O}_{1w/o} \rightleftarrows Cr_3O_{4(s)} \qquad 2.44$$

$$K_{44} = \frac{1}{h_{Cr}^3 h_O^4} \qquad 2.45$$

where the activities of liquid iron and the deoxidation products are taken as unity. In the determination of deoxidation thermodynamics, the equilibrium constants are generally reported for the reverse reactions and correspond to the reciprocal of the values given by equations 2.41, 2.43 and 2.45.

The experimental determinations of the equilibrium constants for these reactions and the free energies of formation of the deoxidation products are reviewed in the following sections. The standard free energy of formation of chromic oxide has been critically assessed due to its importance in calculations of the oxygen activity of the reference electrode used in this work.

2.9 Equilibrium Studies in the Fe-Cr-O System

Chen and Chipman[24] have studied the Fe-Cr-O system at 1595°C. They equilibrated liquid iron-chromium alloys containing up to 20% chromium, with accurately controlled H_2/H_2O gas mixtures in crucibles of either chromite ($FeCr_2O_4$) or chromic oxide. The experiments were carried out in an induction furnace and the temperature was measured by a carefully calibrated 'disappearing filament optical pyrometer'. The melts were quenched after equilibration and analysed for oxygen and chromium.

They have expressed the reaction equilibria as:

$$FeO\cdot Cr_2O_{3(s)} + 4H_{2(g)} \rightleftarrows 4H_2O_{(g)} + Fe_{(\ell)} + 2\underline{Cr}_{1w/o} \qquad 2.46$$

$$K_{46} = h_{Cr}^2 \left(\frac{P_{H_2O}}{P_{H_2}}\right)^4 \qquad 2.47$$

and

$$Cr_2O_{3(s)} + 3H_{2(g)} \rightleftarrows 2\underline{Cr}_{1w/o} + 3H_2O_{(g)} \qquad 2.48$$

$$K_{48} = h_{Cr}^{2}\left(\frac{P_{H_2O}}{P_{H_2}}\right)^{3} \qquad 2.49$$

These data were combined with the standard free energy change for the reaction

$$H_{2(g)} + \underline{O}_{1w/o} \rightleftarrows H_2O_{(g)} \qquad 2.23$$

to obtain the equilibrium data for reactions 2.40 and 2.42.

Since the experiments were carried out in crucibles made of the deoxidation products it was assumed that excess chromium in the melt would oxidize out. Conversely if the melt were deficient in chromium for the particular gas composition, the crucible would dissolve to make up for the deficiency. The chromium content at which the equilibrium deoxidation product changed from chromite to chromic oxide was determined by conducting experiments in chromic oxide crucibles and a fixed ratio of P_{H_2}/P_{H_2O} but with different amounts of chromium in the melt. The Cr content at which a chromite deoxidation product was identified was found to be 5.50% Cr.

The authors combined their data for reaction 2.48 with the free energy of solution of chromium in iron to obtain the free energy change for the reaction:

$$Cr_2O_{3(s)} + 3H_{2(g)} \rightleftarrows 2Cr_{(s)} + 3H_2O_{(g)} \qquad 2.50$$

Since the value of ΔG^{o}_{50} obtained from their data at 1600°C agreed very well with similar data obtained at low temperatures they reported the variation of ΔG^{o}_{48} with the temperature as

$$\Delta G^{o}_{48} = 93210 - 40.83T \text{ cals} \qquad 2.51$$

Further, they found that the analyzed oxygen in the melt exceeded the amount expected to be dissolved in iron in equilibrium with Cr_2O_3. They proposed that this was due to the presence of chromous oxide-CrO-dissolved in the melt, but found no direct evidence of this. This may be interpreted as an association between chromium and oxygen atoms in the melt.

Lintschewski and Samarin[25] did similar work and found that $FeCr_2O_4$ was stable below 6% Cr and Cr_2O_3 above that. They give values of ΔG^o_{46} and ΔG^o_{48} in the temperature range 1625-1710°C as:

$$\Delta G^o_{46} = 336,000 - 167.06T \text{ cals.} \qquad 2.52$$

$$\Delta G^o_{48} = 248,810 - 125.40T \text{ cals.} \qquad 2.51(a)$$

Turkdogan[26] equilibrated Fe-Cr melts containing 3 to 13% Cr with chromic oxide under a gas-mixture of argon-H_2/H_2O in alumina crucibles at 1565°, 1600° and 1660°C. He gives the value of ΔG^o_{42} as

$$\Delta G^o_{42} = -169.210 + 70.95T \text{ cals.} \qquad 2.53$$

Hilty[27] et al., melted Fe-Cr alloys containing up to 50% Cr in rotating magnesia crucibles under an inert atmosphere at 1550°, 1600° and 1650°C. They saturated the melt with oxygen and allowed the equilibrium deoxidation product to form, quenched the melt and analyzed the deoxidation products by X-ray diffraction. They identified the deoxidation products as solid solutions of oxides of iron and chromium and represented them as follows.

	Chromium Content			
	Low	Medium	High	Very High
	Cr<2.5%		Cr>9%	
Deoxidation product	chromite	Distorted spinel	Cr_3O_4	Cr_3O_4
solid solutions of	Fe_3O_4 & $FeO \cdot Cr_2O_3$	Cr_3O_4 & $FeO \cdot Cr_2O_3$	Fe_3O_4 Cr_3O_4	

They explained the observation of Chen and Chipman, that Cr_2O_3 was the stable phase, as being caused by the dissociation of Cr_3O_4 during cooling according to the following reaction:

$$3Cr_3O_{4(s)} \rightleftarrows 4Cr_2O_{3(s)} + Cr_{(s)} \qquad 2.54$$

Based on the results of Hilty et al., Chipman[28] recalculated his earlier data. Assuming that the standard free energy of formation of Cr_3O_4 will be four-thirds that of Cr_2O_3 he obtained

$$3Cr_{(s)} + 2O_{2(g)} \rightleftarrows Cr_3O_{4(s)} \qquad 2.55$$

and $\Delta G^o_{55} = -349{,}000 + 74T$ cals $\qquad 2.56$

He used this value of ΔG^o_{55} to interpret the data of Chen and Chipman[24] for K_{48} in terms of Cr_3O_4 as the deoxidation product rather than Cr_2O_3 as assumed by Chen and Chipman. He reports the standard free energy change for the reaction:

$$Cr_3O_{4(s)} + 4H_{2(g)} \rightleftarrows 3\underline{Cr}_{1w/o} + 4H_2O_{(g)} \qquad 2.57$$

as $\Delta G^{o}_{57} = 121,300 - 51.6T$ cals. 2.58

and that of ΔG^{o}_{40} and ΔG^{o}_{44} as

$$\Delta G^{o}_{40} = -232,200 + 99.1T \text{ cals.} \quad 2.59$$

$$\Delta G^{o}_{44} = -244,800 + 109.6T \text{ cals.} \quad 2.60$$

Sakao and Sano[29] equilibrated Fr-Cr melts containing up to 20% Cr with H_2/H_2O gas mixtures in order to determine the equilibrium deoxidation product. They reported that $FeCr_2O_4$ was stable up to 3% Cr, Cr_3O_4 above 9% Cr and another spinel, $Fe_2Cr_7O_{12}$, between 3 and 9% Cr. However, Kojima et al.[30] repeated this work by adding up to 20% Cr to oxygen saturated iron melts and analyzed the equilibrium deoxidation products by a microprobe analyzer. They reported that $FeO{\cdot}Cr_2O_3$ was stable up to 7% Cr in the melt and a mixture of Cr_2O_3 and Cr_3O_4 above 7% Cr.

Adachi and Iwamoto[30] carried out a series of experiments on Fe-Cr alloys containing up to 65% Cr at 1600°C in magnesia crucibles to confirm the results obtained by Hilty et al. They found no evidence of the formation of Cr_3O_4 or of metallic chromium in the oxide inclusions. They characterized the inclusions by electron diffraction and by microprobe analysis. From lattice parameter measurements they concluded that the 'distorted spinel' of Hilty et al. was in fact a solution of chromite and chromic oxide. They reported that the only deoxidation products observed were chromite and chromic oxide.

Nakamura et al.[31] equilibrated oxygen saturated Fe-Cr melts containing between 3 and 30% chromium at temperatures between 1600 and 1800°C,

under argon atmospheres and in MgO crucibles. They report the stable deoxidation product as Cr_2O_3 in this range, and the value of log K_{42} as:

$$\log K_{42} = -\frac{44040}{T} + 19.42 \qquad 2.61$$

Buzek[46] determined the equilibrium constant for reaction 2.40 by equilibrating Fe-Cr-O melts containing up to 20% Cr, with solid chromite at 1600°C under an argon atmosphere. The chromite was prepared synthetically and characterized before introducing on the melt and the equilibrium deoxidation product was also characterized by X-ray diffraction. He reported the stable deoxidation products as chromite up to 7% Cr and Cr_2O_3 above that. He reports the value of K_{40} at 1600°C as follows

$$\frac{1}{K_{40}} = 2.34 \times 10^{-6} \qquad 2.62$$

A number of investigations in the Fe-Cr-O system have been carried out using solid electrolytes. The experimental techniques have been reviewed in section 2.17. The conclusions of the authors are discussed here.

Fruehan[84] assumed that the stable deoxidation product was chromite below 3% Cr and chromic oxide above that. His results have been interpreted by Turkdogan[1] to give the values of log K_{40} and log K_{42} as

$$\log K_{40} = \frac{50.700}{T} - 21.70 \qquad 2.63$$

$$\log K_{42} = \frac{40740}{T} - 17.78 \qquad 2.64$$

The results of the investigations in the liquid Fe-Cr-O system have been summarized in Table 2.6.

Table 2.6

Equilibrium in the Fe-Cr-O System

Source	Deoxidation Product	Stability Range %Cr	- log K(T)	$1/K_{1873}$	Reaction
Chen and Chipman	$FeCr_2O_4$	<5.5		2.44×10^{-6}	2.40
	Cr_2O_3	5.5 - 25		1.45×10^{-4}	2.42
Lintschewski & Samarin	$FeCr_2O_4$	<6	-106,200/T + 52.23	3.4×10^{-5}	2.40
	Cr_2O_3	6 - 16	-78,950/T + 39.20	1.1×10^{-3}	2.42
Turkdogan	Cr_2O_3	3 - 13	-36,980/T + 15.506	5.8×10^{-5}	2.42
Chipman	$FeCr_2O_4$	<3	-50,740/T + 21.66	3.7×10^{-6}	2.40
	Cr_3O_4	>9	-33,500/T + 23.95	2.4×10^{-5}	2.44
Sakao & Sano	$FeCr_2O_4$	<3		3×10^{-6}	2.40
	$Fe_2Cr_7O_{12}$	3 - 9		1.1×10^{-16}	
	Cr_3O_4	9 - 20		2.1×10^{-5}	2.44
Kojima et al.	$FeCr_2O_4$	<7		8×10^{-6}	2.40
	Cr_2O_3 + Cr_3O_4	7 - 20			

.....

Source	Deoxidation Product	Stability Range %Cr	- log K(T)	$1/K_{1873}$	Reaction
Turkdogan	$FeCr_2O_4$	<3	-50700/T + 21.70	4.0×10^{-6}	2.40
	Cr_2O_3	3 - 20	-40740/T + 17.78	1.1×10^{-4}	2.42
Nakumura et al.	Cr_2O_3		-44040/T + 19.42	8.1×10^{-5}	2.42
Buzek	$FeCr_2O_4$	0 - 7		2.34×10^{-6}	2.40
	Cr_2O_3	7 - 20			

$$Fe_{(\ell)} + 2\underline{Cr}_{1w/o} + 4\underline{O}_{1w/o} \rightleftarrows FeCr_2O_{4(s)} \qquad (2.40)$$

$$2\underline{Cr}_{1w/o} + 3\underline{O}_{1w/o} \rightleftarrows Cr_2O_{3(s)} \qquad (2.42)$$

$$3\underline{Cr}_{1w/o} + 4\underline{O}_{1w/o} \rightleftarrows Cr_3O_{4(s)} \qquad (2.44)$$

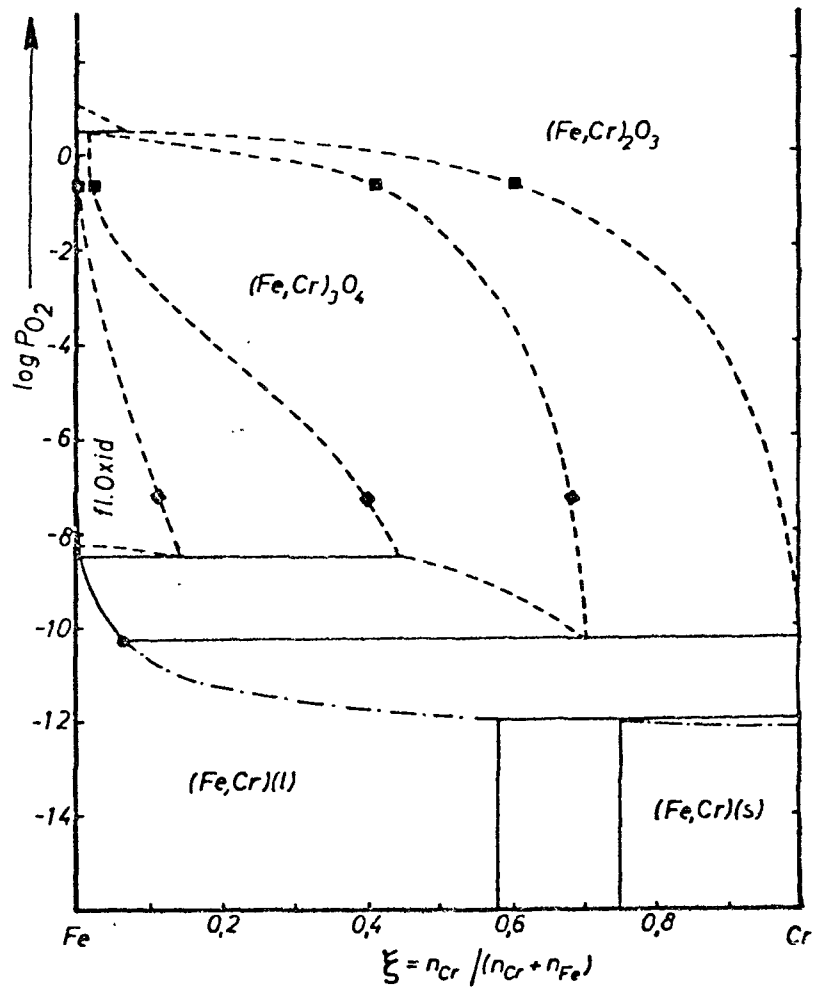

Fig. 2.2 Phase diagram ($\frac{n_{Cr}}{n_{Fe}+n_{Cr}}$ vs log P_{O_2}) of the Fe-Cr-O system at 1600°C (Sticher & Schmalzried)

It has been suggested that CrO would form as a stable deoxidation product in the Fe-Cr-O system,[32] and some thermodynamic data for 'CrO' have been reported.[35,45] Healey and Schottmiller[36] have reported the formation of CrO in silica saturated slags and its behaviour in slags has been studied.[33,34] However, it has been pointed out that CrO is stabilized by the presence of silica in slags and there are no reports of its formation as a stable deoxidation product in the Fe-Cr-O system.

Sticher and Schmalzried[20] have reviwed the Fe-Cr-O system both in the solid state and also above the melting point given. They have presented a summary of numerous determinations in the form of diagrams of log P_{O_2} vs $\frac{n_{Cr}}{n_{Fe}+n_{Cr}}$ at various temperatures. Their diagram at 1600°C is shown in Fig. 2.2.

It can be seen from Fig. 2.2 and Table 2.6 that the Fe-Cr-O system forms a number of oxides which are stable over various ranges of oxygen activity and temperature. Investigations of the Fe-Cr-O system are complicated by the following factors:

1. Oxides like Cr_3O_4 and the distorted spinel disproportionate on cooling. Hence, even though the deoxidation product can be characterized at room temperature, it does not necessarily correspond to the product formed at high temperature.

2. For the same reason, it is difficult to estimate the chromium contents where one deoxidation product transforms to another. This can explain the disagreements in the stability domains reported in Table 2.6.

3. It is difficult to determine whether equilibrium has been attained in the system.

4. When a Fe-Cr-O melt is 'equilibrated' with a preformed deoxidation product it is difficult to determine whether that product is the true equilibrium product at the reaction temperature.

5. In the equilibration techniques employed in the investigations it is not possible to determine whether the 'distorted spinel' has a definite composition or if it represents a continuous range of solid solutions of Cr_3O_4 in $FeO \cdot Cr_2O_3$.

2.10 Free Energies of Formation of the Deoxidation Products

2.10.1 Chromite-$FeCr_2O_4$

Chen and Chipman[24] determined the free energy change for the reaction:

$$Fe_{(\ell)} + 4\underline{O}_{1w/o} + 2\underline{Cr}_{1w/o} \rightleftarrows FeCr_2O_{4(s)} \qquad 2.40$$

and combined this with the standard free energy change for the reaction:

$$2\underline{Cr}_{1w/o} + 3\underline{O}_{1w/o} \rightleftarrows Cr_2O_{3(s)} \qquad 2.42$$

to obtain the ΔG^o for the reaction:

$$Fe_{(\ell)} + \underline{O}_{1w/o} + Cr_2O_{3(s)} \rightleftarrows FeCr_2O_{4(s)} \qquad 2.65$$

as $\Delta G^o_{65} = -15.2$ kcal/mole at 1595^oC.

Fruehan,[84] using a solid electrolyte galvanic cell determined the standard free energy change for the reaction

$$Fe_{(\ell)} + 2Cr_{(\ell)} + 4\underline{O}_{1w/o} \rightleftarrows FeCr_2O_4 \qquad 2.66$$

as -79.8 ± 1.5 kcal/mole at 1600°C. Calculations based on Chen and Chipman's data for ΔG^{o}_{66} gives a value of -81.2 kcal/mole at 1600°C. The values of ΔG^{o}_{66} similarly calculated from the equilibrium data of Samarin,[25] Sakao and Samo[29], and Turkdogan[1] are shown in Table 2.7.

Jacob and Alcock[55] have used a solid electrolyte galvanic cell to study the oxygen potential of the system $Fe_{(s,\ell)} + Cr_2O_{3(s)} + FeCr_2O_{4(s)}$ in the temperature range 750° to 1700°C. They report the cell reaction and its standard free energy change as

$$2Fe_{(s,\ell)} + O_{2(g)} + 2Cr_2O_{3(s)} \rightleftarrows 2FeCr_2O_{4(s)} \qquad 2.67$$

$$\Delta G^{o}_{67} = -151{,}400 + 34.7T \pm 300 \text{ cals.} \quad (750^{o} - 1536^{o}C)$$

$$\Delta G^{o}_{67} = -158{,}000 + 38.4T \pm 300 \text{ cals.} \quad (1536^{o} - 1700^{o}C) \qquad 2.68$$

They have also presented a theoretical treatment of the standard free energy of formation of spinels. In spinel systems at high temperatures the cations can interchange between the tetrahedral and octahedral sites thus making a significant contribution to the total entropy of the spinel. They calculated the lattice site preference energy for the cations from crystal field theory[(82)] and report the free energy of formation of chromite from $FeO_{(s)}$ and $Cr_2O_{3(s)}$ as

$$\Delta G^{o}_{FeCr_2O_4} = -12{,}450 + 1.73T \text{ cals.} \quad (750^{o} - 1400^{o}C) \qquad 2.69$$

Katsura and Muan[37] have studied equilibria in the $FeO\text{-}Fe_2O_3\text{-}Cr_2O_3$ system at 1300°C under oxygen partial pressures ranging from 0.21 atm (air) to 1.5×10^{-11} atm. They synthesized solid solutions of Fe_2O_3 and Cr_2O_3, from

analytical grade Fe_2O_3 and Cr_2O_3 by a series of operations consisting of heating the appropriate powder mixture, grinding, and remixing. The partial pressure of oxygen was controlled with gas mixtures of CO/CO_2 and CO/CO_2-H_2 or by using air.

They measured the weight changes of a specimen at 1300°C at fixed partial pressures of oxygen, by a thermogravimetric technique to determine the partial pressure of oxygen in equilibrium with $Fe_{(s)}$, $Cr_2O_{3(s)}$ and $FeCr_2O_{4(s)}$. The oxide phases were determined by X-ray diffraction of samples quenched from 1300°C and the free energy changes of the reactions were calculated as follows:

$$2Fe_{(s)} + 2Cr_2O_{3(s)} + O_{2(g)} \rightleftarrows 2FeO\cdot Cr_2O_{3(s)} \qquad 2.70$$

and $$1.90Fe_{(s)} + O_{2(g)} = 2Fe_{0.95}O_{(s)} \qquad 2.71$$

By subtracting ΔG^o_{71} from ΔG^o_{70} they obtained the value of ΔG^o for the reaction

$$2Fe_{0.95}O_{(s)} + 2Cr_2O_{3(s)} + 0.1Fe_{(s)} \rightleftarrows 2FeO\cdot Cr_2O_{3(s)} \qquad 2.72$$

They reported the value of ΔG^o_{72} as -19.8 kcal at 1300°C.

Kunnmann et al.[10] employed a technique similar to the one used for vanadite (sec. 2.6) to determine the standard free energy change for the reaction

$$FeCr_2O_{4(s)} \rightleftarrows Fe_{(s)} + Cr_2O_{3(s)} + \tfrac{1}{2}O_{2(g)} \qquad 2.70a$$

They reported $\Delta G^o_{70.a}$ at various temperatures as follows:

$T^{o}K$	1380	1320	1234	1073	
$\Delta G^{o}_{70.a}$ kcal/formula wt.	46.20	46.65	47.95	51.15	(±0.25)

Novokhatski and Lenev[38] have used a technique similar to that of Katsura and Muan using H_2/H_2O gas mixtures to study the thermodynamic properties of chromite in the temperature range 1300-1500°C. They report the values of ΔG^{o} for reactions 2.70 and 2.72 and the reaction

$$Fe_{(s)} + 2Cr_{(s)} + 2O_{2(g)} \rightleftarrows FeCr_2O_{4(s)} \qquad 2.73$$

as follows

$$\Delta G^{o}_{70} = -154{,}640 + 33.87T \quad (\pm 1000 \text{ cal/mole}) \qquad 2.74$$

$$\Delta G^{o}_{72} = -15850 + 2.60T \quad (\pm 700 \text{ cal/mole}) \qquad 2.75$$

$$\Delta G^{o}_{73} = -348{,}100 + 78.66T \quad (\pm 1200 \text{ cal/mole}) \qquad 2.76$$

Rezukhina et al.[39] used a solid electrolyte galvanic cell, of the same type as used by Jacob and Alcok but with a ThO_2-La_2O_3 solid electrolyte to determine the standard free energy change for the reaction

$$FeO_{(s)} + Cr_2O_{3(s)} \rightleftarrows FeCr_2O_{4(s)} \qquad 2.77$$

in the temperature range 1300° - 1433°K. They report the value of ΔG^{o}_{77} in this temperature range and of ΔG^{o}_{73} at 298°K as

$$\Delta G^{o}_{77} = -14.885 + 3.746T \text{ cals.} \qquad 2.78$$

$$\Delta G^{o}_{73}(298^{o}K) = -325 \pm 1 \text{ kcal} \qquad 2.79$$

Table 2.7

Standard Free Energy Change for Selected Reactions for $FeCr_2O_4$

Source	Reaction	Temperature (Range) ^oK	$\Delta G^o(T_i)$ cals/mole	ΔG^o_{1873} cals/mole
Chen & Chipman	$Fe_{(\ell)} + \underline{O}_{1w/o} + Cr_2O_{3(s)} \rightarrow FeCr_2O_4$	1868	(1868^o) - 15200	
Lintschewski		1898 - 1983	-485,865 + 239T±1000	-38300
Turkdogan	$Fe_{(\ell)} + 2\underline{Cr}_{1w/o} + 4\underline{O}_{1w/o} \rightleftarrows FeCr_2O_{4(s)}$	1933^o	(1933^o) - 52880	
Chipman		1823 - 1923	-232135 + 99.1T	-46540
Sakao & Sano		1873		-47325
Kojima et al.		1873		-43675
Turkdogan			-231925/T + 99.3T	-46200
Fruehan	$Fe_{(\ell)} + 2Cr_{(\ell)} + 4\underline{O}_{1w/o} \rightleftarrows FeCr_2O_{4(s)}$	1873		-79800 ± 1500
Jacob & Alcock	$FeO_{(s)} + Cr_2O_{3(s)} \rightleftarrows FeCr_2O_4$	1023 - 1673	-12450 + 1.73T±300	

.....

Source	Reaction	Temperature (Range) ^{o}K	$\Delta G^{o}(T)$ cals/mole	ΔG^{o}_{1873} cals/mole
Tretjakow		1000 - 1500	-13750 + 3.93T	
Rezakhina et al.	$FeO + Cr_2O_3 \rightleftarrows FeCr_2O_4$	1300 - 1433	-14885 + 3.746T	
Katsura & Muan	$Fe_{0.95}O_{(s)} + Cr_2O_{3(s)} + 0.05Fe_{(s)} \rightleftarrows FeCr_2O_{4(s)}$	1573	(1573^{o}) - 9900	
Jacob & Alcock	$Fe_{(s,\ell)} + \frac{1}{2}O_{2(g)} + Cr_2O_{3(s)} \rightleftarrows FeCr_2O_4$	1023 - 1809	-75700 + 17.35T	
		1809 - 1973	-79,000 + 19.2T	-43038
Kunnmann	$Fe_{(s)} + Cr_2O_{3(s)} + \frac{1}{2}O_{2(g)} \rightleftarrows FeCr_2O_4$	1073 - 1380	(1073^{o}) - 51150	
			(1380^{o}) - 46200	
Novokhatski & Lenev		1573 - 1773	-77320 + 16.94T	

Tretjakow and Schmalzried[40] used a similar technique with calcia stabilized zirconia electrolytes in the temperature range 1000^{o} - $1500^{o}K$. They report the value of ΔG^{o} for the reaction

$$FeO_{(s)} + Cr_2O_{3(s)} \rightleftarrows FeCr_2O_{4(s)} \qquad 2.77$$

$$\Delta G^{o}_{77} = -13,750 + 3.93 \times T \quad cal/mole \qquad 2.80$$

These results have been summarized in table 2.7. The results show a spread of 8.6 kcal at $1000^{o}C$. The results of Chen and Chipman,[24] Jacob and Alcock[55] and Fruehan[84] are within 3 kcal at $1600^{o}C$, though Jacob and Alcock report their value from an extrapolation of their data in the temperature range 750^{o} to $1400^{o}C$. The values of Lintschewski and Samarin[25] are significantly different from those of Chen and Chipman. This is also reflected in their value of K_{40} reported in table 2.7, and is probably due to errors in analysis for chromium and oxygen.

2.10.2 Chromic Oxide-Cr_2O_3

Jeannin et al.[41] determined the standard free energy of formation of Cr_2O_3 from chromium metal and oxygen in the temperature range 1300^{o} - $1600^{o}K$. They mixed powders of Cr and Cr_2O_3 and heated them in an alumina boat under purified argon. The atmosphere was then changed to hydrogen at slightly above atmospheric pressure. The system was closed, and the hydrogen circulated in the system. The reaction may be written as:

$$Cr_2O_{3(s)} + 3H_{2(g)} \rightleftarrows 2Cr_{(s)} + 3H_2O_{(g)} \qquad 2.81$$

After equilibration, the gas was isolated, and the water separated by condensation. The water was reevaporated to a definite volume and its

pressure measured by a manometer. They reported the value of the standard free energy of formation of Cr_2O_3 corresponding to a reaction:

$$2Cr_{(s)} + \frac{3}{2}O_{2(g)} \rightleftarrows Cr_2O_{3(s)} \qquad 2.82$$

by the following equation:

$$\Delta G^o_{82} = -266,700 + 59.95T \pm 300 \text{ cals.} \quad (1300 - 1600^oK) \qquad 2.83$$

In a recent investigation, Pehlke et al.[83] report the measurement of the standard free energy of formation of Cr_2O_3 using an EMF technique with Yttria doped Thoria as the solid electrolyte in the temperature range 857° - 1250°C. The details of their technique are described in section 2.17. They have employed two cells using Mn/MnO and Co/CoO mixtures as reference electrodes and since the agreement between the cells was within ±200 cals/mole they report the average value of ΔG^o_{82} as a function of temperature by the relation:

$$\Delta G^o_{82} = -266,600 + 59.78T \text{ cals.} \qquad 2.84$$

Tretjakow and Schmalzried[40] and Pugliese and Fitterer[42] have made similar measurements with calcia stabilized zirconia as the electrolyte and air as the reference electrode in the temperature range 1000 to 1500°K. Tretjakow and Schmalzried have expressed ΔG^o_{82} by the relation:

$$\Delta G^o_{82} = -258,600 + 55.2T \text{ cals.} \qquad 2.85$$

While Pugliese and Fitterer have not reported their data in the form of a relation between ΔG^o_{82} and temperature, their values of ΔG^o_{82} are about

3 to 5 kcal/mole less negative than those of Pehlke et al., and 1 to 3 kcal/mole less negative than those of Tretjakow and Schmalzried (Table 2.8).

Finally Coughlin,[43] has made theoretical calculations based on the free energy of formation at 298°K and specific heat data in the temperature range 298 to 1823°K. He reports the value of ΔG^{o}_{82} as

$$\Delta G^{o}_{82} = -271,300 + 61.82T \text{ cals.} \qquad 2.86$$

Chen and Chipman have determined the equilibrium constant for the reaction

$$2\underline{Cr}_{1w/o} + 3\underline{O}_{1w/o} \rightleftarrows Cr_2O_{3(s)} \qquad 2.42$$

The free energy change for reaction 2.42 can be calculated from their data of the equilibrium constant. The value of ΔG^{o}_{42} at 1595°C obtained from their data is -32,800 cals/mole. The value of ΔG^{o}_{42} can be similarly calculated from the data of Samarin, Turkdogan and other investigators. This can be combined with the free energy changes associated with the fusion of oxygen and chromium in liquid iron to obtain the standard free energy of formation of Cr_2O_3.

The results of all these determinations are summarized in table 2.8 and fig. 2.3. Table 2.8 also shows the extrapolation of the data to 1600°C.

It can be seen from fig. 2.3 that while the data of Pehlke et al., Jeannin et al. and Coughlin is in good agreement, that of Tretjakow and Schmalzried as well as Pugliese and Fitterer is in consistent disagreement. This has been attributed to electronic conduction in calcia stabilized

Table 2.8

Standard Free Energy Changes for Selected Reactions for Cr_2O_3

Source	Reaction	Temperature (Range) ^oK	$\Delta G^o(T_i)$ cals/mole	ΔG^o_{1873} cals/mole
Chen & Chipman		1868	(1868^o)- 32800	
Samarin et al.	$2\underline{Cr}_{1w/o} + 3\underline{O}_{1w/o} \rightleftarrows Cr_2O_{3(s)}$	1898 - 1983	-361196 + 179.3T	
Turkdogan		1838 - 1933	-169183 + 70.9T±1000	-36350
Turkdogan (Fruehan)			-186385 + 81.3T	-34030
Jeannin et al.	$2Cr_{(s)} + \frac{3}{2}O_{2(g)} \rightleftarrows Cr_2O_{3(s)}$	1300 - 1600	-266700 + 59.95T±300	-154413*
Pehlke et al.		1148 - 152[illegible]	-266600 + 59.78T±300	-154632*
Tretjakow		1000 - 150[illegible]	-258,600 + 55.2T±600	-155210
Pugliese		1000 - 1500	(1448^o) - 175019	
Coughlin		298 - 1823	-271300 + 61.82T	-155511*
Barin & Knacke		298 - 1800	(1800^o) - 158.344	
Wicks and Block		298 - 1800	-274750 - -.11TℓnT $+2.01x10^{-3}T^2+105.95T$	-155490*

*Extrapolated

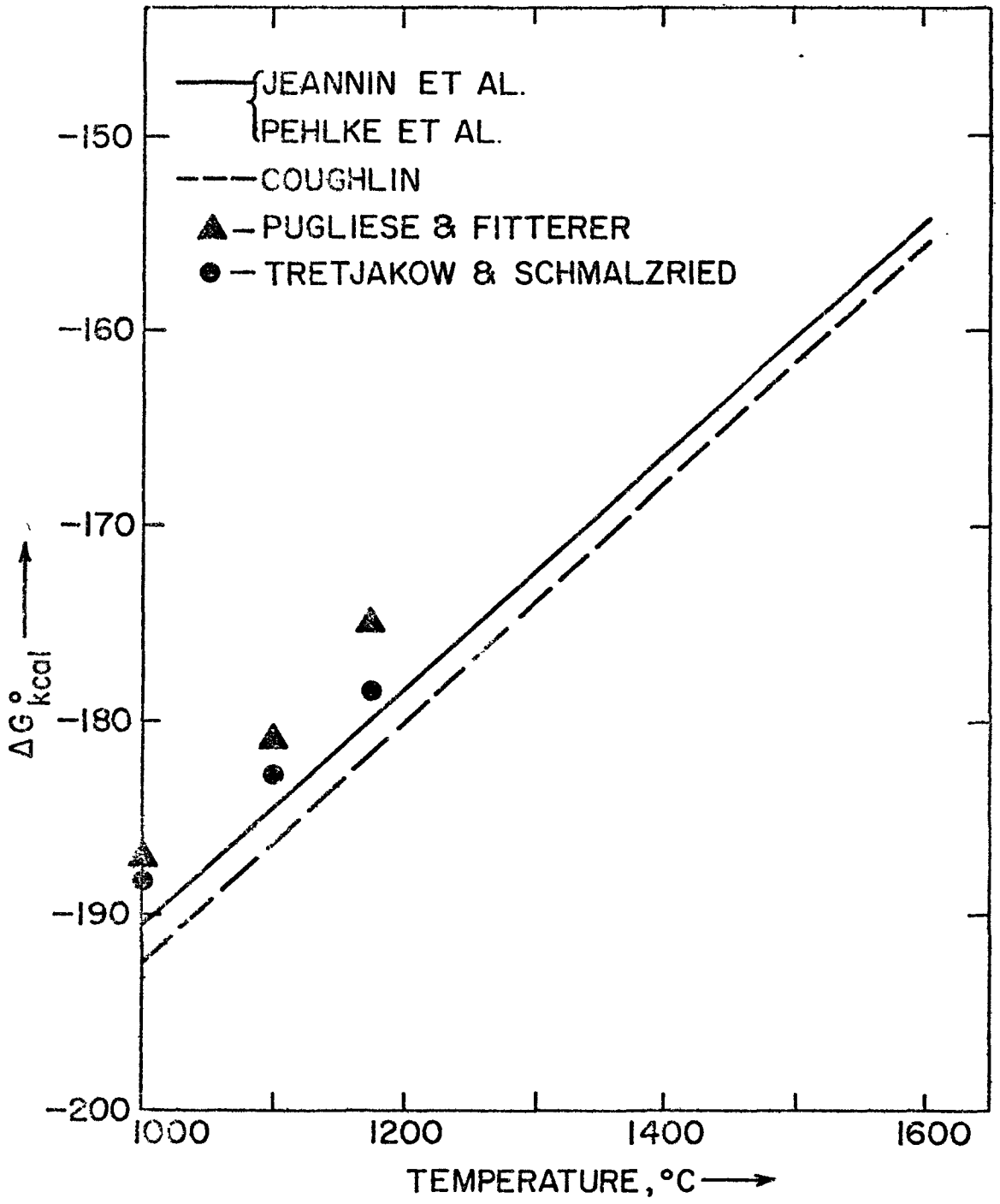

Fig. 2.3 Standard free energy of formation of Cr_2O_3 from the literature

zirconia and other sources of error to be discussed in Chapter 5. The data of Jeannin et al. has been used in this work.

Barin and Knacke[22] and Wicks and Block[44] have compiled the free energy, enthalpy and entropy data for Cr_2O_3 based on heats of formation at 298°K and empirically determined heat capacity data.

2.10.3 Lower Oxides of Chromium (Cr_3O_4 and CrO)

There have been no reported experimental investigations in the standard free energy of formation of Cr_3O_4. The only reported value is due to an estimation by Chipman.[28] He estimated the heat of formation of Cr_3O_4 to be roughly four thirds that of Cr_2O_3. Further he assumed the entropy change to be equal to that of Mn_3O_4, which is known, and also that the effect of temperature would be the same as for Mn_3O_4, and reported the approximate equation

$$3Cr_{(s)} + 2O_{2(g)} \rightleftarrows Cr_3O_{4(s)} \qquad 2.55$$

and $$\Delta G_f^o = -349{,}000 + 74T \text{ cals.} \qquad 2.56$$

2.11 Free Energy of Solution of Chromium in Molten Iron

Chipman[28] has calculated the standard free energy change for the reaction:

$$Cr_{(s)} \rightleftarrows \underline{Cr}_{1w/o} \qquad 2.87$$

as:

$$\Delta G_{87}^o = 4350 - 11.11T \text{ cals.} \qquad 2.88$$

He assumed Raoultian behaviour of chromium in iron due to the physical

similarity between the two elements.

Turkdogan[26] has calculated ΔG^{o}_{87} by combining the standard free energy changes for the reactions

$$Cr_{(s)} \rightleftarrows Cr_{(\ell)} \qquad 2.89$$

$$\Delta G^{o}_{89} = 3500 - 1.61T \text{ cals/mole} \quad \text{(heat of fusion)} \qquad 2.90$$

and

$$Cr_{(\ell)} \rightleftarrows \underline{Cr}_{1w/o} \qquad 2.91$$

$$\Delta G^{o}_{91} = 4.575T \log \frac{0.5585}{52} = -9.01T \text{ cals.} \qquad 2.92$$

to obtain the expression

$$\Delta G^{o}_{87} = 3500 - 10.62T \text{ cals.} \qquad 2.93$$

However, the two expressions 2.88 and 2.93 differ by only 100 cals/mole at 1600°C.

Fruehan[84] has studied the behaviour of chromium in molten iron with a solid electrolyte galvanic cell as well as by a mass spectrometric technique and found that solutions of Cr in iron show very small negative deviations from Raoult's law.

(C) Solid Electrolytes

2.12 Solid Electrolytes in the Study of Deoxidation Thermodynamics

In 1957 Kiukkola & Wagner[51] successfully demonstrated the use of several solid oxide electrolytes for measuring the free energy changes of several chemical reactions. Since that time this technique has been employed

in a number of studies of the thermodynamics of the deoxidation of steel and deoxidation products as well as a number of other systems involving oxygen.[49,55] Provided that a suitable electrolyte is available and with proper care in cell design, this technique offers numerous advantages over the conventional equilibration techniques.

A number of excellent reviews of the properties of various solid electrolytes, their applications and experimental techniques have been published.[50,51,56-59] Hence only salient features of the criteria for the choice of a solid electrolyte, the cell design and the properties of the electrolytes will be discussed in this section. Further, the expressions for the various quantities measured with the present cell design will also be outlined.

2.12.1 The Oxygen Cell

The solid oxide electrolyte is employed in oxygen concentration cells as a 'bridge' that permits transport of only oxygen ions between two isolated electrodes with different oxygen chemical potentials μ^{I} and μ^{II}. The cell can be represented as:

$$\text{Pt} , \; \mu^{I}_{O_2} \; \left| \begin{array}{c} \text{Solid Oxide} \\ \text{Electrolyte} \end{array} \right| \; \mu^{II}_{O_2} , \; \text{Pt} \qquad 2.94$$

with a cell reaction

$$\mu^{II}_{O_2} \rightleftarrows \mu^{I}_{O_2} \qquad 2.95$$

The free energy change associated with the cell reaction involving 'n'

electrons may be expressed as

$$\Delta G_{95} = \mu^{I}_{O_2} - \mu^{II}_{O_2} \text{ cals/mole} \qquad 2.96$$

$$= -nFE \qquad 2.97$$

where E is the EMF of the cell and F is a Faraday.

When the chemical potential of oxygen at one electrode is kept at a known constant value (the reference electrode), the oxygen potential at the other electrode can be determined by measurement of the EMF of the cell. Further, reactions involving oxygen at this electrode can be studied by monitoring the cell EMF, provided the solid electrolyte and the reference electrode are not affected.

The solid electrolytes most commonly used are ZrO_2-CaO and ThO_2-Y_2O_3. Of these, ZrO_2-CaO is more frequently used because of difficulties in the fabrication, purity and handling of ThO_2-Y_2O_3. ZrO_2-CaO was used exclusively in this work and hence the ZrO_2-CaO system is disucssed in detail in subsequent sections. The ThO_2-Y_2O_3 system has been reviewed extensively by Etsell and Flengas[56] and a detailed discussion of this electrolyte has not been included.

2.13 Significance of 'Ionic Transport Number'

The relation between the cell EMF and the free energy change for the cell reaction as given by equation 2.97 is strictly valid only when the solid electrolyte is a purely ionic conductor. However, it has been pointed out by Rapp[57] that crystalline solids exhibit appreciable electronic conductivities. Wagner[51] has demonstrated that the EMF of

a galvanic cell based on a solid electrolyte which exhibits only slight deviation from ideal stoichiometry, can be expressed as:

$$E_{cell} = \frac{1}{2ZF} \int_{\mu_{O_2}^{I}}^{\mu_{O_2}^{II}} t_{ion}\, d\mu_{O_2} \qquad 2.98$$

where (Z=-2) is the valence of oxygen and t_{ion} is the transport number of the oxygen ion in the electrolyte.

Further, since $t_{ion} + t_e = 1$, this expression can be written as

$$E_{cell} = \frac{\mu_{O_2}^{I} - \mu_{O_2}^{II}}{2ZF} - \frac{1}{2ZF} \int_{\mu_{O_2}^{I}}^{\mu_{O_2}^{II}} t_e\, d\mu_{O_2} \qquad 2.99$$

Thus when $t_e \approx 0$ (electronic conduction is negligible)

$$E_{cell} = \frac{\mu_{O_2}^{I} - \mu_{O_2}^{II}}{2ZF} \qquad 2.100$$

It is obvious from these equations that the ionic transport number should be as close to unity as possible under the conditions of operation of the electrochemical cell. If $t_e \neq 0$ the cell voltage does not correspond to that given by eq. 2.100, and the cell cannot be used to determine the chemical potential of oxygen. Heyne and Beekmans[61] have pointed out that under such conditions oxygen transport takes place through the electrolyte even if the cell is not loaded externally. The charge carried by the oxygen transported forms the exact equivalent of the charge leak-through by electronic conductivity, thereby polarising the cell.

2.14 Dependence of t_{ion} on P_{O_2} and Other Factors

Schmalzried[62] has proposed an expression to describe the functional dependence of t_{ion} on oxygen activity in solid electrolytes

$$t_{ion} = \frac{\sigma_{ion}}{\sigma_{ion}+\sigma_{\oplus}+\sigma_{\ominus}} \qquad 2.101$$

$$= \left[1 + \left(\frac{P_{O_2}}{P_{\oplus}}\right)^{1/n} + \left(\frac{P_{O_2}}{P_{\ominus}}\right)^{-1/n}\right]^{-1} \qquad 2.102$$

For a given temperature, the parameters $P_{\oplus}$ and $P_{\ominus}$ represent those oxygen activities at which the p-type and n-type electronic conductivities $\sigma_{\oplus}$ and $\sigma_{\ominus}$ respectively equal the ionic conductivity, σ_{ion}. The $P_{O_2}^{1/n}$ and $P_{O_2}^{-1/n}$ dependencies result from the defect equilibria which describe the introduction of electronic defects into the electrolyte structure.

It follows that for any solid electrolyte there exists a range of oxygen activity outside of which the value of t_{ion} will vary significantly from unity.

Patterson[63] has studied the temperature dependence of the ionic and electronic conductivities of solid electrolytes. He has suggested that at elevated temperatures the ionic conductivities are virtually independent of P_{O_2} whereas the excess electronic conductivities are proportional to $P_{O_2}^{1/n}$ and $P_{O_2}^{-1/n}$ for holes and electrons respectively. Thus the value of $P_{\oplus}$ and $P_{\ominus}$ are temperature dependent and may be expressed as

$$\log P_{\oplus} = -n\left(\frac{Q_{ion}-Q_{\oplus}}{2.303R}\right)\frac{1}{T} + n \log \frac{\sigma^{o}_{ion}}{\sigma^{o}_{\oplus}} \qquad 2.103$$

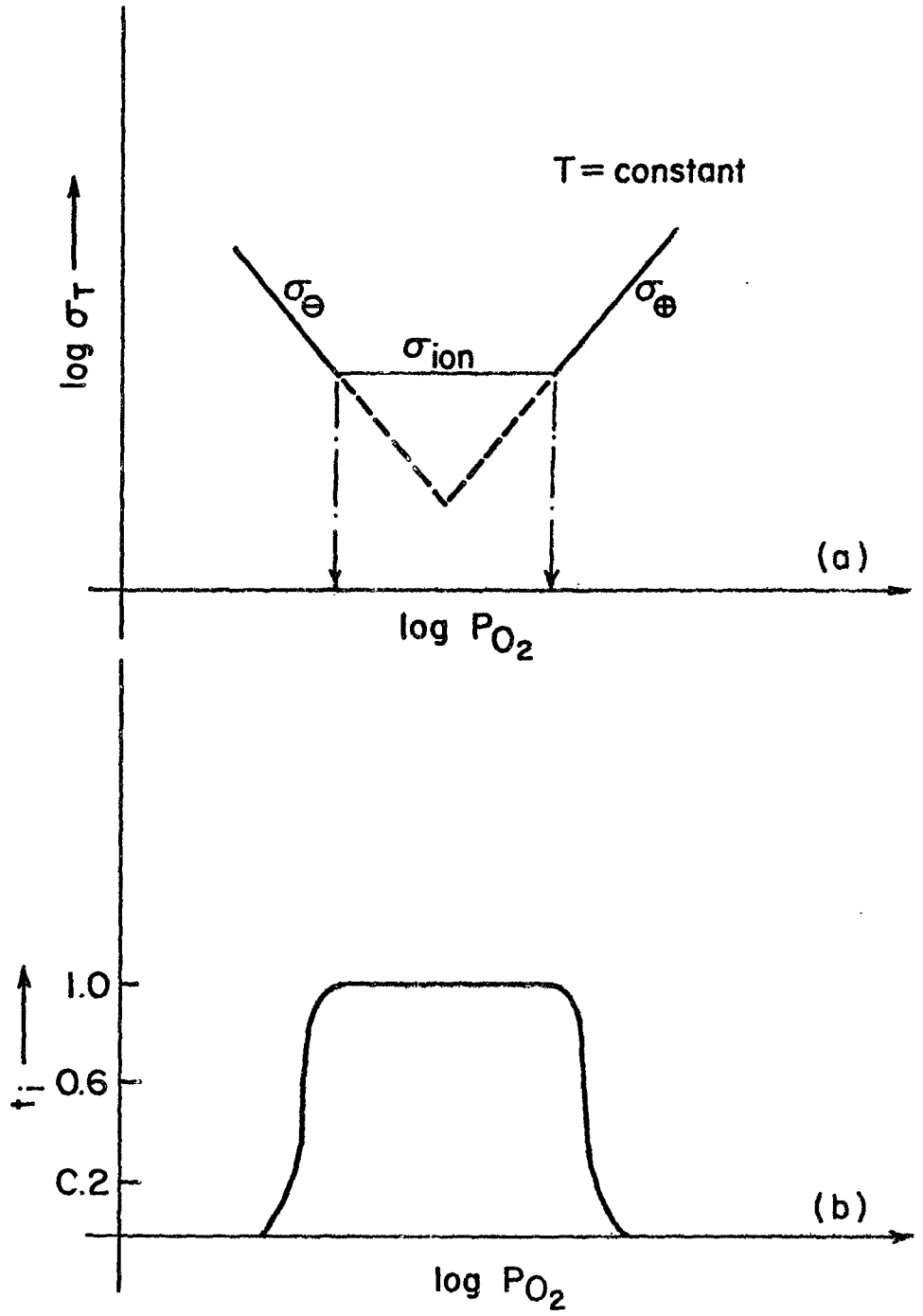

Fig. 2.4 Schematic representation of the variation of total conductivity (a) and ionic transport number (b) with oxygen partial pressure

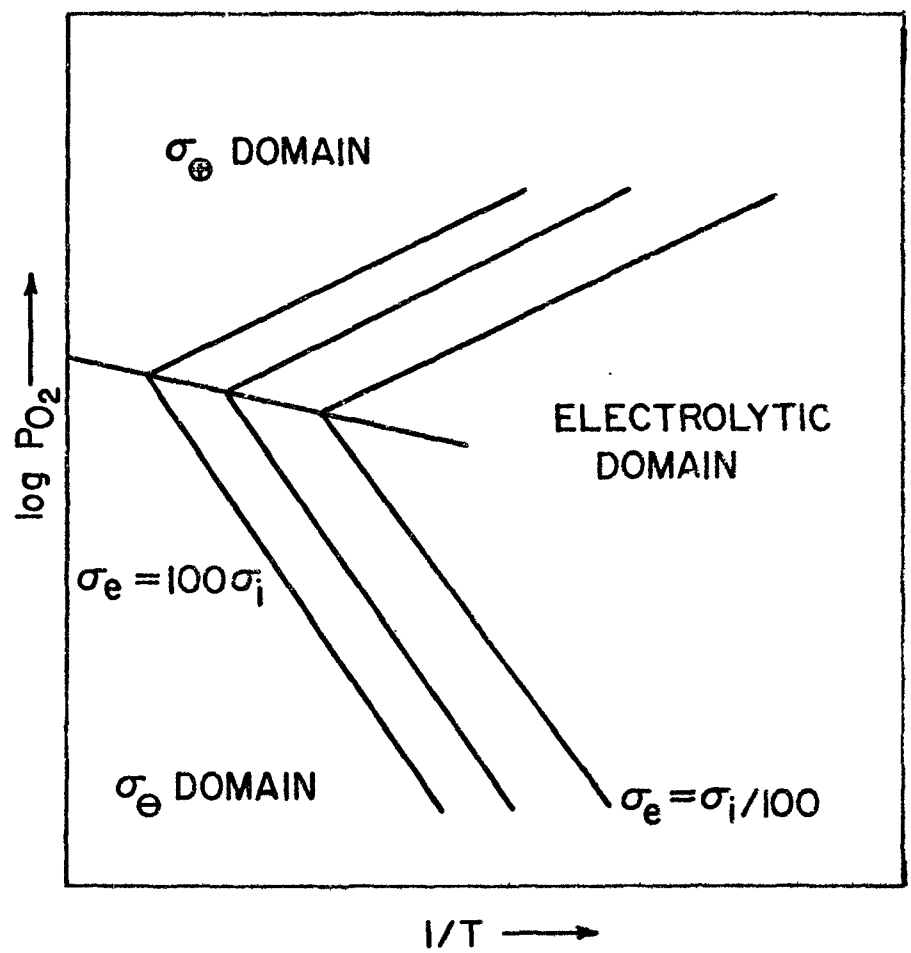

Fig. 2.5 Schematic representation of the dependence of the electrolytic domain on the temperature

2.15 CSZ as a Solid Electrolyte

Calcia stabilized zirconia is used extensively as a solid electrolyte at about 1000°C in research as well as in commercial oxygen probes and fuel cells. The composition of the electrolyte used most frequently is one with 15 mole % of calcium oxide.

Etsell and Flengas[56] have summarized determinations of the phase boundaries, lattice parameters, ionic conductivities, diffusion coefficients and also the critical partial pressures beyond which the ionic transport number becomes less than 0.99 at 1000°C. While a large value of ionic conductivity is desirable, only the electrolytic domain is of critical significance in this work. Hence only the determinations of the electrolytic domain will be discussed in this section.

The upper limit of oxygen partial pressure - above which electronic conduction by holes becomes significant - has been determined by Steele and Alcock[64] as 1 atm and by Tretyakov and Muan[65] as 100 atm. at 1000°C. Patterson[63] has used the data from these and other workers[66-68] to obtain the variation of the electrolytic domain with temperature (Fig. 2.6). The value for the upper limit at 1000°C from this figure can be seen to be 10^8 atm. Even at 1600°C the upper limit, from this diagram, is at about 1 atm. This value is beyond the region of interest in studies of deoxidation thermodynamics.

However, the limit of oxygen partial pressure below which electronic conduction becomes significant is of critical importance in studies of deoxidation thermodynamics. Schmalzried,[69] Steele and Alcock,[64] and Tretyakov and Muan[65] have determined this limit from EMF measurements on cells with electrodes consisting of metal, metal oxide mixtures up to 1000°C.

Table 2.9

Lower Limit of the Electrolytic Domain for Calcia Stabilized Zirconia (CSZ)

Critical Oxygen Pressure -log P_{O_2}

Temperature Source	1000°C	1600°C
Schmalzried	-16	-
Steele & Alcock	-17	-
Tretyakov & Muan	-20	-
Baker and West	-17.5	-8.4
Fischer & Janke	-	-10.0
Fruehan	-	-13.0
Patterson et al.	-19	-8.4

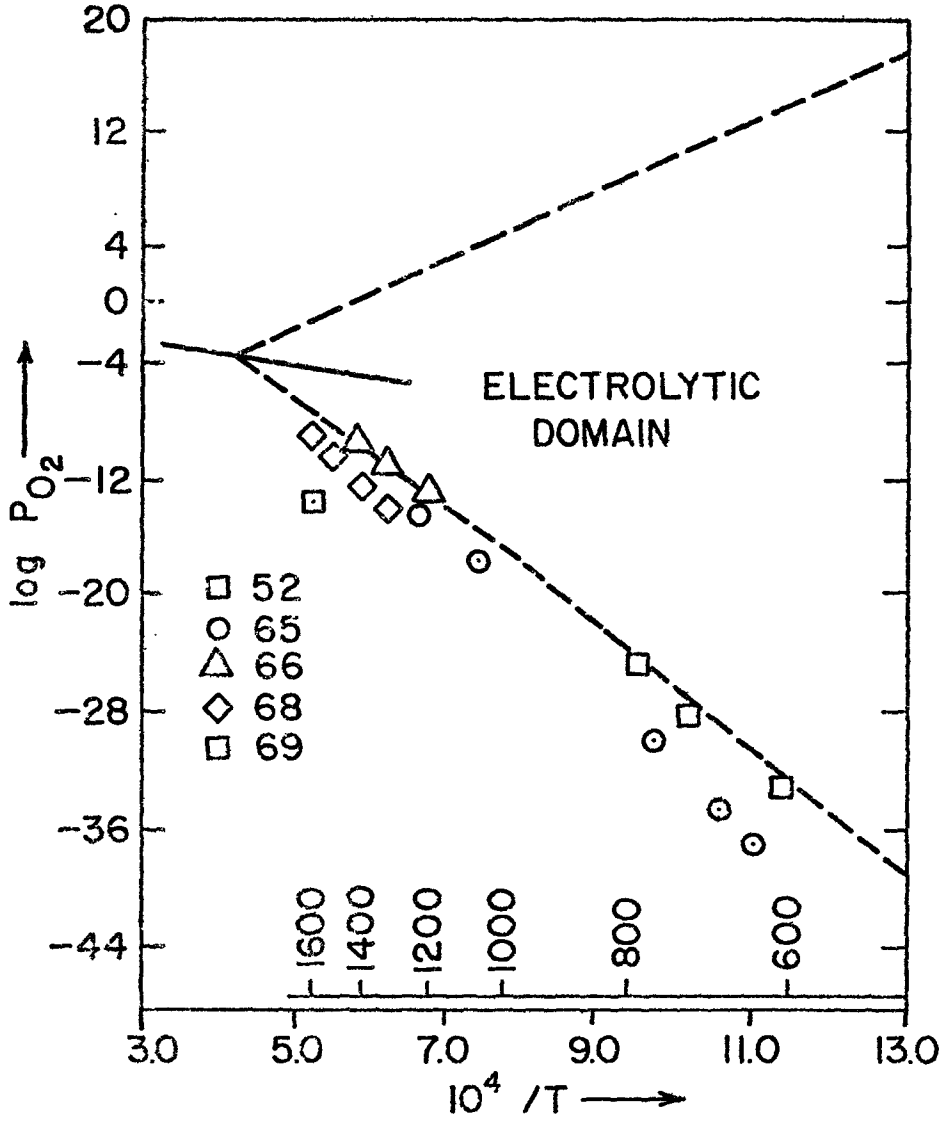

Fig. 2.6 Lower limits of the electrolytic domain for C.S.Z. as reported in the literature

The oxygen partial pressures at the two electrodes are fixed and can be calculated from thermodynamic data. The ratio of the measured EMF to the theoretical value can be related to the value of P_θ by using equations 2.99 and 2.102. Their results are summarized in Table 2.9.

An EMF method using air as one electrode and H_2/H_2O mixtures of predetermined composition as the other electrode, was used by Baker and West[66] and by Fischer and Janke.[68] Fruehan[(88)] determined the limit at liquid iron temperatures by determining the activity of oxygen in molten iron and comparing it with the analyzed concentrations. These values are also listed in Table 2.9.

Patterson[67] et al. have determined this limit from A.C. and D.C. conductivity measurements by the polarised cell technique. Heyne and Beekmans[61] have used a technique involving the differential transport of oxygen between three concentric tubes of CSZ to determine the dependence of conductivity of the solid electrolytes on the partial pressure of oxygen.

The lower limit of the electrolytic domain for CSZ at 1600°C can be obtained from Pattersons[63] work as $P_{O_2} \approx 10^{-8.4}$ atm. Fischer and Janke[68] determined this limit as 2.8×10^{-10} atm. Fruehan[88] compared results obtained from CSZ electrolytes with those from a cell using Yttria doped Thoria known to be ionic at 1600°C down to $P_{O_2} = 2 \times 10^{-16}$ atm - and concluded that CSZ can be used at 1600°C at least down to $P_{O_2} = 8 \times 10^{-13}$ atm.

2.16 The Reference Electrodes

It was pointed out in Sec. 2.12 that in order to use the EMF cell to determine thermodynamic data, one of the electrodes has to act as a

reference with a fixed oxygen activity.

Air has been used as a reference electrode in early works on deoxidation thermodynamics by Fitterer.[70] Air has the advantage that it is a direct reference with a fixed oxygen activity independent of temperature and also it does not polarise easily. However, the oxygen potential is very far from the oxygen activities of interest in these studies, and also it tends to permeate through the electrolyte especially at steelmaking temperatures.

Rapp[57] has reviewed a number of solid state coexistence electrodes used with solid oxide electrolytes. They comprise of a mixture of fine powders of a metal and its stable oxide. With these electrodes the lower limit of temperature for successful application is determined by diffusivities in the solid state. Generally such electrodes can be used above $600^{o}C$.

The electrodes used commonly in the temperature range $700^{o}C$ - $1200^{o}C$ are Fe-FeO, Cu-Cu_2O, and Ni-NiO. This choice is determined by the reliability of the available thermodynamic data, as well as the resistance to polarization of these electrodes.

At steelmaking temperatures the electrodes used most commonly are Cr/Cr_2O_3 and Mo/MoO_2. The oxygen partial pressure in equilibrium with these electrodes at $1600^{o}C$ is 8×10^{-13} atm and 7.1×10^{-8} atm.

Exchange electrodes are used in cells where no solid electrolyte is available for the ions involved in the reaction. Exchange electrodes have been reviewed by Rapp.[57] However, they are generally not employed in the determination of deoxidation thermodynamics.

Most of the practical criteria for choosing the reference electrode

are pointed out in section 3.2. One of the main conditions is that the oxygen activity has to be uniform throughout the electrode. If the diffusional processes do not make up for any imbalance introduced at this electrode a layer of oxide or metal forms at the electrode electrolyte interface thus polarizing the cell.

2.17 Deoxidation Studies Using Solid Electrolytes

A number of studies using solid electrolytes for the study of deoxidation thermodynamics, the free energies of formation of oxides, and also for oxygen activities in other metals and slags have been reported in the literature.[70-81] The details of the various cell designs used in these works have been reviewed by Turkdogan[71] and also by Shores and Rapp,[57] and will not be discussed in great detail here. Further, only those studies of deoxidation thermodynamics that deal with the Fe-Cr-O and Fe-V-O systems are reviewed in detail.

While most of the studies referred to have used a ZrO_2-CaO electrolyte, Olette[76] et al. have used a ThO_2-10%Y_2O_3 solid electrolyte to study the Fe-Zr-O, and Fe-Ce-O systems. Other electrolytes like ZrO_2-MgO, and ZrO_2-Y_2O_3 have been used[3,82] but not for the Fe-Cr-O and Fe-V-O systems.

Fruehan[84-85] studied the Fe-V-O and Fe-Cr-O systems using cells which can be expressed as:

$$\text{or } \begin{matrix}\text{Mo}\\\text{Pt}\end{matrix} \mid \text{Cr-}Cr_2O_3 \mid \begin{matrix}\text{CaO-}ZrO_2\\\text{or}\\ThO_2\text{-}Y_2O_3\end{matrix} \mid \begin{matrix}\text{Fe-V-O}\\\text{or}\\\text{Fe-Cr-O}\end{matrix} \quad \begin{matrix}\text{oxygen}\\\text{saturated}\end{matrix} \quad \mid \begin{matrix}\text{Mo-}Al_2O_3\\\text{Cermet}\end{matrix} \qquad (2105)$$

The cell consisted of a disc of the electrolyte about 3 mm x 3 mm D

sealed into a silica tube, with a Cr/Cr_2O_3 reference electrode and suitable leads to the reference and iron electrodes. The iron melt was saturated with oxygen by adding Fe_2O_3 and various quantities of either V or Cr were added. The melt was then equilibrated and the oxygen activity measured by immersing the cell. For the Fe-V-O system both electrolytes were used and since no significant difference between the two electrolytes was noticed, ZrO_2-CaO was used for the Fe-Cr-O system. V and Cr were determined by chemical analysis and oxygen was analyzed by neutron activation.

The virtual cell reaction for the cell used by Fruehan can be written as

$$\frac{2}{3}Cr_{(s)} + \underline{O}_{1w/o} \rightleftarrows \frac{1}{3}Cr_2O_{3(s)} \qquad 2.106$$

for which $\Delta G^o_{106} = \frac{-RT}{nF} \ell n \frac{1}{h_O}$ 2.107

This was combined with the data for the oxygen partial pressure in equilibrium with Cr/Cr_2O_3 mixture at the reaction temperature and the analyzed deoxidizer content to determine the equilibrium for the reactions

$$FeV_2O_{4(s)} \rightleftarrows Fe_{(\ell)} + 2\underline{V}_{1w/o} + 4\underline{O}_{1w/o} \qquad 2.11$$

$$V_2O_{3(s)} \rightleftarrows 2\underline{V}_{1w/o} + 3\underline{O}_{1w/o} \qquad 2.13$$

$$FeCr_2O_{4(s)} \rightleftarrows 2Fe_{(\ell)} + 2\underline{Cr}_{1w/o} + 4\underline{O}_{1w/o} \qquad 2.40$$

and $$Cr_2O_{3(s)} \rightleftarrows 2\underline{Cr}_{1w/o} + 3\underline{O}_{1w/o} \qquad 2.42$$

These results were then used to calculate the activity coefficients. The results on the Fe-V-O and Fe-Cr-O have been summarized in Tables 2.2 and 2.7.

Kay and Kontopolous[12] have used a similar technique to study the Fe-V-O system using a ZrO_2-CaO electrolyte. However, in this case the oxygen was analysed by the inert gas fusion method. Their results are also summarized in Table 2.2.

Kontopolous[78] has also used the EMF technique to determine the free energy of formation of lower oxides of vanadium in the temperature range 700-1450°C. The cell used can be represented as

$$\text{Pt, } \begin{matrix}\text{Fe/FeO}\\ \text{or}\\ \text{Cr/Cr}_2\text{O}_3\end{matrix} \;\Big|\; ThO_2\text{-}Y_2O_3 \;\Big|\; V + \begin{matrix}\text{vanadium}\\ \text{vanadium}\\ \text{oxide}\end{matrix}\text{, Pt} \qquad 2.108$$

The virtual cell reaction can be expressed as

$$y(\text{Fe or Cr})_{(s)} + V_xO_{y(s)} \rightleftarrows yFeO \text{ or } \frac{2y}{3} Cr_2O_3 + xV_{(s)} \qquad 2.109$$

The cell EMF was a measure of the ratio of the partial pressure of oxygen in equilibrium with the reference electrode and that in equilibrium with vanadium and its oxide. The latter was calculated by using thermodynamic data for the reference electrode.

The cell was made by thoroughly mixing powders of vanadium and one of its oxides which was synthesised and carefully characterized. The mixture was pressed into a pellet and sintered. This pellet and a pellet of the reference electrode, made in a similar fashion, were placed on opposite sides of a disc of the CSZ electrolyte to form the cell. The cell was spring loaded to ensure good contact with the electrolyte and had platinum leads to the two electrodes.

The cell was allowed to equilibrate at the desired temperature and

the EMF measured. The two electrodes were either isolated or were flushed by argon, in the latter case, under the assumption that this method would prevent the formation of mixed potentials. The free energies of formation of VO and V_2O_3 determined by Kontopoulos are of significance in this investigation and have been listed in Tables 2.3 and 2.4.

Jacob and Alcock[55] have used similar techniques to determine the free energy changes for the reactions:

$$2Fe_{(s,\ell)} + O_{2(g)} + 2Cr_2O_{3(s)} \rightleftarrows 2FeCr_2O_{4(s)} \qquad 2.67$$

and $$2Fe_{(s,\ell)} + O_{2(g)} + 2V_2O_{3(s)} \rightleftarrows 2FeV_2O_{4(s)} \qquad 2.25$$

in the temperature range 750°C to 1600°C. Their cells can be represented as:

$$\text{Pt, reference electrode} \mid \begin{matrix}\text{solid} \\ \text{electrolyte}\end{matrix} \mid \begin{matrix}\text{Fe + Preformed} \\ \text{deoxidation} \\ \text{products}\end{matrix}, \text{ Pt or Mo}$$

Fe, FeO and Mo, MoO_2 were used as reference electrodes and ZrO_2-CaO and ThO_2-Y_2O_3 pellets or both were used as solid electrolytes. The oxides of V and Cr were preformed, characterized by X-ray diffraction, mixed with iron powder, pressed and sintered. Above the melting point of iron, the oxides were merely placed on the melt and the cell was used in the form of a probe. The cells were allowed to equilibrate, tested for reversibility and the open circuit EMF measured and used to calculate the free energy changes for reactions 2.67 and 2.25. The results obtained have been summarized in Tables 2.2 and 2.7.

Pehlke et al.[83] used a cell similar to that used by Kontopolous[78] with ThO_2-8 mole % Y_2O_3 solid electrolytes and Co/CoO and Mn/MnO reference electrodes to determine the free energy of formation of Cr_2O_3 in the range 875°C to 1250°C. The experimental technique was similar to that of Kontopolous. Pugliese and Fitterer[42] and Tretjakow and Schmalzried[40] have also determined the free energy of formation of Cr_2O_3 by a similar technique but with a CaO-ZrO_2 electrolyte and an air reference electrode. The results of all these studies have been listed in Table 2.8.

Finally, Vahed[77] has used a cell of a type similar to that used by Fruehan with ZrO_2-CaO solid electrolytes and a ThO_2-Y_2O_3 cell of the type used in this work to determine the free energy change for the reaction:

$$Fe_{(\ell)} + \underline{O}_{1w/o} + V_2O_{3(s)} \rightleftarrows FeV_2O_{4(s)} \qquad 2.110$$

in the temperature range 1550°C to 1650°C. The melts were over-oxidized either with Fe_2O_3 or a gas mixture of H_2/H_2O and subsequently reduced by passing H_2 gas. The EMF was measured at definite time intervals during the reduction period. An arrest in EMF with respect to time indicated fixed oxygen activity at which the above mentioned reaction occurred. From this activity of oxygen the free energy change for reaction 2.110 was calculated.

CHAPTER 3

EXPERIMENTAL TECHNIQUE

3.1 Introduction

As mentioned in Chapter (1) the galvanic cells used in these experiments to determine the deoxidation thermodynamics of iron by vanadium and chromium in the temperature range 1550^{o}-1605^{o}C can be represented as:

$$Mo_{(s)}, \begin{matrix} Cr_{(s)}\text{-}Cr_2O_{3(s)} \\ \text{or} \\ Mo_{(s)}\text{-}MoO_{2(s)} \end{matrix} \Big| \begin{matrix} \text{calcia stabilized} \\ \text{zirconia} \\ \text{(solid electrolyte)} \end{matrix} \Big| \begin{matrix} Fe\text{-}Cr\text{-}O_{(\ell)}, \\ \text{or} \\ Fe\text{-}V\text{-}O_{(\ell)} \end{matrix} \begin{matrix} Mo\text{-}ZrO_2 \\ \text{Cermet} \\ (s) \end{matrix} \qquad (3.1)$$

This chapter describes the construction of the cell, and other apparatus used in the experiments. Various considerations that led to the design of the cell as well as the procedure followed in a typical run are also outlined. However, the features and shortcomings of the overall design are discussed in Chapter 5.

3.2 Design of the Cell

A schematic cross section of the cell, including the leads to the two electrodes, is shown in Fig. 3.1. It is an oxygen concentration galvanic cell employing a solid oxide electrolyte for oxygen. The details of the construction of the cell are outlined in this section.

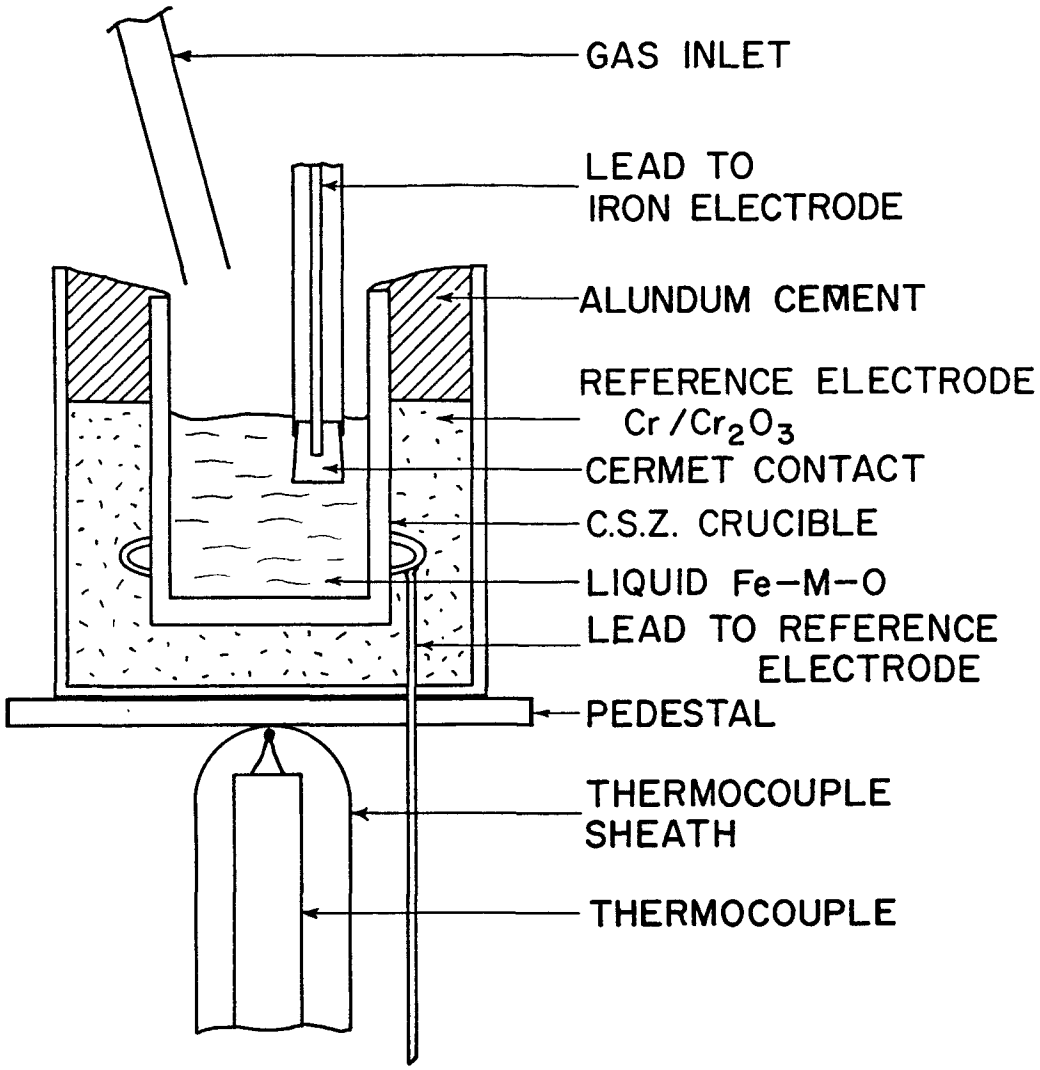

Fig. 3.1 Schematic cross-section of the cell

3.2.1 The Container

The cell was held in a recrystallized alumina crucible (Morganite, Triangle RR, XN50) with an inner diameter of 1,5/16". The crucibles were cut to a length of 1¼" from their original size and a 0.050" diameter hole was drilled near the outer edge of the bottom for the lead from the reference electrode. The containers were visually inspected for cracks before using them to make a cell.

3.2.2 The Reference Electrode

The criteria for the choice of the reference electrode are:

1. It should provide a well known, stable and reversible activity of the element whose ions carry the charge (oxygen in these experiments)

2. The equilibrium oxygen activity at the electrode should be in the range where the solid electrolyte is essentially an ionic conductor.

3. It should not react with the container or the solid electrolyte.

4. It should not polarize easily.

5. In order to improve the sensitivity of the measurements the EMF corresponding to the half cell reaction should be of a value comparable to that at the electrode under investigation.

6. It should be easy to make and handle.

These conditions are fulfilled by a solid state co-existence electrode. The electrodes used were powder mixtures of a metal and its oxide - Cr and Cr_2O_3 or Mo and MoO_2. These electrodes have an internal equilibrium between the metal and its oxide as well as an equilibrium with the electrolyte. In these electrodes the oxide used has to be stable at the temperature of the reaction. Both Cr/Cr_2O_3 and Mo/MoO_2 electrodes were used in this work, but

for reasons outlined in Chapter 5 the Cr/Cr_2O_3 reference electrode was used in most of the experiments.

The reference electrode was made by weighing out the appropriate amounts of the metal and oxide powders. These were mixed in a ball mill for 12 hours. A small quantity of this mixture was put at the bottom of the alumina container and rammed down. The solid electrolyte crucible was placed on this rammed mixture. More powder was then put all around the solid electrolyte crucible and rammed down again. The reference electrode was isolated by 3 layers of alumdum cement. The cement was dried slowly at about $80^{o}C$ and care was taken to check that there were no cracks in the cement. No cracks were formed in the cement during the experiment and it thus ensured complete isolation of the reference electrode compartment.

Mixing ratios of 90/10 and 80/20 by weight as well as 1/1 mole ratios of metal/metal oxide have been reported in the literature.[55,88] Both these mixtures were tried and no effect was notice on the EMF. In view of the fact that the electrode is solid and for equilibrium the metal and metal oxide particles should be in contact, the mixture used in this work had equal volumes of metal and metal oxide powders which is equivalent to a 70:30 ratio by weight.

3.2.3 The Solid Electrolyte

Calcia stabilized zirconia (CSZ) was used as the solid electrolyte for oxygen. The criteria for choosing the solid electrolyte are listed in Chapter 2.

CSZ crucibles (1" O.D. x 3/4" I.D. x 1" high) were supplied by Zircoa and from preliminary experiments it was found that the crucibles had

to meet the following conditions for satisfactory performance:

1. The bulk density should exceed 95% of the theoretical density
2. The crucibles should be impervious
3. The crucibles should have a single phase microstructure - i.e. the materials used in making the crucibles should be 'pure' - and careful sintering is necessary to prevent the formation of microcracks.

It was observed that whenever the crucibles failed to meet these conditions they performed unsatisfactorily. A silicate phase at the grain boundaries was found to be especially harmful for both ionic conductivity as well as high temperature mechanical strength.

All crucibles and the sintered cement were tested for porosity by Helium or Freon leak detection techniques under a vacuum of 1×10^{-6} torr. Only those crucibles that did not show leaks were used for the experiments.

The bulk density of the crucibles was measured by a mercury displacement method and crucibles having a bulk density in excess of 96% of the theoretical value only were used.

Random samples from the crucibles were polished at the top edge and examined under a microscope to ensure that there were no grain boundary precipitates. If any precipitate was observed, a piece from the crucible was examined under a scanning electron microscope. Figure 3.2 show micrographs of a crucible - with a grain boundary phase which was identified as complex silicates. The crucibles were also inspected for color - good crucibles were yellowish white and translucent - which could act as sources of of electronic conductivity.

The most suitable electrolyte for the study of deoxidation thermodynamics at $1600^{o}C$ is ThO_2- Y_2O_3. Commercially available crucibles could not meet the above conditions and failed under the extreme experimental conditions.

3.2.4 The 'Iron' Electrode

The electrodes under study were molten alloys in the Fe-V-O and Fe-Cr-O systems which were contained in the CSZ crucible.

The alloys were made in the course of the experiment. The oxygen potential of these electrodes was altered by passing an oxidizing or reducing mixture of argon and oxygen over the melt. A Mo-ZrO_2 cermet made contact with the iron electrodes.

3.2.5 The Electrical Leads

The lead to the reference electrode was a molybdenum wire, 0.050" diameter supplied by General Electric. A ring was made at one end of the wire which encircles the CSZ crucible (Fig. 3.1). The wire was passed through the hole at the bottom of the alumina container and was led out of the furnace through one of the ports in the brass head at the bottom of the furnace tube, using an insulating stopper.

The lead to the molten metal was a 0.050"D molybdenum attached to the cermet. The cermet was mechanically fitted into a recrystallized alumina tube (McDanel, 1/8" I.D.), and a 1/4" layer of alundum cement was packed into the tube above the cermet. The other end of the tube was sealed with 'plyseal'. The cermet contact and lead is shown in Fig. 3.3. Details of the design, manufacture and the need for making these cermets are outlined in section 3.3.

3.3 Cermets

Molybdenum wire has been used as an electrical lead to molten iron in a number of works.[12,77] However, the dissolution of molybdenum alters

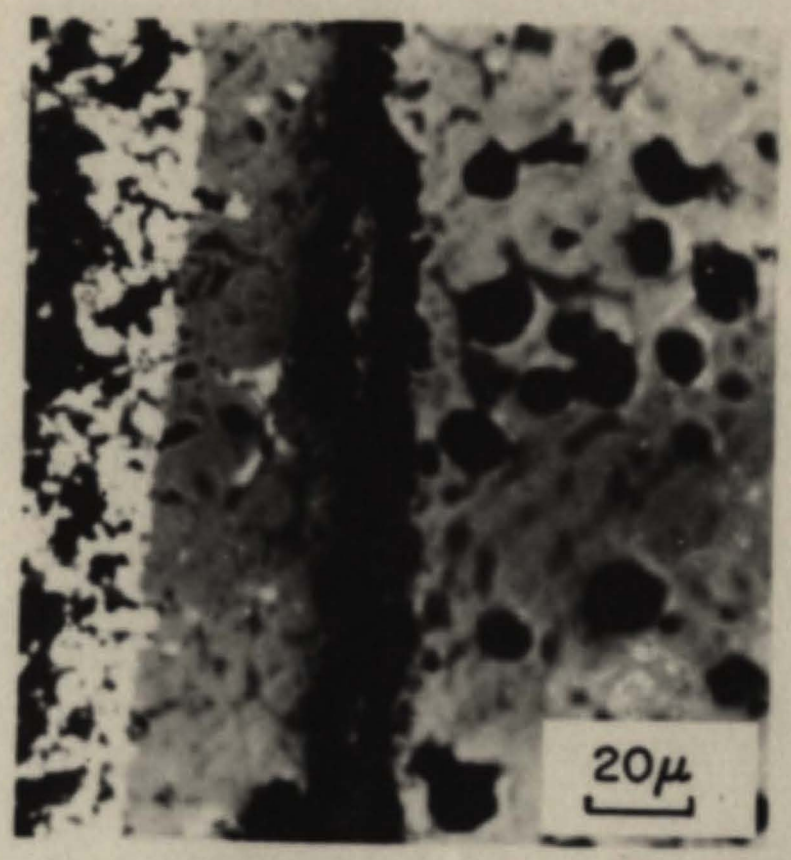

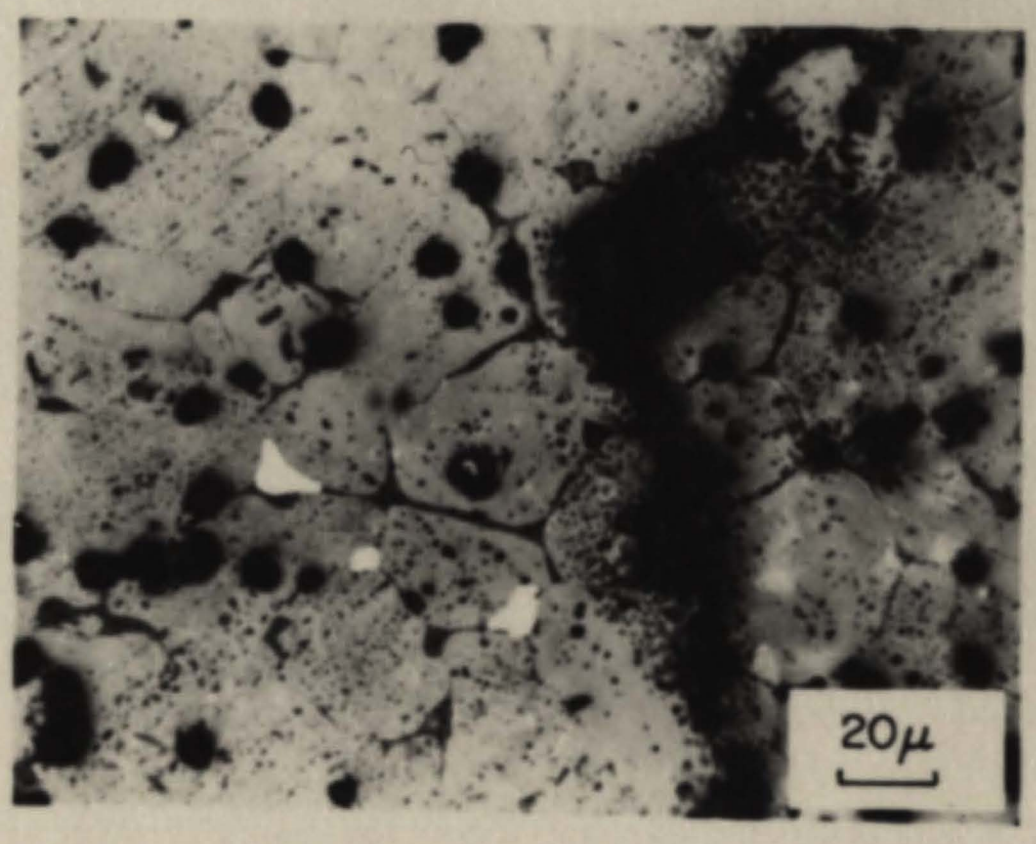

Fig. 3.2 Micrographs of an unsatisfactory C.S.Z. crucible (showing grain boundary films of complex silicates).

the composition of the melts and can result in the loss of electrical contact. Hence the wire should be used only for spot measurements in large melts.

Cermets (sintered ceramic-metal composites) have been used as contacts for molten metals including iron.[1,88,74] On sintering a pressed mixture of a metal and a ceramic, a ceramic network is formed with metal powder in the interstices. This network inhibits attack by the molten metal while still maintaining good electrical contact. However, electrical contact with the cermet has been made by mechanically winding platinum wire around it. This makes the lead difficult to handle and can also introduce errors at the contact between the air and the cermet. Further, when molybdenum is used as a lead to the reference electrode, the measured EMF has to be corrected for the appropriate thermal EMF. Hence, a technique to form and sinter a cermet at the end of a long (30 inches) molybdenum wire had to be developed.

The first batch of cermets produced were made from molybdenum and alumina powder. However, since zirconia is much more stable than alumina at steelmaking temperatures, most of the cermets used were made from molybdenum and zirconia. Molybdenum powder (99.9% pure, -200 mesh) and alumina powder (99.99% pure, 1 micron) were supplied by Alfa Inorganics. Zirconia powder (high purity, silica free) was supplied by Magnesium Elektron Inc.

Since the decrease in the extent of dissolution is due to reduced contact between the melt and the metallic part of the contact, the compositions were chosen to include the maximum amount of the ceramic as long as the following conditions were met:

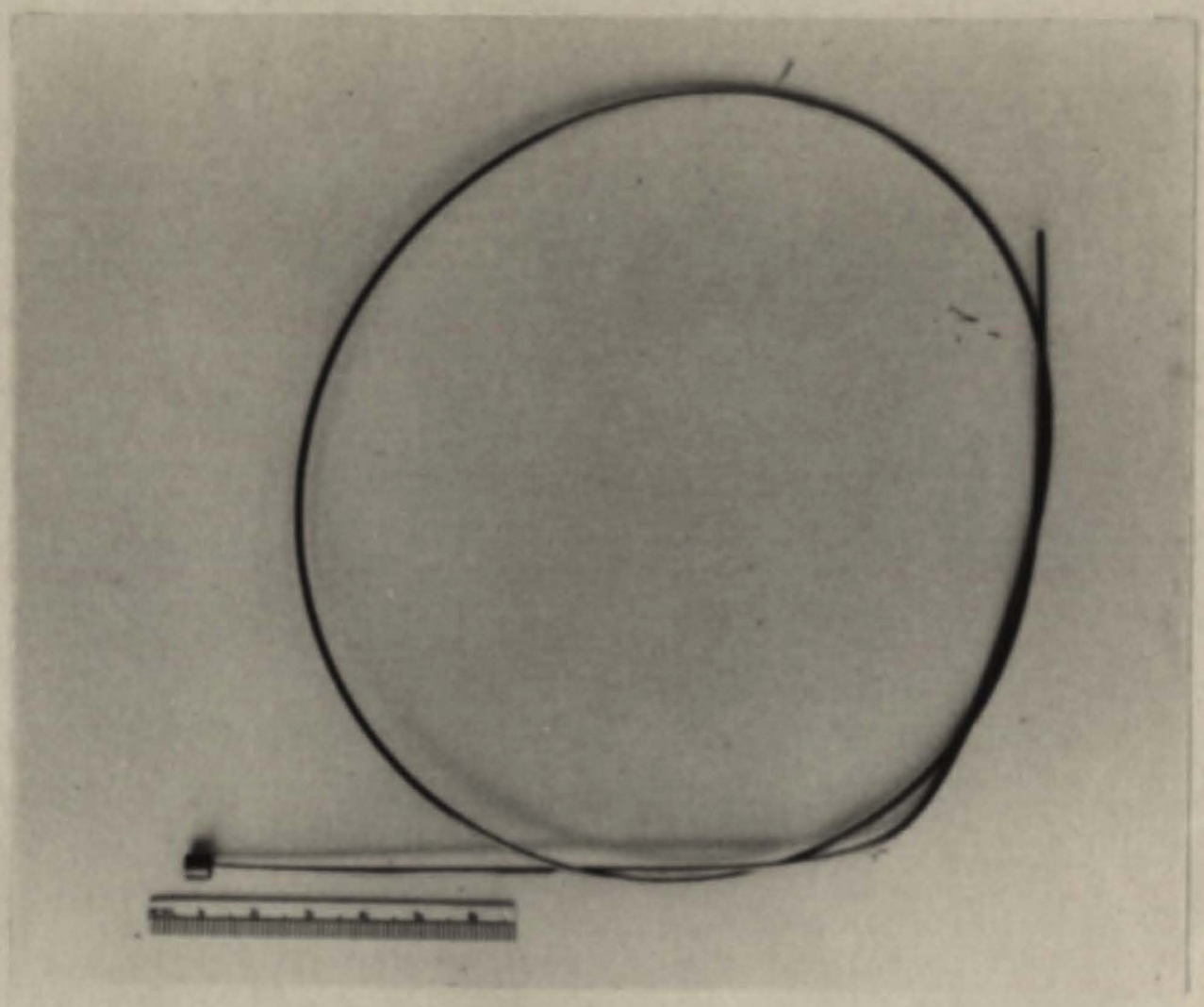

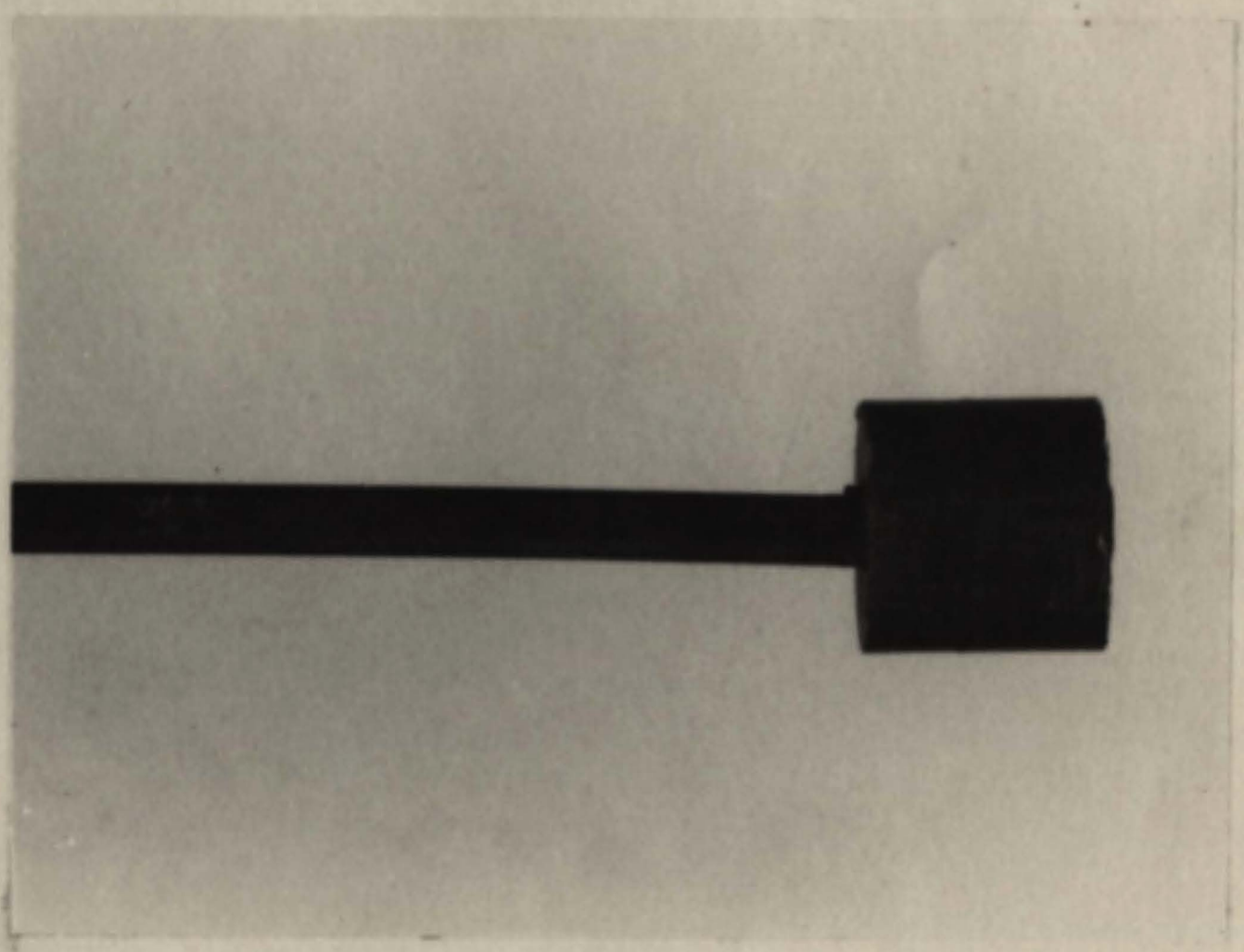

Fig. 3.3 The cermet lead as produced.

1. The cermet should be easily pressed and sintered.

2. The cermet should have excellent electrical conductivity.

It was observed that a powder mixture containing 40:60 volume ratio of metal to ceramic met these conditions. Appropriate amounts of the metal and ceramic powders were mixed in a ball mill for about 12 hours.

The powder mixture was pressed in a 1/4" D die, shown in Fig. 3.4. A 0.050" D hole passed through the bottom plungers and plates of the die. A long (30") molybdenum wire was passed through the die as shown in Fig. 3.4. About 2 g of the powder mix was placed in the die and pressed at a pressure of about 120 kpsi. When removed from the die, the molybdenum wire was an integral part of the cermet.

The cermets were sintered by induction heating in a quartz tube (1/2" D) and oxidation of the molybdenum wire was prevented by flowing hydrogen over the cermet. The maximum temperature during sintering was measured by a disappearing filament optical pyrometer and was estimated to be about 1900^{o}C. In case of the zirconia cermets, the heating and cooling rate had to be slowed down at about 1000^{o}C to allow for the phase change, cubic-monoclinic, in zirconia. In all cases dense crack-free cermets were produced with the wire firmly embedded in them. The cermets could be ground easily to fit in an alumina tube (1/8" I.D.).

The cermets produced were inspected for cracks and their conductivity measured. The cermets as produced and before and after use in the alumina sheath, are shown in Fig. 3.5. It can be seen that there is hardly any deterioration of the cermet even after one hour in the melt and this made it possible to monitor the cell EMF continuously. The electrical conductivity

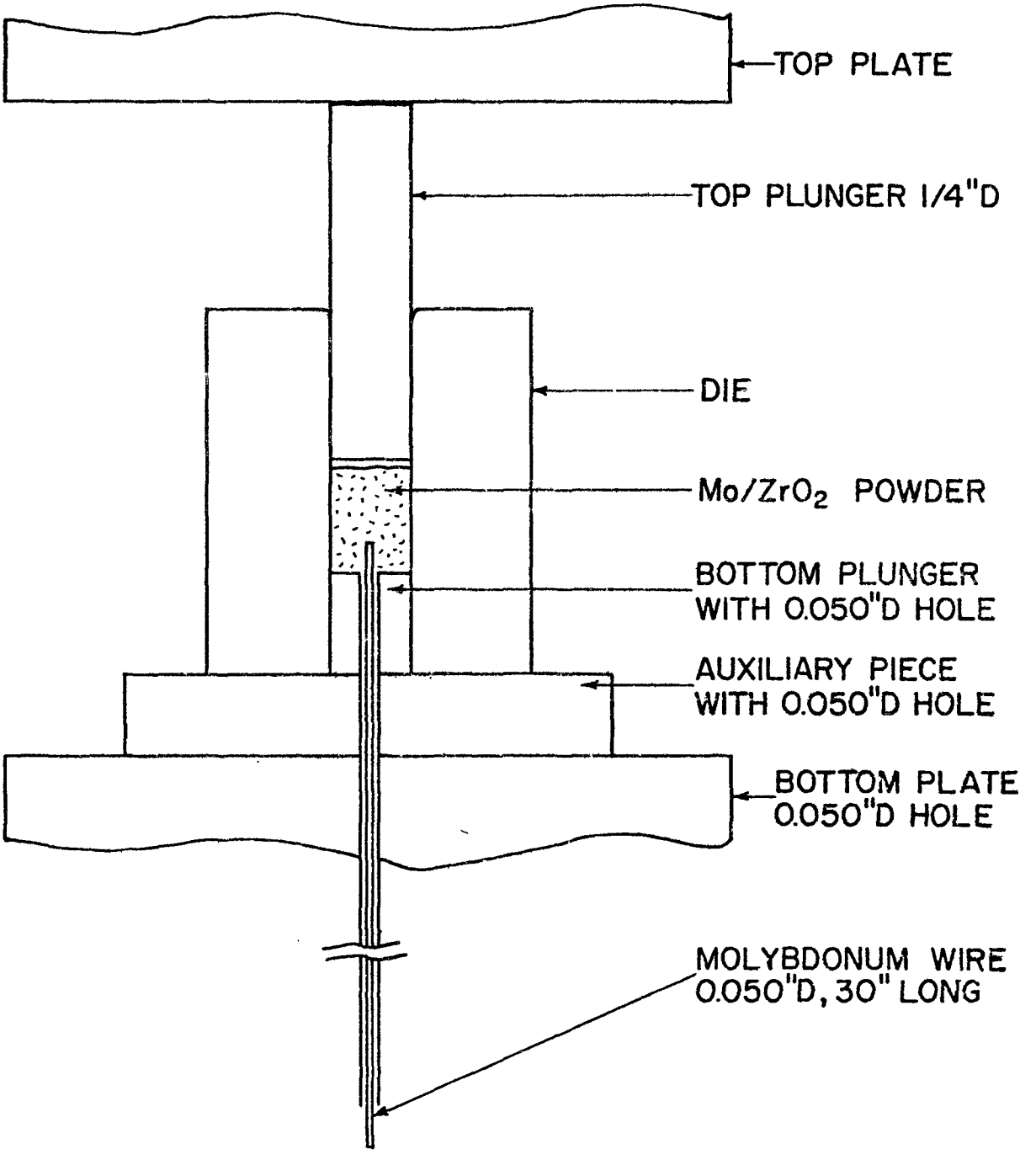

Fig. 3.4 Die for making cermets

of the cermets was measured after use and they continued to show excellent conductivity.

A number of steel samples were analyzed for molybdenum after the experiments, by atomic absorption. In all cases the analyzed molybdenum content was less than 0.005%.

3.4 The Furnace

The furnace (Fig. 3.6) used for the experiments was basically the same as that described in detail by Kontopolous.[12] In brief, it was a tubular, vertically mounted, resistance furnace with molybdenum as the heating element.

The working tube was recrystallized alumina (McDanel 997) of 1 5/8" I.D. The furnace was closed top and bottom with water cooled brass heads mounted on 'O' ring seals. The top head had ports for gas inlet, an electrical lead, a thermocouple and a quartz prism for viewing. The bottom head had ports for the cell support, an electrical lead and for gas outlet. All ports were closed by swagelok fittings with teflon ferrules and made gas tight.

The furnace drew power from a proportional power controller (Barber-Coleman, Series 621) driven by a null balance mullivoltmeter controller (Barber-Coleman, Model 377) which received the output of a Pt/Pt-10% Rh 'Control' thermocouple. The power controller limited temperature variation of the furnace to within $\pm 2^{o}C$.

The winding of the furnace was designed to give a zone about two inches long where the temperature was substantially uniform. This was checked by using a Pt/Pt-10% Rh thermocouple and temperature variation in

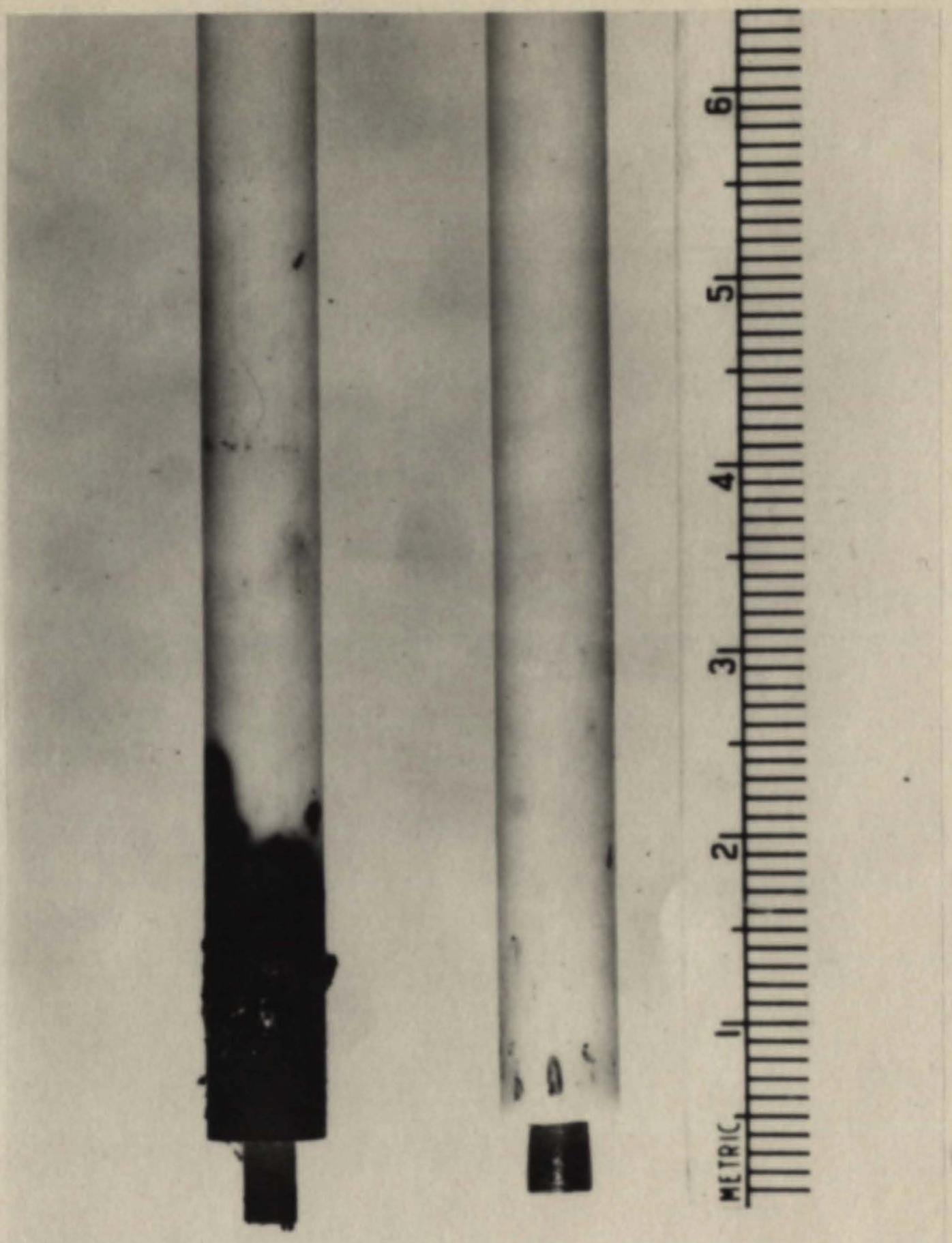

Fig. 3.5 Mo/ZrO_2 cermets in alumina sheaths before and after use.

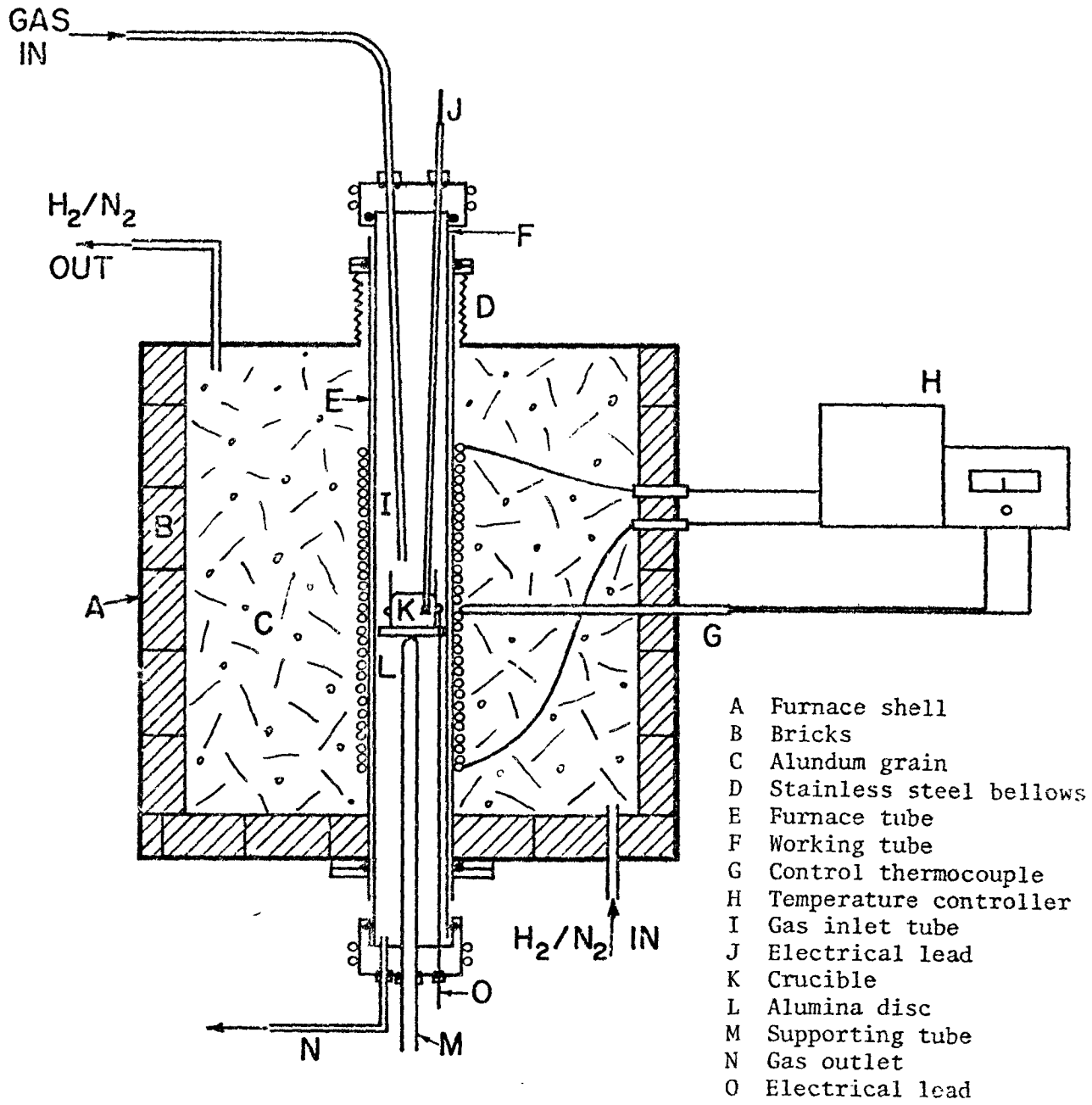

Fig. 3.6 Schematic cross-section of the furnace

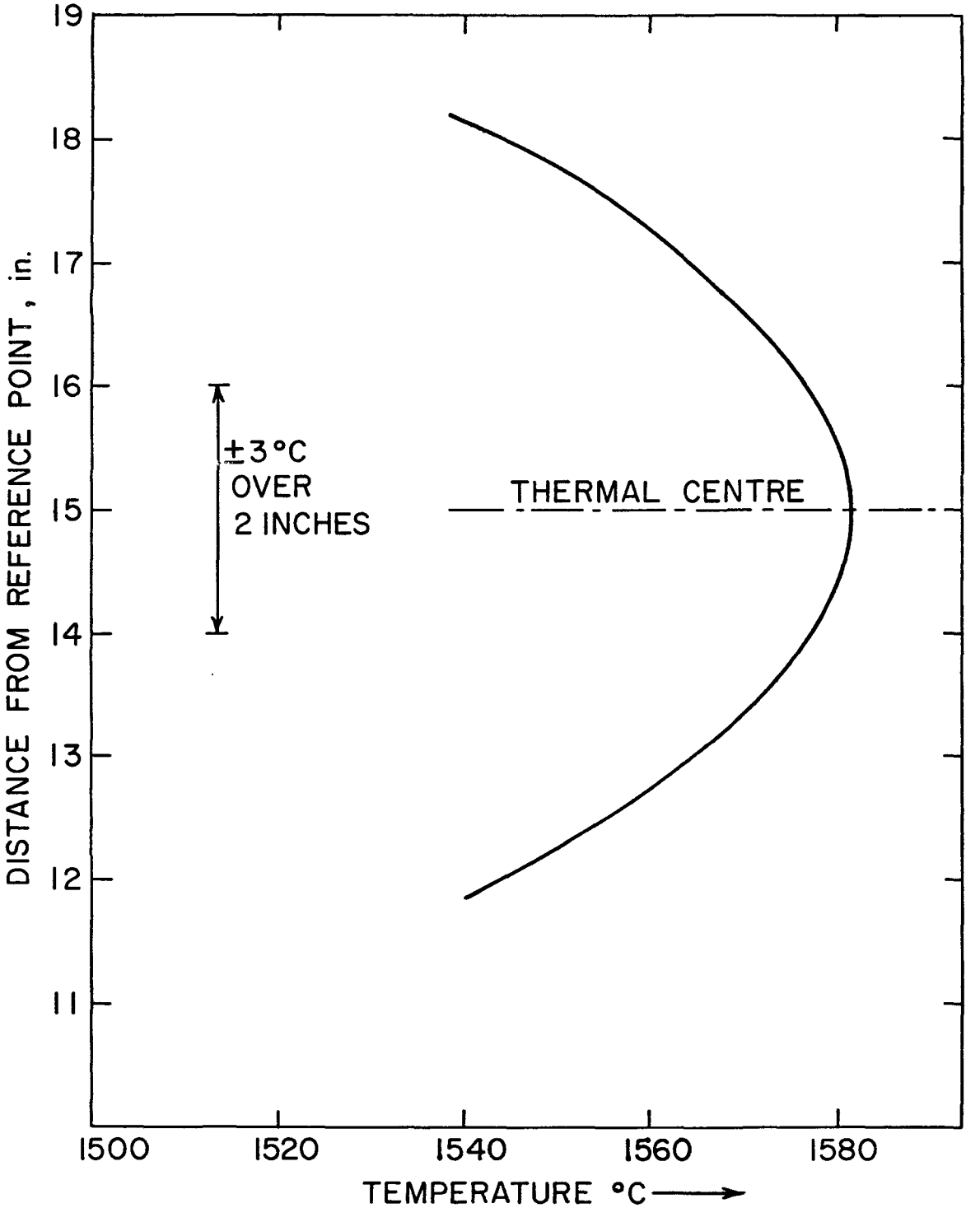

Fig. 3.7 Temperature profile of the furnace

the furnace is shown in Fig. 3.7 where the distance in inches is measured from the outer edge of the brass head at the bottom of the tube. The temperature in the hot zone varied by $\pm 3^{o}C$ over two inches and hence this zone was considered to be at uniform temperature. Further, this uniformity was repeatedly checked during the experiments as well as periodically after five or six runs.

The maximum temperature that could be attained with the 0.050"D molybdenum wire used in this furnace was about $1620^{o}C$. However, the cooling effect of the flowing gas in the furnace made it difficult to stabilize the temperature at this limit. Hence, experiments had to be restricted to about $1605^{o}C$.

3.5 The Gas Train

The gas train was designed to provide inert, oxidizing and reducing atmospheres in the working tube of the furnace. All gases were supplied by Matheson and prepurified argon was used to provide the inert atmosphere to dilute the oxidizing and reducing gases. It was passed over tubes containing ascarite to remove CO_2, magnesium perchlorate to remove H_2O and zirconium chips held at about $800^{o}C$ to remove O_2, and then passed through a flowmeter and a valve into the gas line to the furnace.

Commercial purity hydrogen was passed at room temperature over a palladium catalyst to remove free O_2, over soda lime to remove CO_2 and through a flowmeter and a valve to the main gas line.

Oxidizing atmospheres were produced by using a mixture of argon and 1% oxygen. The premixed gas and its analysis was supplied by Matheson.

All three gas lines were connected through valves to a main line

which in turn was connected to an alumina tube. This alumina tube was fitted with a swagelok and could be placed with the open end just above the cell assembly.

3.6 EMF Measurement

The EMF of the cell was measured on a potentiometer as well as an electrometer with a high input impedance. The true reversible value of the EMF is obtained only when measurements are made in 'open circuit' - i.e. without drawing any current from the cell.

A null balance potentiometer (Croydon, type P3) was connected in parallel to a high input impedance (2×10^{14} ohms) electrometer (Keithly, Model 616) through a single pole double throw switch. At null balance, the potentiometer fulfilled the 'open circuit' condition. When slightly off balance it drew a current through the cell. In fact, the stable reading was approached from both above and below and this provided a rough indication of the reversibility of the cell.

The current drawn by the electrometer was comparable to that drawn by the potentiometer when the latter was off balance. However, the electrometer provided a continuous, rapid and digital readout and hence it was used along with the potentiometer. The measurements of the two instruments were compared frequently during each experiment and agreed to within $\pm$ 1 mV.

The instruments were affected by induction effects from the furnace winding when placed close to the furnace. However, no such effect was observed when the instruments were moved further away from the furnace. This was verified in every experiment by shutting off the furnace momentarily while the measurement was made.

The leads from the cell were connected to the two instruments by insulated, multistrand copper wire, through 'alligator' clamps. The effect of improper contact as well as imbalance due to unmatched fields of the two leads was tested by changing the input impedance of the electrometer manually, in the first experiments. Since it was observed that there was no effect on the measurements, subsequent measurements were made with the maximum input impedance.

3.7 Temperature Measurement

In all experiments the temperature was measured using a platinum/platinum-10% rhodium thermocouple. This thermocouple was insulated using a double bore mullite sheath and placedin a thermocouple sheath which also supported the cell. Thus, the head of the thermocouple was about 1 1/4" below the top of the cell assembly. Care was taken to ensure that the head was well within the two inch long uniform temperature zone of the furnace. This was ensured by moving the crucible about 1/4" up and down with respect to its final position and checking the temperature before each experiment was started.

The temperature uniformity was also checked periodically by inserting a platinum/platinum-13% rhodium thermocouple from the top of the furnace. In all cases the temperature was found to be well within the accuracy of temperature measurement possible with these thermocouples.

All thermocouples were made from 0.020" diameter wires supplied by Johnson, Matthey and Mallory. The suppliers guarantee an accuracy of better than $\pm 3^{o}C$. Further, both the thermocouples were calibrated against a standard thermocouple supplied by the National Research Council of Canada.

Since the agreement was found to be within $\pm 1^{o}C$ and no systematic differences were observed, the measured temperatures were taken as the true temperatures within the limits of accuracy mentioned above.

After every three experiments, the thermocouple bead and about half an inch of the wires were cut off and new bead made. This was done to avoid any errors due to rhodium evaporation and impurity pick up that could have occurred during the experiments.

The EMF of the thermocouple was measured on the potentiometer as well as the electrometer referred to earlier. In order to ensure that there was no induction effects, the measured EMF was checked by switching off the furnace momentarily. It was found that there was no effect on the measurement due to induction and hence the temperature was measured with the furnace 'on'. The temperature was also monitored on a Honeywell chart recorder. The thermocouple was connected to these instruments using compensating leads and hence a cold junction correction had to be included in the measurements. All values of temperature include the appropriate correction.

3.8 Materials

Alloys were made in the course of the experiment itself. Ferrovac 'E' was used as the iron base and was supplied by Crucible Steel Corp. The analysis is given in Table 3.1. The iron was supplied as rods 1" dia. x 6" long and small pieces were cut off to make the alloys.

Vanadium in the form of flakes, chromium crystallites for alloys, chromium and molybdenum powders for the reference electrodes were supplied by Alfa Inorganics. Their analysis and size are listed in Table 3.1.

Table 3.1

Analysis of Ferrovac E

C - 0.008	Mo - 0.001
Mn - 0.001	Co - 0.004
P - 0.002	Cu - 0.001
S - 0.005	Sn - 0.002
Si - 0.005	Pb - 0.005
Ni - 0.025	Al < 0.01
Cr - 0.001	N_2 - 0.00015
V - 0.004	O_2 - 0.0012
W - 0.01	H_2 - 0.00006

Fe = 99.92

All compositions expressed in weight percent.

Vanadium Analysis in ppm

Fe - 1000	C - 900
Si - 800	Cr - 600
Al - 200	Others - 100

	Metallic Impurity	Total Impurity	Size
Chromium crystallites	0.002%	0.005%	
Chromium powder	0.02%	0.1%	-140 mesh
Molybdenum powder	<0.1	0.3%	-200 mesh
MoO_2	-	<1%	-200 mesh

Cr_2O_3 for the reference electrode was Fisher 'Certified Reagent' grade and MoO_2 was again supplied by Alfa Inorganics.

3.9 Experimental Procedure

About 25 to 30 gms of Ferrovac 'E' and an appropriate amount of vanadium or chromium metal were weighed out accurately. The weighed metals were put in the calcia stabilized zirconia crucible of the cell and introduced at the bottom of the furnace. The cells were supported by a recrystallized alumina tube closed at one end, which housed the Pt/Pt-10% Rh thermocouple. The cermet in its sheath was introduced at the top of the furnace which was then flushed with purified argon gas.

The furnace was generally maintained at about 1200^{o}C between experiments and while the furnace was heated to the experimental temperature, the cell was raised and the cermet lowered into the hot zone. Care was taken to ensure that the average heating rate did not exceed 150^{o}C per hour, and that the cell was not subjected to excessively large thermal shocks.

When the crucible reached the 'hot zone' of the furnace and the experimental temperature was reached, the melt was allowed to homogenize for about 10 minutes. When chromium was used, the alloy was melted under a mixture of argon and hydrogen to prevent the formation of an oxide film which made a homogenization difficult. The cermet was introduced into the melt and the EMF of the cell was measured (time zero). The value of the EMF was checked on the potentiometer and the effect of induction was checked by switching the furnace 'off' momentarily while the EMF was measured.

The hydrogen flow was shut off and the argon-oxygen mixture was passed into the furnace. The EMF was measured about every two minutes on

the electrometer and every second measurement was checked on the potentiometer. Since the cermet lead could be left in the melt the EMF could be continuously measured on a recorder. However, this was generally not done in order to avoid polarization of the cell. After the first two or three measurements the gas flow rates were adjusted to give a controlled rate of oxidation.

The oxides formed a film on the surface of the melt which often slowed down the rate of oxidation and could also give an erroneous indication of an EMF arrest. The melt was therefore stirred by moving the cermet lead after every 3 or 4 minutes. In order to make sure that the position of the cermet in the melt did not have any effect on the readings, the EMF was measured with the cermet immersed at various depths in the melt. In all cases the EMF remained steady to within ±1 m.V. The temperature was monitored every four minutes, and was found to be steady within ±2^{o}C. Even when the furnace was shut 'off' to check the effect of induction, the temperature did not fall by more than 3^{o}C.

Whenever an EMF arrest occurred it was checked by:

1. Stirring
2. Reversibility tests
3. Altering the rate of gas flow
4. Induction effect tests

In order to be able to obtain a sample for identification of the deoxidation product, the cells were quenched from any desired stage of oxidation. This was done by shutting off the oxidizing gas, increasing the flow rate of purged argon, and lowering the crucible by about five inches (1000^{o}C).

The cell was removed from the furnace in two stages and stored in a dessicator.

3.9.1 Principles of the Technique

Starting with a highly reduced melt of iron and deoxidizer, the melt is oxidized at a slow rate by the flowing gas mixture. The EMF of the cell represents the oxygen activity of the melt. While oxygen dissolves in the melt or while one deoxidation product is being formed, the oxygen activity of the melt and hence the cell EMF increases continuously. However at a particular oxygen and deoxidizer concentration the stable deoxidation product changes, and two deoxidation products are in simultaneous equilibrium with the melt. The oxygen activity in the melt remains constant while one oxide transforms to the other as indicated by an arrest in the cell EMF. Hence, if the melt is continuously oxidized one such arrest or plateau is observed for every two deoxidation products and each plateau corresponds directly to the invariant point between the two oxides. The EMF of a cell during oxidation is shown schematically in Fig. 3.8. A similar output is obtained for the reduction of an oxidized melt, though the oxides are formed in the reverse sequence.

3.10 Characterization of Deoxidation Products

3.10.1 X-Ray Analysis

Samples for X-ray analysis were obtained by scraping the top layer of the ingot with a clean, sharp knife edge. Pieces of iron were removed with a magnet and the samples ground in an agate mortar.

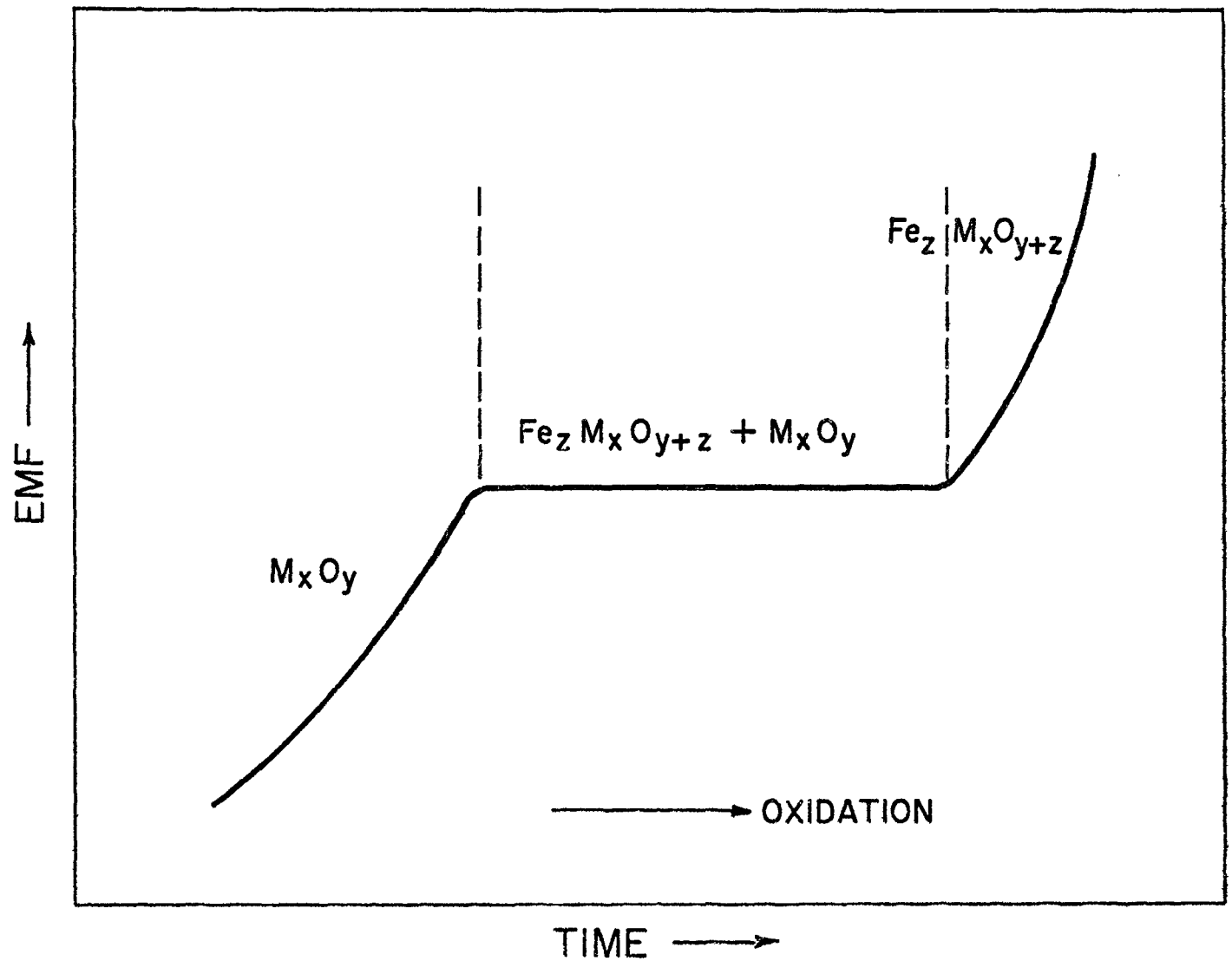

Fig. 3.8 Schematic diagram of a EMF vs time trace

The powder was rolled onto a glass fibre with glue and mounted on a Debye-Scherrer camera. The samples were X-rayed for about 10 hours using Cu radiation filtered through a Ni window.

3.10.2 Micrographic Examination

A thin slice, about 1/8" thick, was sectioned from the top of an ingot and treated by an iodine etching technique.[86] The process involves a low temperature selective reaction between iron and iodine to form a gaseous iodide which can be decomposed at a higher temperature to solid iron and gaseous iodine, which can be used again for further etching. Thus the iron is continually removed from the sample while the deoxidation products do not react with iodine. The etching reactions may be written as:

$$Fe_{(s)} + I_{2(g)} \rightleftarrows FeI_{2(g)} \qquad (3.2)$$

$$FeI_{2(g)} + 1/2\ I_{2(g)} \rightleftarrows FeI_{3(g)} \qquad (3.3)$$

and

$$FeI_{3(g)} \rightleftarrows Fe_{(s)} + 3/2\ I_{2(g)} \qquad (3.4)$$

The sample and an appropriate amount of iodine were sealed in an evacuated quartz tube (11" long) and heated in a three zone furnace having individual temperature controls for each zone. The experimental arrangement and the temperature profile in the furnace are shown schematically in Fig. 3.9. The sample was etched for about 24 hours and the deoxidation products examined by scanning electron microscopy.

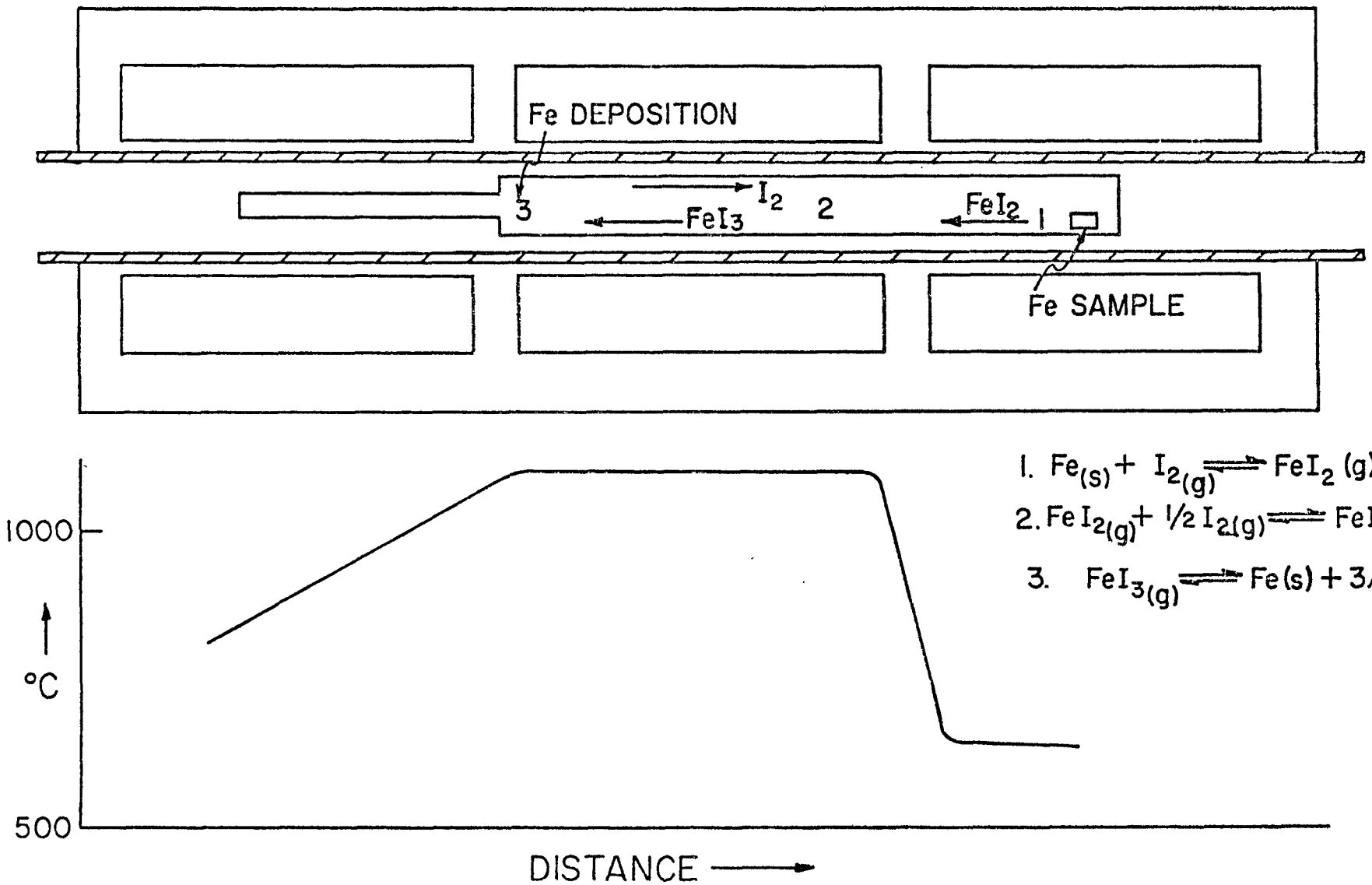

Fig. 3.9 Schematic cross-section and temperature profile of the "Iodine Etching Furnace"

CHAPTER 4

RESULTS

4.1 Relation Between Cell EMF and Oxygen Activity

The galvanic cell used in the investigation may be represented as

$$\underset{(s)}{Mo} \;|\; \underset{(s)}{Cr+Cr_2O_3} \;||\; C.S.Z. \;||\; \underset{(\ell)}{Fe\text{-}M\text{-}O} \;|\; \underset{Cermet\ (s)}{Mo\text{-}ZrO_2} \qquad (4.1)$$

where 'M' represents either V or Cr. Since current flows through the circuit only when the EMF is being measured, 10^{-14} amps, the cell EMF corresponds to a 'virtual' transfer of oxygen from the melt to the reference electrode. The virtual cell reaction can be written as:

$$\frac{2}{3}\,Cr_{(s)} + \underline{O}_{1w/o} \rightleftarrows \frac{1}{3}\,Cr_2O_{3(s)} \qquad (4.2)$$

for which

$$\Delta G_2 = \Delta G_2^o + RT\ell n\,\frac{1}{h_O} \qquad (4.3)$$

$$= -2FE \qquad (4.4)$$

The value of ΔG_2^o, can be obtained by combining the standard free energy changes of the reactions:

$$\frac{2}{3}\,Cr_{(s)} + \frac{1}{2}\,O_{2(g)} \rightleftarrows \frac{1}{3}\,Cr_2O_{3(s)} \qquad (4.5)$$

and $\frac{1}{2}O_{2(g)} \rightleftarrows \underline{O}_{1w/o}$ (4.6)

to obtain

$$\Delta G_2^o = \Delta G_5^o - \Delta G_6^o$$

Expressing the value of ΔG_5^o and ΔG_6^o in terms of the equilibrium constants for reactions 4.5 and 4.6, the value of ΔG_2^o can be obtained as a function of temperature and the activity of oxygen in equilibrium with $Cr\text{-}Cr_2O_3$ at the reaction temperature. Further, using the values of K_6 and ΔG_5^o reviewed in Chapter 2, a relation between log h_0, T and EMF can be obtained.

Employing the value of Jeannin et al.[41] for ΔG_5^o and the value reported in sec. 2.7 for ΔG_5^o, the final relation can be expressed as:

$$\log h_0 = 4.52 - \frac{13{,}500 - 10.08E}{T} \qquad (4.7)$$

where E, the cell EMF, is expressed in millivolts.[91]

A similar relation can be obtained for Mo/MoO_2 reference electrodes. Using the standard free energy of formation of MoO_2 as reported in JANAF tables,[89] the relation can be expressed as:

$$\log h_0 = 4.42 - \frac{8780 - 10.05E(mV)}{T} \qquad (4.8)$$

Equations 4.7 and 4.8 have been used for calculating the value of log h_0 at the EMF plateaus in this work.

4.2 EMF Data in the Fe-V-O System

Experiments were conducted with melts having initial vanadium contents ranging from 1.1 to 1.5% V in solution in iron.

The results obtained from the experiments have been shown as plots of EMF in millivolts vs time in Figs. 4.1 to 4.6. In general the solid electrolytes allowed about one hour of chemical reactions. It can be seen from Fig. 4.1 that the curves show a maximum of two arrests in the EMF vs time plot as the melt was oxidized. While both the arrests were determined in initial experiments, subsequent experiments were focussed on one or the other of the plateaus to characterize them properly.

In a number of experiments the melt was oxidized for about ten to fifteen minutes after the EMF had exceeded the value given by the upper plateau. In all cases, the EMF either increased continuously or the iron oxide formed attacked the crucible and resulted in unstable EMF readings.

In some of the experiments the melt was quenched from different stages of oxidation, as indicated by the EMF trace, to obtain samples of the deoxidation products stable at each oxidation stage.

On the basis of the identification of the deoxidation products (sec.4.3) the reactions at the two plateaus are represented as:

a) Lower plateau:

$$2VO_{(s)} + \underline{O}_{1w/o} \rightleftarrows V_2O_{3(s)} \qquad (4.9)$$

b) Upper plateau:

$$Fe_{(\ell)} + V_2O_{3(s)} + \underline{O}_{1w/o} \rightleftarrows FeV_2O_{4(s)} \qquad (4.10)$$

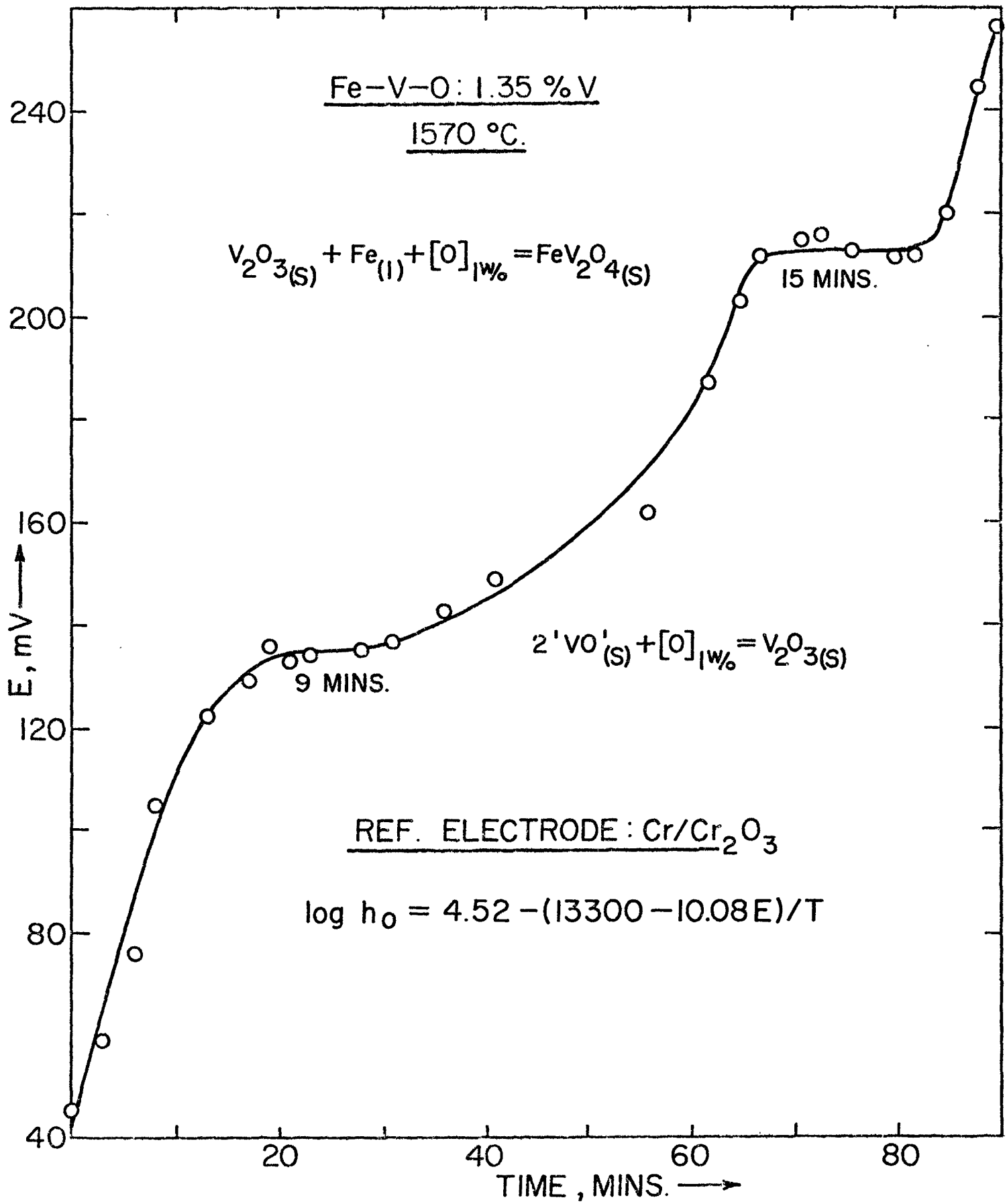

Fig. 4.1 EMF vs Time curve in the Fe-V-O System

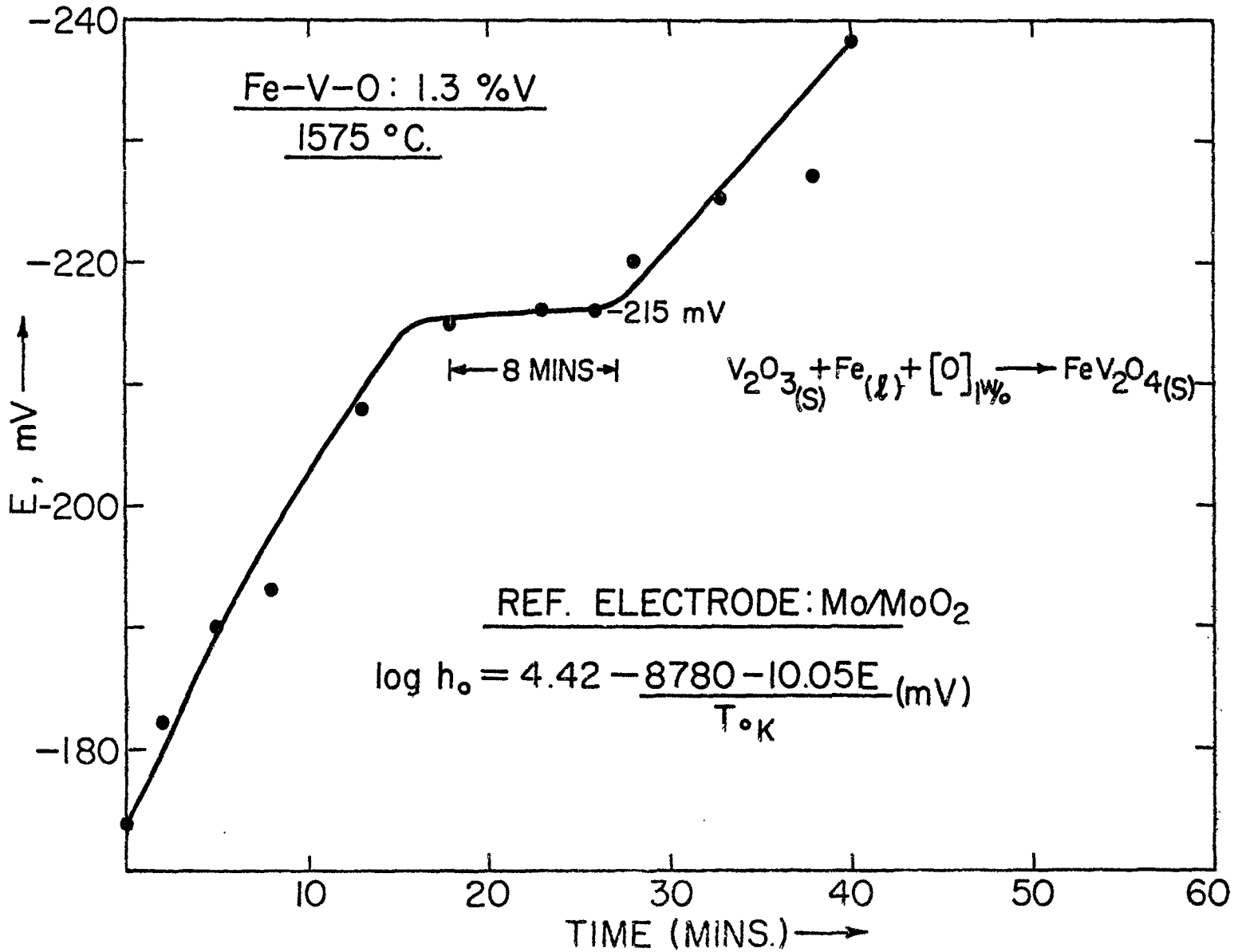

Fig. 4.2 EMF vs time curve in the Fe-V-O system

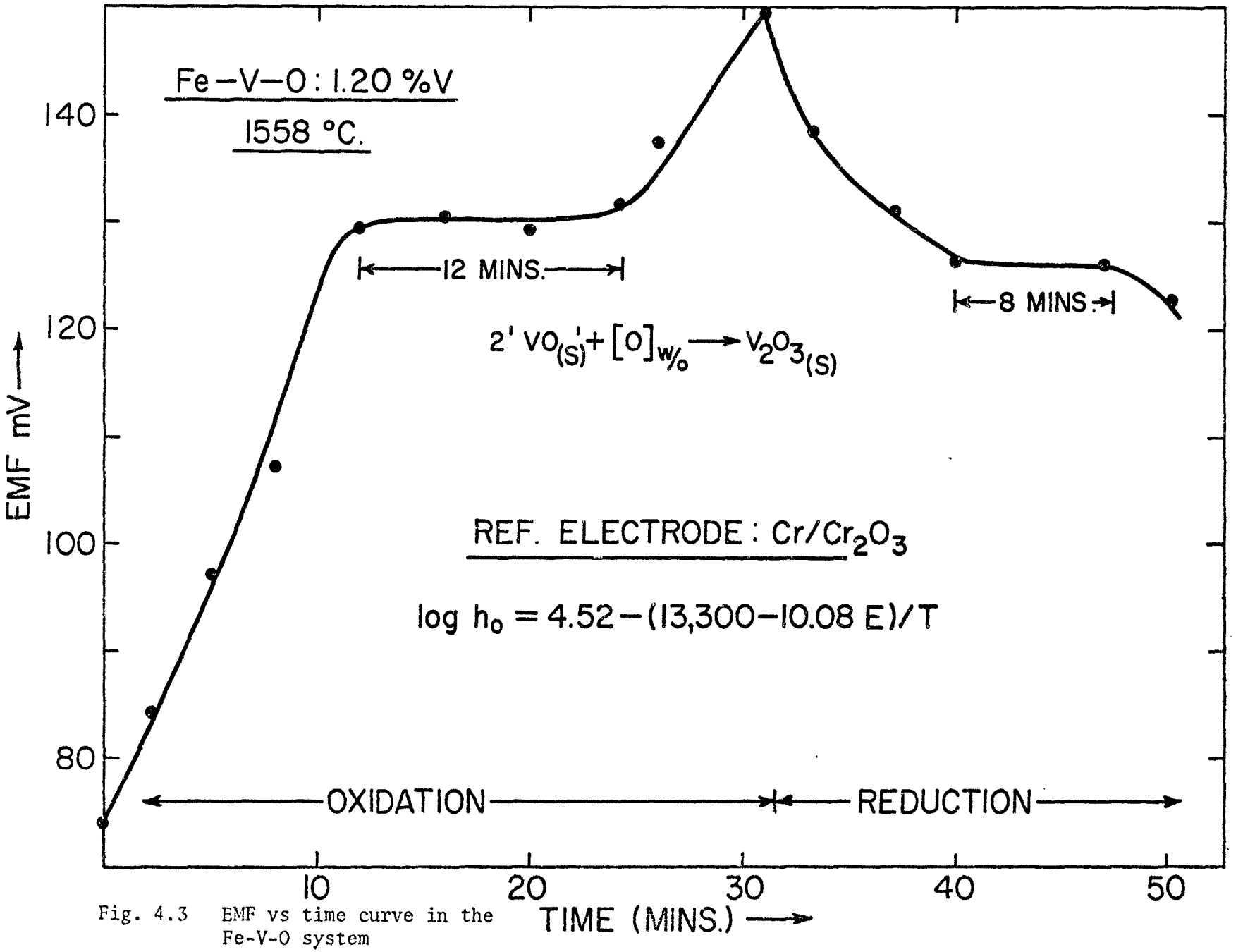

Fig. 4.3 EMF vs time curve in the Fe-V-O system

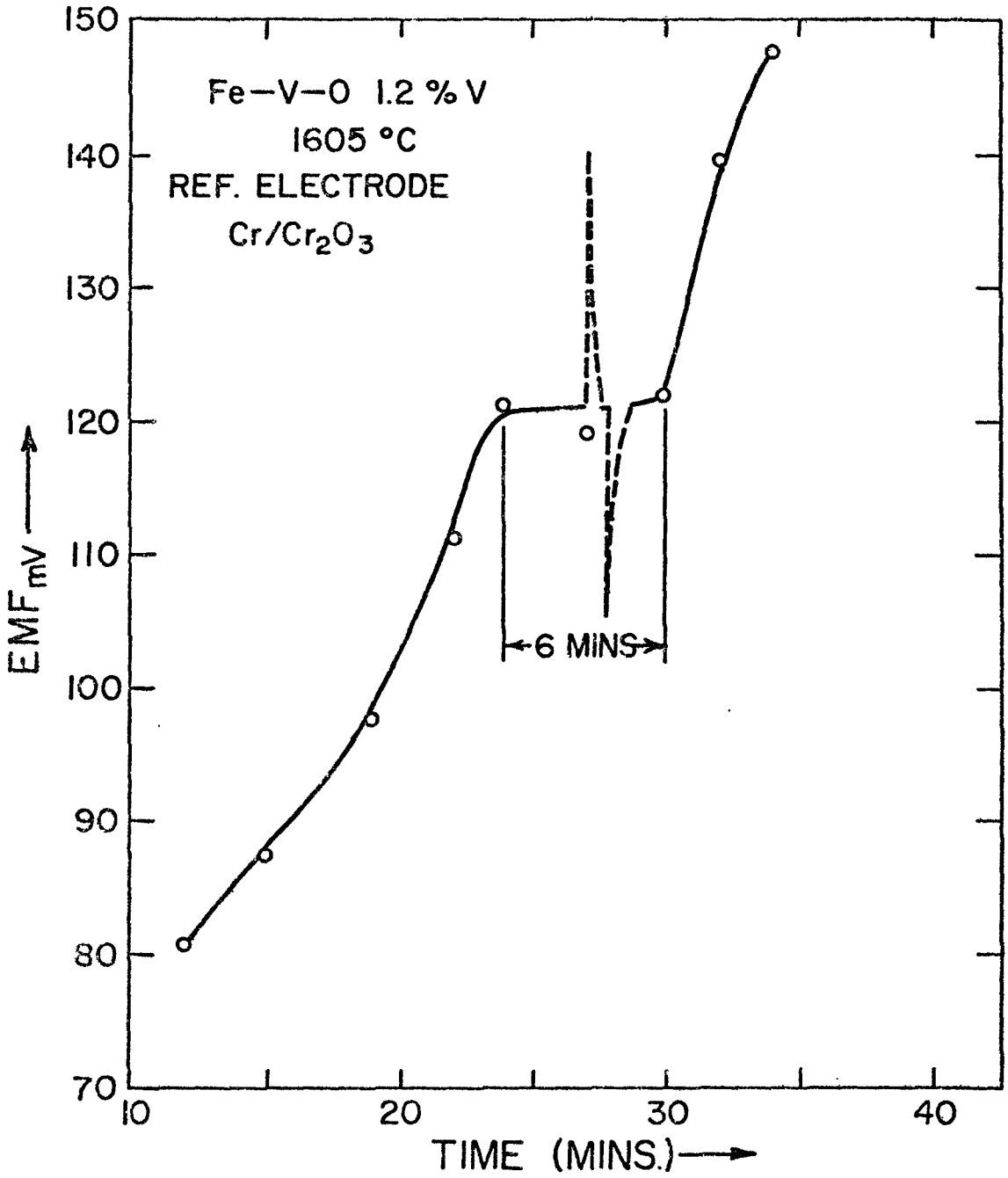

Fig. 4.4 EMF vs time curve in the Fe-V-O system

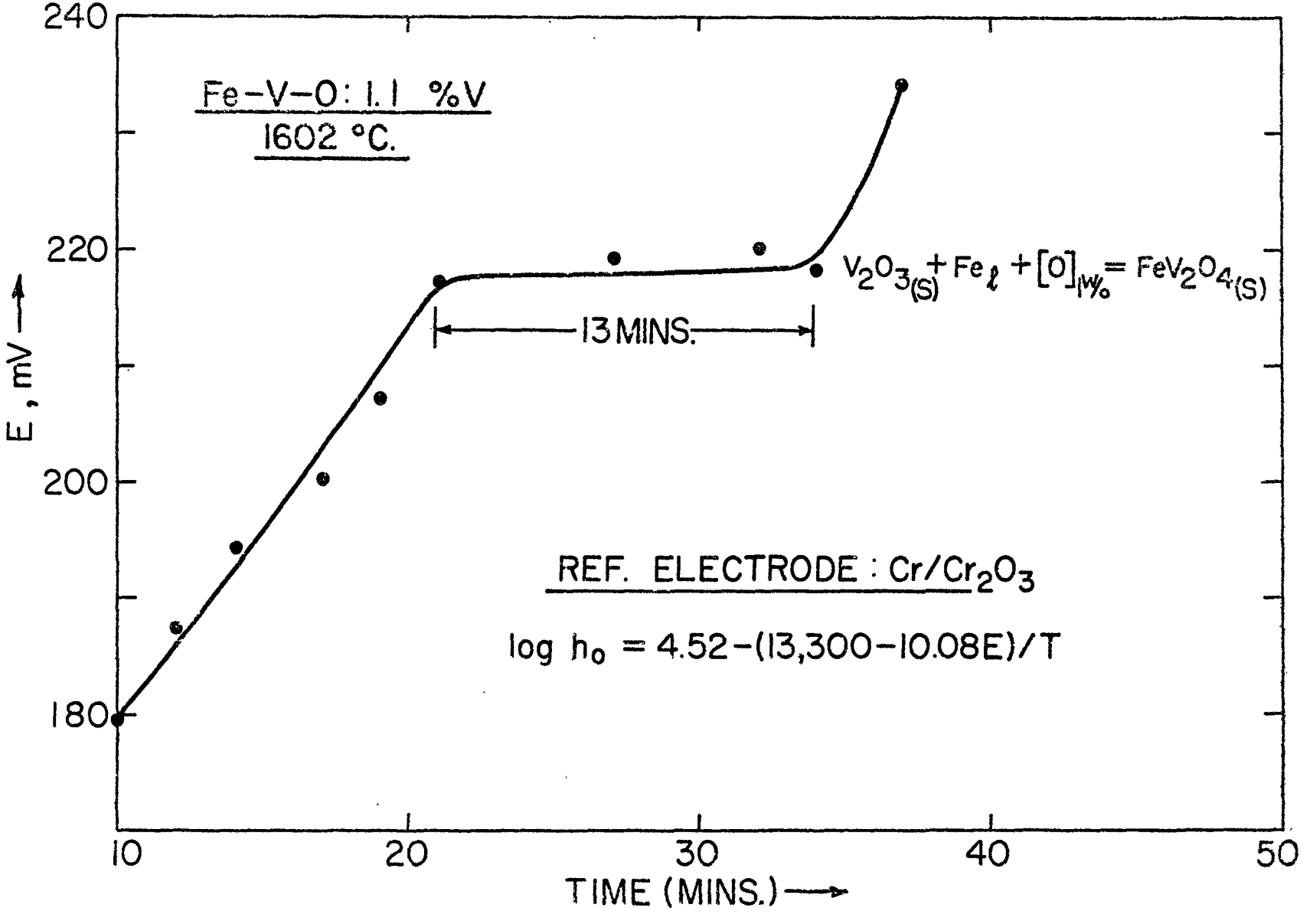

Fig. 4.5 EMF vs time curve in the Fe-V-O system

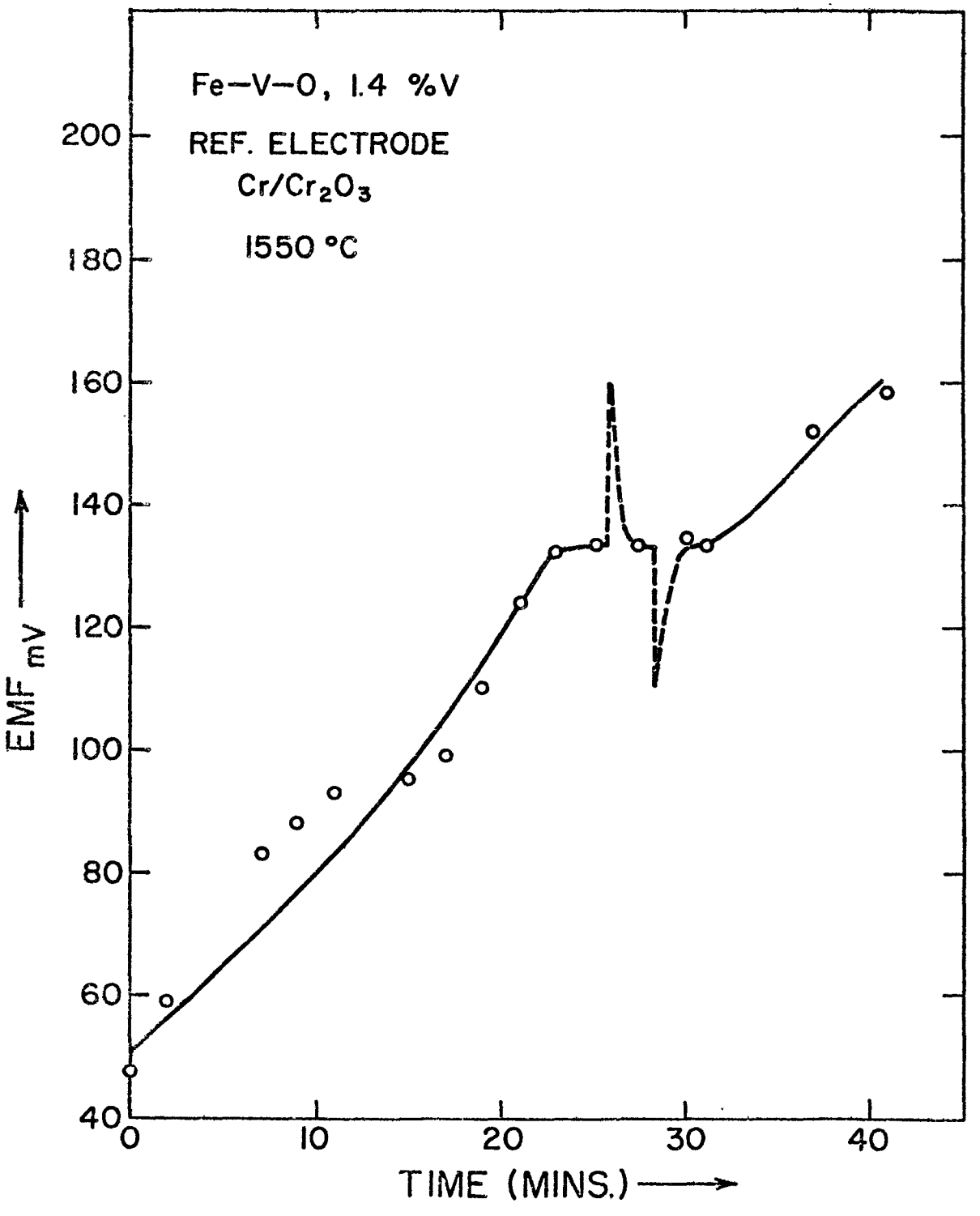

Fig. 4.6 EMF vs time curve in the Fe-V-O system

The stability of the plateaus was tested by

a) Imposing an external EMF of about 30 to 50 mV higher than the observed EMF

b) Discharging the cell through an external resistance for short times.

In each case the EMF returned to the original stable value within seconds.

Whenever possible the reversibility of the plateaus was tested by reducing the melt with H_2 gas after an EMF arrest was over and started to increase. As shown in Fig. 4.3 the plateau EMF during reduction was within ±3 mV of the plateau obtained during oxidation.

It was observed that after the EMF arrest at the upper plateau, the solid electrolyte deteriorated very rapidly, probably due to iron oxide attack.

The values of log h_0 corresponding to the plateaus were calculated using equations 4.7 and the standard free energy changes for reactions 4.9 and 4.10 were calculated using the relation:

$$\Delta G^{o} = +RT\ell n\ h_0 \tag{4.11}$$

Further, the values of ΔG^{o} for reactions 4.9 and 4.10 were combined with the standard free energy change for reaction 4.6 to obtain ΔG^{o} for the reactions:

$$2VO_{(s)} + \frac{1}{2}O_{2(g)} \rightleftarrows V_2O_{3(s)} \tag{4.12}$$

$$Fe_{(\ell)} + V_2O_{3(s)} + \frac{1}{2}O_{2(g)} \rightleftarrows FeV_2O_{4(s)} \tag{4.13}$$

These results have been summarized in Tables 4.1 and 4.2 and a plot of log h_0 vs 1/T is shown in Fig. 4.7.

Table 4.1

Thermodynamic Data from the Upper Plateau in the Fe-V-O System

Temperature ^{o}C	Temperature ^{o}K	EMF mV	$-\log h_O$	$-\Delta G^{o}_{4.10}$ cals/mole	$-\Delta G^{o}_{4.13}$ cals/mole
1575	1848	215*±3	1.50	12700	42000
1570	1843	215±3	1.52	12800	42100
1602	1875	218±3	1.40	12000	41300

*Reference Electorde - Mo/MoO_2

$$Fe_{(\ell)} + \underline{O}_{1w/o} + V_2O_{3(s)} \rightleftarrows FeV_2O_{4(s)} \qquad (4.10)$$

$$Fe_{(\ell)} + \frac{1}{2}O_{2(g)} + V_2O_{3(s)} \rightleftarrows FeV_2O_{4(s)} \qquad (4.13)$$

Table 4.2

Thermodynamic Data in the Fe-V-O System from the Lower Plateau

Temperature °C	Temperature °K	EMF mV	-log h_O	$-\Delta G^o_{4.9}$ cals/mole	$-\Delta G^o_{4.12}$ cals/mole
1555	1828	133±3	2.00	16926	46190
1558	1831	129±3	2.03	17000	46200
1570	1843	135±3	1.96	16560	45830
1570	1843	133±3	1.97	16610	45880
1605	1878	120±3	1.92	16480	45770

$$2VO_{(s)} + \underline{O}_{1w/o} \rightleftarrows V_2O_{3(s)} \qquad (4.9)$$

$$2VO_{(s)} + \frac{1}{2}O_{2(g)} \rightleftarrows V_2O_{3(s)} \qquad (4.12)$$

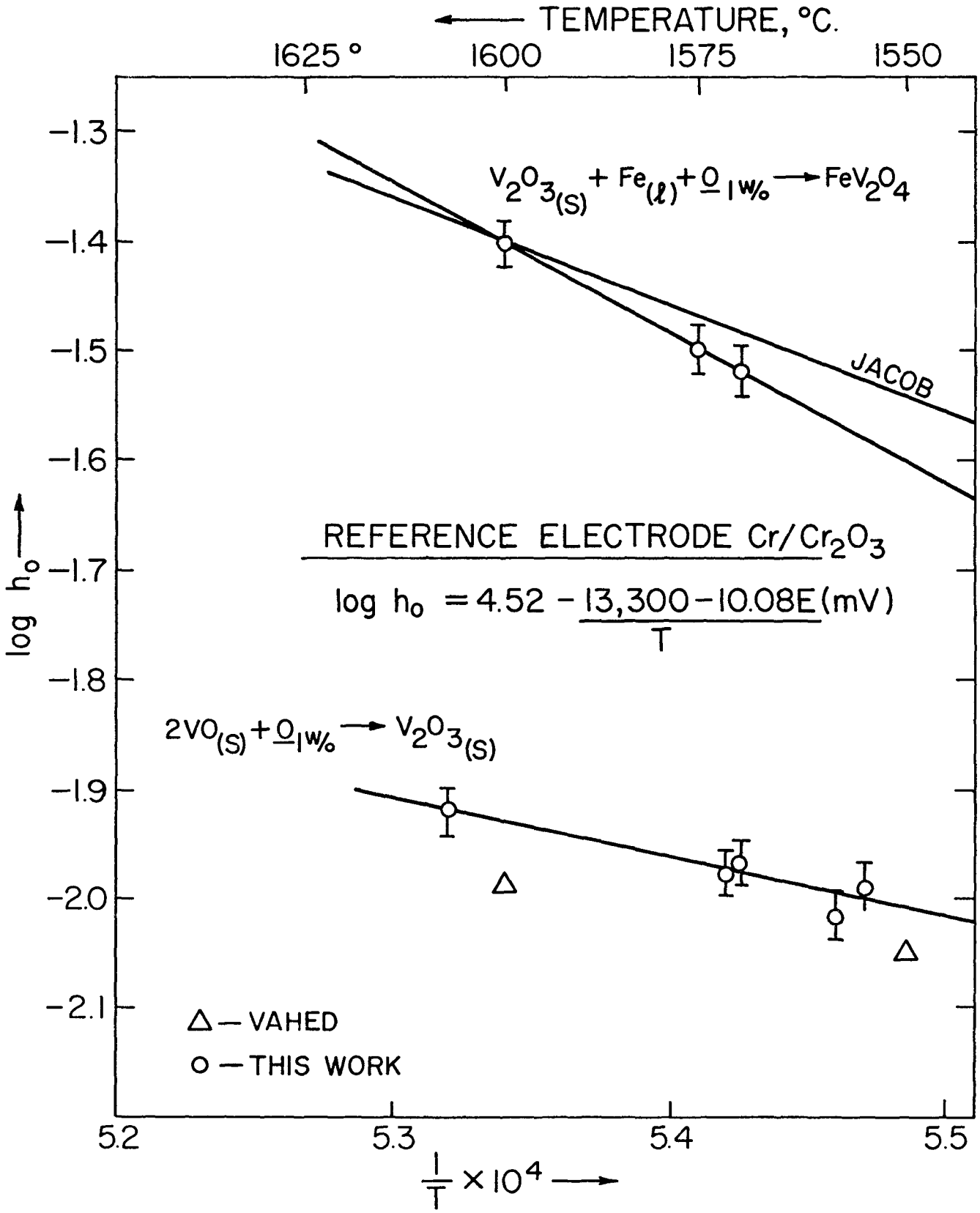

Fig. 4.7 Plot of log h_0 vs 1/T in the Fe-V-O system

4.3 X-Ray Analysis of Oxides in the Fe-V-O System

As pointed out earlier, the present technique offers the possibility of examining the deoxidation products at any desired stage of oxidation or reduction.

The melts were quenched from three different regions:

a) From above the upper plateau

b) Between the two plateaus

c) From the lower plateau

The films obtained from the Debye-Scherrer camera were compared with reported diffraction data from JCPDS standards.[90] In all cases at least two samples were analyzed and the products were identified as:

a) FeV_2O_4 above the upper plateau

b) V_2O_3 between the two plateaus

c) A mixture of V_2O_3 and VO at the lower plateau.

In all cases the oxides are bound to have some oxides of iron in solution. However, since neither iron or its oxides could be identified by X-ray analysis the scheme given above represents the deoxidation products formed in the Fe-V-O system.

The lines obtained and the positions of the lines from the standard data are shown in Tables 4.3 - 4.5 and appendix 1 respectively. The lines were characterized visually ranging from 'very, very strong' to very, very weak in seven steps and compared with the intensity ratios from the standard tables.

Table 4.3

X-Ray Diffraction Pattern of Deoxidation Products in the Fe-V-O System

Between the two plateaus

Radiation Cu, K_{α}, $\lambda = 1.5418A^{o}$

No.	Intensity	d, A^{o}	Matches the standard* line of
1	S	3.62	V_2O_3
2	VS	2.72	"
3	S	2.45	"
4	VW	2.21	"
5	W	1.80	"
6	VVS	1.70	"
7	M	1.45	"

*Source - Joint Committee on Powder Diffraction Standards[90]

S - Strong
M - Medium
W - Weak
V - Very

Table 4.4

X-Ray Diffraction Pattern of Deoxidation Products in the Fe-V-O System

Above the Upper Plateau

Radiation Cu, K_α, $\lambda = 1.5418A^o$

No.	Intensity	d, A^o	Matches the standard* line of
1	M	4.80	FeV_2O_4
2	S	2.92	"
3	VVS	2.52	"
4	VS	2.05	"
5	M	1.71	"
6	S	1.63	"
7	VS	1.46	"
8	VW	1.27	"

*Source - Joint Committee on Powder Diffraction Standards[90]

S - Strong

M - Medium

W - Weak

V - Very

Table 4.5

X-Ray Diffraction Pattern of Deoxidation Products in the Fe-V-O System

At the Lower Plateau

Radiation Cu, K_α, $\lambda = 1.5418A^o$

No.	Intensity	d, A^o	Matches the standard* line of
1	M	3.64	V_2O_3
2	S	2.71	"
3	M	2.48	"
4	W	2.40	VO
5	VW	2.18	V_2O_3
6	S	2.04	VO
7	VW	1.83	V_2O_3
8	VVS	1.70	"
9	M	1.47	V_2O_3
10	VS	1.43	VO
11	M	1.21	VO
12	M	1.17	VO
13	VW	1.05	VO
14	VW	0.94	VO
15	M	0.91	VO

*Source - Joint Committee on Powder Diffraction Standards[90]

S - Strong

M - Medium

W - Weak

V - Very

4.4 EMF Data in the Fe-Cr-O System

The chromium content of the melts studied ranged between 1.8 and 6% and the EMF vs time curves obtained are shown in Figs. 4.8 - 4.11. Higher chromium contents could not be used because of the tendency of chromium oxides to form a thick film on the surface of the melt which made further oxidation extremely difficult.

The Fe-Cr-O system also showed two stable, reproducible plateaus with EMF vs time curve. The EMF arrests were all subjected to reversibility tests after the initial run, which was carried out merely to get an idea of the EMF vs time curve. In the Fe-Cr-O system the reversibility tests were very critical since the system showed a number of other EMF arrests above the upper plateau none of which satisfied the reversibility tests. These spurious arrests were found to be caused by formation of the oxide layer on the surface, which restricted oxygen transfer to the melt and the EMF continued to rise when the melt was stirred.

The transformation reaction at the two plateaus can be represented as:

a) Upper plateau:

$$3Fe_{(\ell)} + 2Fe_2Cr_7O_{12(s)} + 4\underline{O}_{1w/o} \rightleftarrows 7FeCr_2O_{4(s)} \qquad (4.14)$$

b) Lower plateau:

$$6Fe_{(\ell)} + 7Cr_3O_{4(s)} + 8\underline{O}_{1w/o} \rightleftarrows 3Fe_2Cr_7O_{12(s)} \qquad (4.15)$$

While X-ray examination of the deoxidation products confirm the reaction at the upper plateau, a similar confirmation could not be obtained for the lower plateau. The validity of reactions 4.14 and 4.15 will be discussed in detail in Chapter 5.

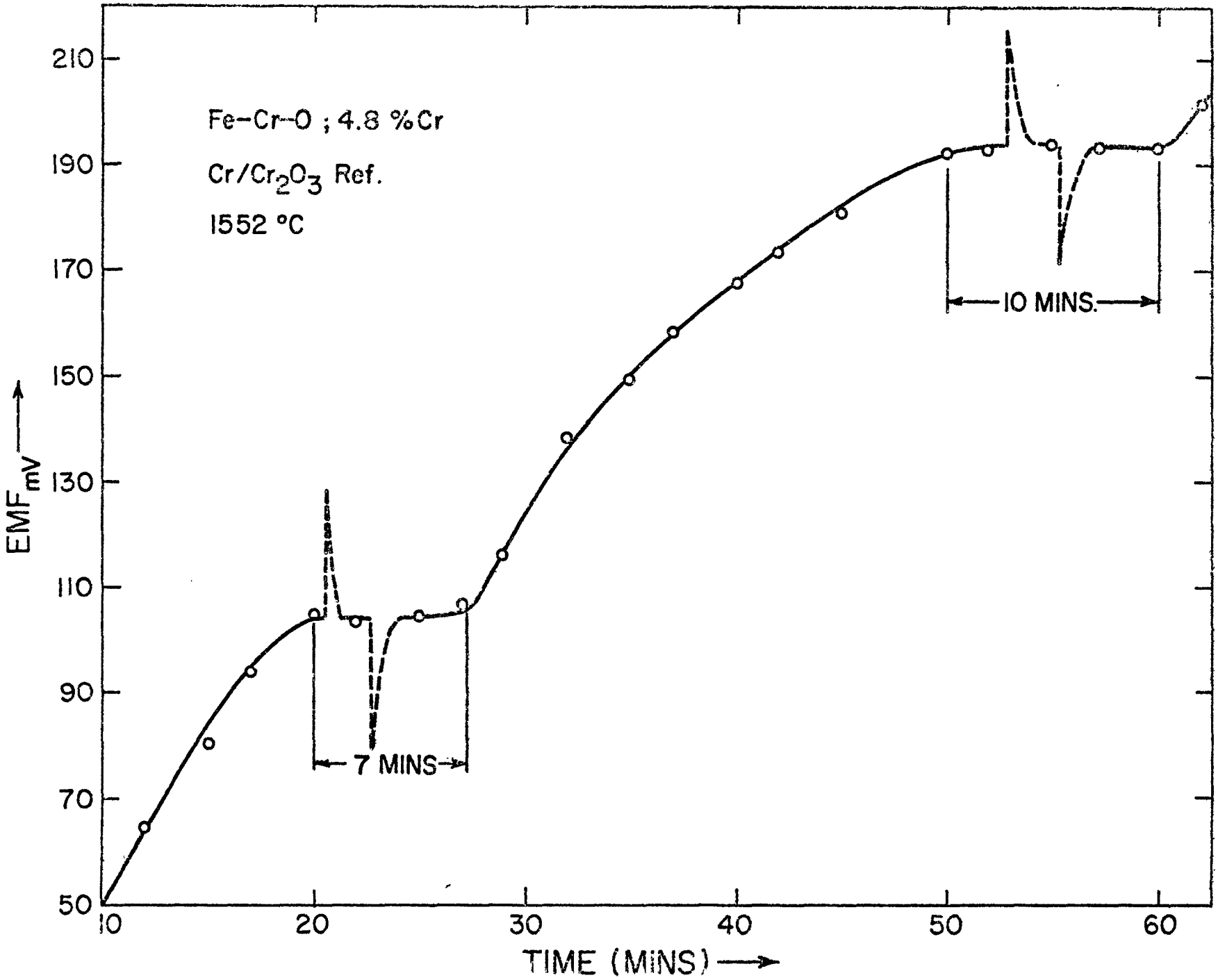

Fig. 4.8 EMF vs time curve in the Fe-Cr-O system

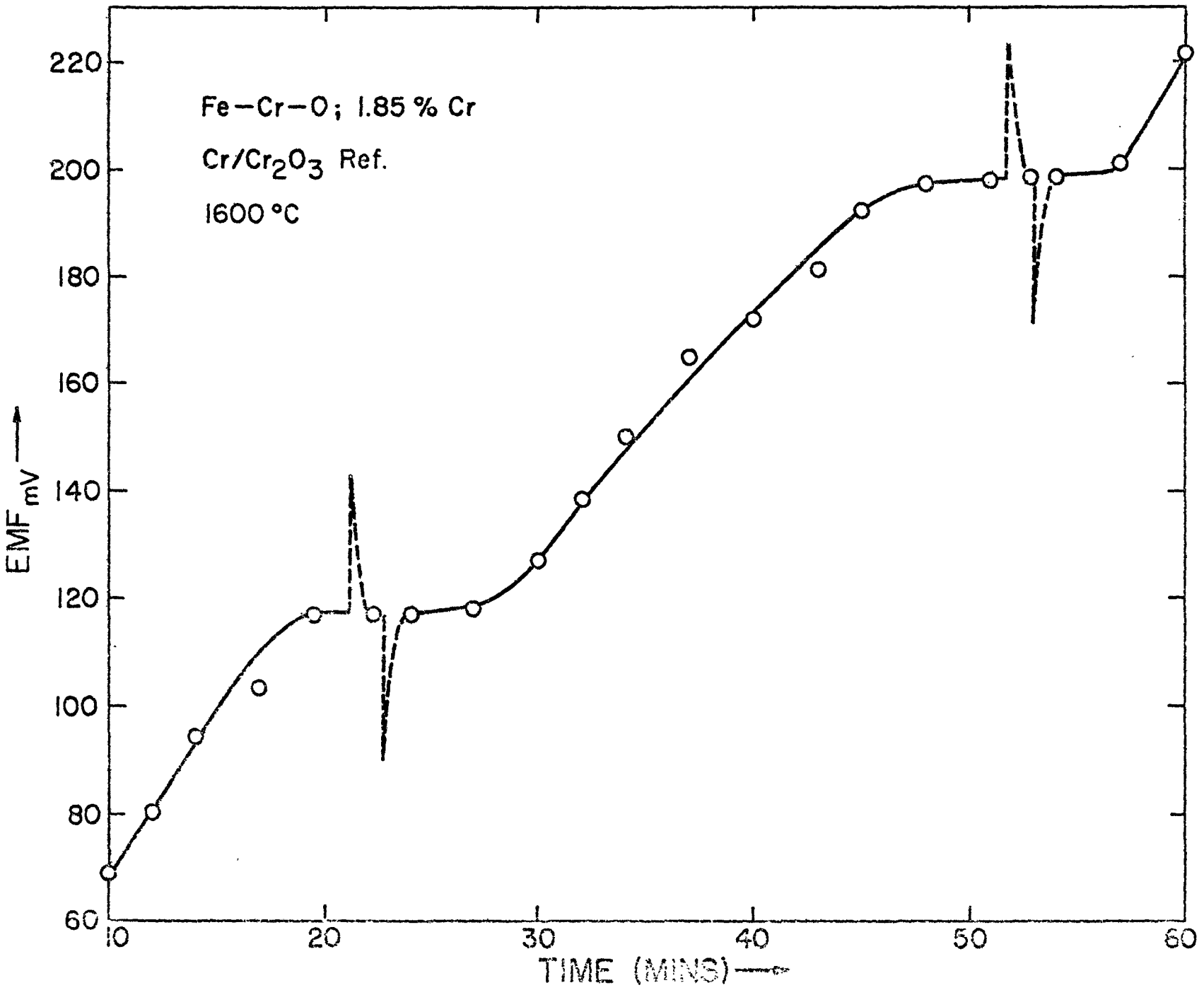

Fig. 4.9 EMF vs time curves in the Fe-Cr-O system

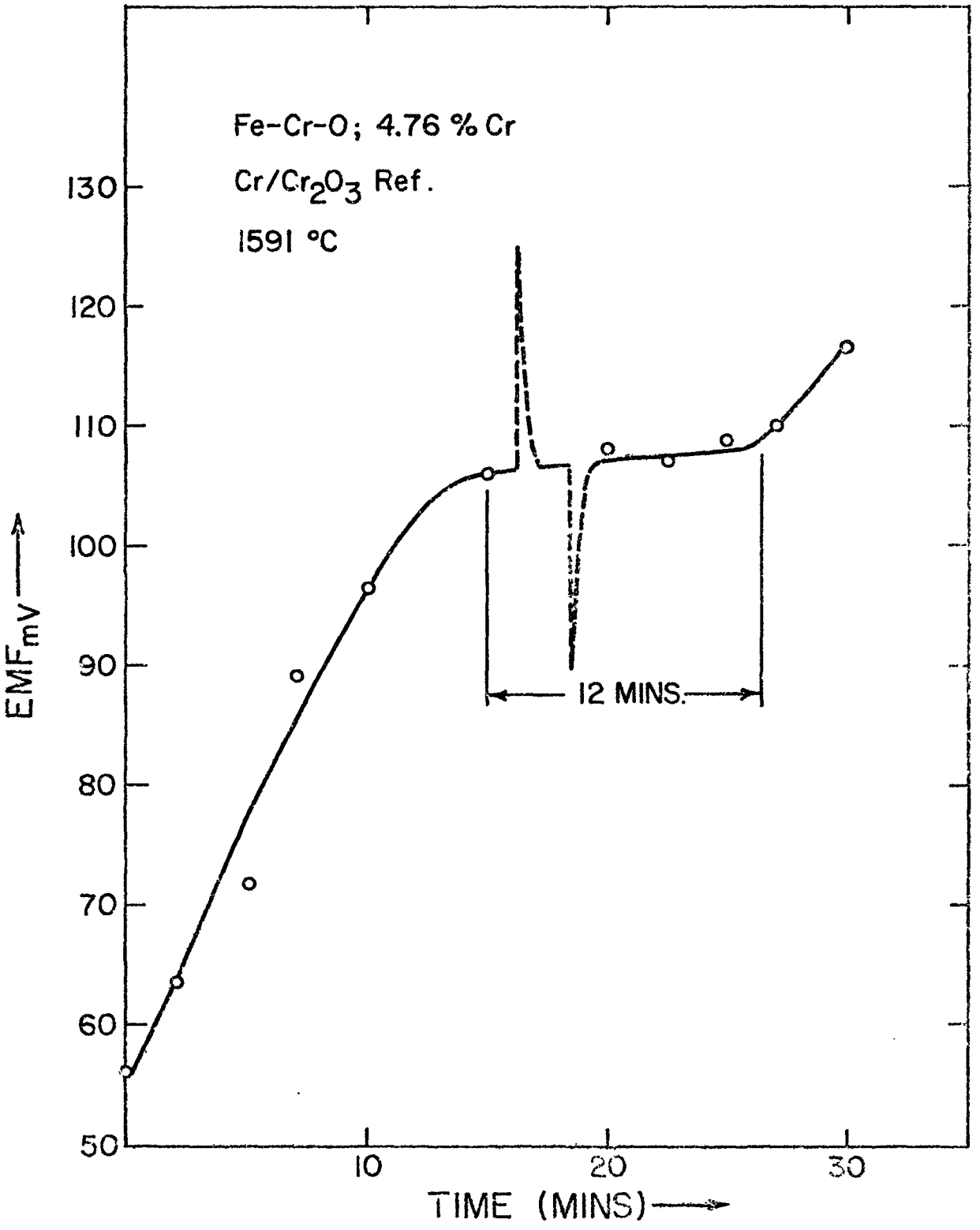

Fig. 4.10 EMF vs time curves in the Fe-Cr-O system

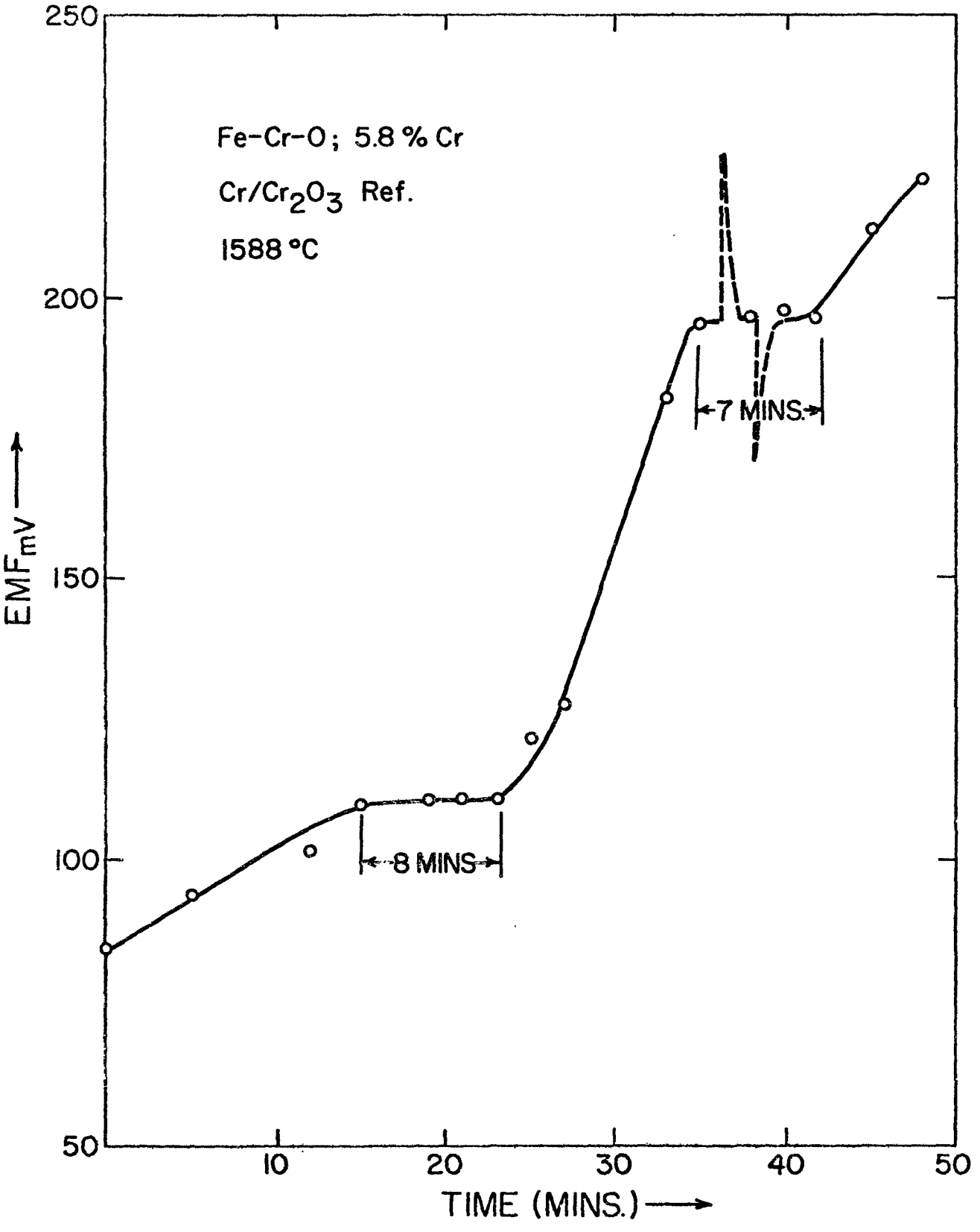

Fig. 4.11 EMF vs time curves in the Fe-Cr-O system

As before, the stability of the plateaus was tested by imposing an external EMF of about 20 to 30 mV in both the positive and negative sense relative to the value at the arrest. In both cases the EMF returned to the stable value of the plateau within a few seconds.

The experiments were terminated after the EMF started to increase after the upper plateau. However, generally the cell became unstable at these stages of oxidation due to reaction between the oxide product and the solid electrolyte. This was also confirmed after the cell was cooled down - the ingot tended to stick to the crucible if the melt was oxidized to a level above that given by the upper plateau.

The plateau EMF values have been used to calculate the activities of oxygen corresponding to the transformation of the deoxidation products, using equation 4.7.

The equilibrium constants for reactions 4.14 and 4.15 can be written as:

$$K_{14} = \frac{1}{h_O^4} \tag{4.16}$$

and $$K_{15} = \frac{1}{h_O^8} \tag{4.17}$$

Hence the standard free energy changes for reactions 4.14 and 4.15 per mole of the product can be expressed as:

$$\Delta G^o_{14} = \frac{4}{7} RT\ell n\ h_O \tag{4.18}$$

$$\Delta G^o_{15} = \frac{8}{3} RT\ell n\ h_O \tag{4.19}$$

The values of the plateau EMF's and the calculated values of ΔG^{o}_{14} and ΔG^{o}_{15} are summarized in Tables 4.6 and 4.7. The value of log h_0 is plotted against 1/T in Figure 4.12.

4.5 X-Ray Analysis of the Deoxidation Products in the Fe-Cr-O System

As in the Fe-V-O system, the melts were quenched from three stages of oxidation, as indicated by the EMF measurements. The three regions were:

1. Above the upper plateau
2. Between the two plateaus
3. Below the lower plateau

The powders were exposed for ten hours in a Debye-Scherrer camera and the 'd' spacings determined from the pattern obtained. The products from ingots quenched from regions 1 and 2 were identified as $FeCr_2O_4$ and a "distorted spinel". The measured 'd' spacings are reported in Tables 4.8 to 4.10 and the values from the 'standard' diffraction patterns as reported in JCPDS[90] and the data from the work of Hilty et al.[27] are listed in Appendix 1.

The deoxidation product formed below the lower plateau could not be identified positively. However, the 'd' spacings obtained from the X-ray patterns and listed in Table 4.10 indicate the presence of chromium metal. However, the quantity of deoxidation product formed was very small and hence a reliable diffraction pattern could not be obtained. The significance of the pattern will be discussed in Chapter 5.

In the case of the "distorted spinel" the agreement between the lines is reasonable. Hilty et al. refer to two "distorted spinels" in their study though they do not report any chemical formulae. The reasons

Table 4.6

Thermodynamic Data from the Upper Plateau in the Fe-Cr-O System

Temperature		EMF	$-\log h_O$	$-\Delta G^o_{4.14}$
^oC	^oK	mV		cals/mole
1552	1825	193±3	1.70	8100
1588	1861	198±3	1.55	7600
1600	1873	198±3	1.51	7400

$$3Fe_{(\ell)} + 4\underline{O}_{1w/o} + 2Fe_2Cr_7O_{12(s)} \rightleftarrows 7FeCr_2O_{4(s)} \quad (4.14)$$

Table 4.7

Thermodynamic Data from the Lower Plateau in the Fe-Cr-O System

Temperature °C	Temperature °K	EMF mV	$-\log h_O$	$-\Delta G^o_{4.15}$ cals/mole
1552	1825	104±3	2.19	48800
1554	1827	104±3	2.186	48700
1588	1861	110±3	2.03	46100
1591	1864	108±3	2.03	46200
1600	1873	117±3	1.95	44600

$$6Fe_{(\ell)} + 7Cr_3O_{4(s)} + 8\underline{O}_{1w/o} \rightleftarrows 3Fe_2Cr_7O_{12(s)} \quad (4.15)$$

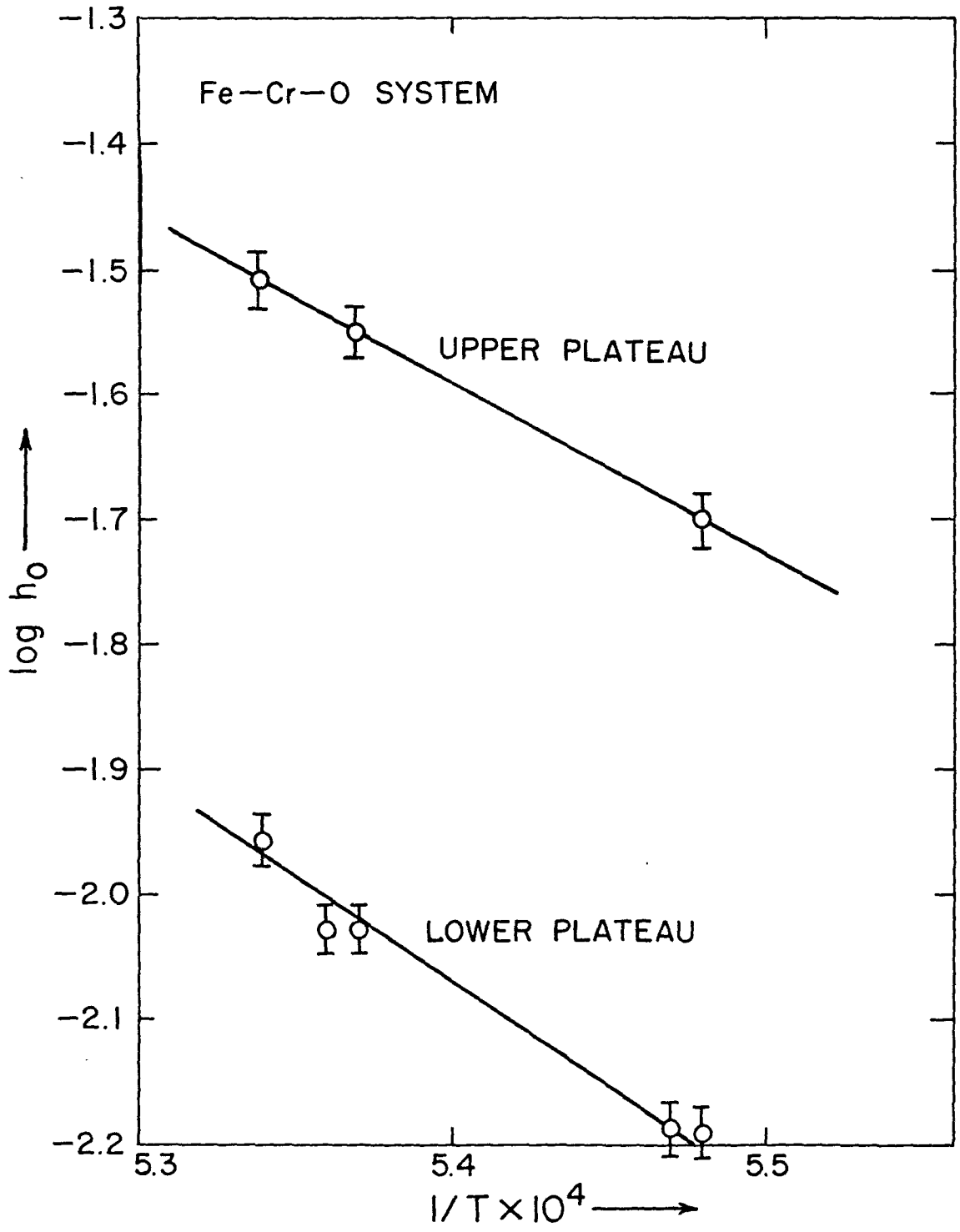

Fig. 4.12 Plot of log h_0 vs 1/T in the Fe-Cr-O system

Table 4.8

X-Ray Diffraction Pattern of Deoxidation Products in the Fe-Cr-O System

Between the two plateaus

Radiation Cu, K_α, λ = 1.5418A, Ni window

No.	Intensity	dA^o	Matches the standard* line of
1	M	4.81	Distorted Spinel
2	M	3.01	" "
3	S	2.95	" "
4	VVS	2.50	" "
5	W	2.41	" "
6	M	2.14	" "
7	W	2.08	" "
8	S	2.03	Cr
9	M	1.65	Distorted Spinel
10	M	1.57	" "
11	W	1.51	" "
12	M	1.47	" "
13	W	1.29	" "

*Source - Hilty et al.[27]

V - Very

S - Strong

M - Medium

W - Weak

Table 4.9

X-Ray Diffraction Pattern of Deoxidation Products in the Fe-Cr-O System

Above the upper plateau

Radiation Cu, K_α λ = 1.5418A

No.	Intensity	dA°	Matches the standard* line of
1	M	4.83	$FeCr_2O_4$
2	S	2.94	"
3	VVS	2.53	"
4	S	2.04	"
5	M	1.67	Cr_2O_3
6	VS	1.58	$FeCr_2O_4$
7	VS	1.45	"
8	VW	1.43	
9	W	1.25	

*Source - Joint Committee on Powder Diffraction Standards[90]

V - Very

S - Strong

M - Medium

W - Weak

Table 4.10

X-Ray Diffraction Pattern for Deoxidation Products in the Fe-Cr-O System

Below the lower plateau

Radiation Cu, K_α, λ = 1.5418A^{o}, Ni, window

No.	Intensity	dA^{o}	Matches the standard* line of
1	W	2.84	Cr_3O_4
2	S	2.61	Cr_3O_4
3	W	2.2	Cr_3O_4
4	VVS	2.05	Cr
5	VW	1.78	Cr
6	VVW	1.00	Cr
7	VW	0.93	Cr

*Source - Joint Committee on Powder Diffraction Standards[90]

V - Very

S - Strong

M - Medium

W - Weak

for concluding that the diffraction pattern corresponds to a "distorted spinel" and for assuming that the 'distorted spinel' is actually $Fe_2Cr_7O_{12}$ are again discussed in Chapter 5.

4.6 Third Law Analysis of Free Energy Data

The standard free energy data determined for the reaction

$$2VO_{(s)} + \frac{1}{2}O_{2(g)} \rightleftarrows V_2O_{3(s)} \qquad (4.12)$$

was analyzed by the 'Third Law' method. The data for reactions 4.13, 4.14 and 4.15 could not be analyzed in a similar fashion since heat capacity data for FeV_2O_4, Cr_3O_4, and $Fe_2Cr_7O_{12}$ are not available.

The Gibbs free energy function gef_T, given by

$$gef_T = (G^o_T - H^o_{298})/T \qquad (4.20)$$

was determined for the reactants and products in reaction 4.12 using the relation

$$gef_T = -S^o_T + \frac{H^o_T - H^o_{298}}{T} \qquad (4.21)$$

The thermochemical data for all components of reaction 4.12 were obtained from the compilation of Wicks and Block.[44]

The heat capacity data available for all oxides are reported in the temperature range 298^o-1800^oK. Since all the oxides are stable at steelmaking temperatures the data were extraplated to the experimental reaction temperatures.

The value of ΔH^o_{298} for the reaction was then calculated from the

Table 4.11

Third Law Analysis of ΔG^{o} Data for the Reaction

$$2VO_{(s)} + \frac{1}{2}O_{2(g)} \rightleftarrows V_2O_{3(s)}$$

a) Thermochemical Data

Component	$H_T - H_{298}$	S^{o}_{298}
V_2O_3	$-10780 + 29.35T + 2.38 \times 10^{-3}T^2 + 5.42 \times 10^{5}T^{-1}$	23.58
VO	$-3940 + 11.32T + 1.61 \times 10^{-3}T^2 + 1.26 \times 10^{5}T^{-1}$	9.3
O_2	$-2313 + 7.16T + 0.5 \times 10^{-3}T^2 + 0.40 \times 10^{5}T^{-1}$	49.01

$$gef_T = gef_T(V_2O_3) - 2gef_T(VO) - \frac{1}{2}gef_T(O_2)$$

b)

Temperature $T^{o}K$	$-\Delta G^{o}_T$ cals/mole	$T \times \Delta gef_T$ cals/mole	$-\Delta H^{o}_{298}$ cals/mole
1828	46190	34588	80800
1831	46267	34657	80900
1843	45881	34882	80800
1843	45829	34882	80700
1878	45774	35535	81300

Average of $\Delta H^{o}_{298} = -80,900$

experimental free energy data using the equation

$$\Delta H^{o}_{298} = \Delta G^{o}_{T} - T\Delta gef_{T} \qquad (4.22)$$

where Δgef_T is given by

$$\Delta gef_{T} = \Sigma gef_{T} \text{ (products)} - \Sigma gef_{T} \text{ (reactants)} \qquad (4.23)$$

The results of the calculations for the change in the Gibbs energy function and ΔH^{o}_{298} for reaction 4.12, as well as the pertinent data used in the calculations are given in Table 4.11.

4.7 Microscopic Examination of the Deoxidation Products

The distribution of inclusions in the quenched ingots was determined by micrographical examination of ingot sections.

The surface oxides were examined under a scanning electron microscope after iodine etching. The inclusions appear as 'globules' at low magnification but at high magnification the 'globules' are seen to be faceted. They appear, in fact, as an agglomeration of small crystallites of deoxidation products. The oxides also appear as thin filaments but X-ray analysis of inclusion material using an energy dispersion analyzer, showed the presence of impurities such as S, Si, Mn and Ni in the filaments while the 'globules' were impurity free.

Figs. 4.13 and 4.14 show scanning electron micrographs of the inclusions at various magnifications, obtained from a number of ingots quenched from different stages of oxidation.

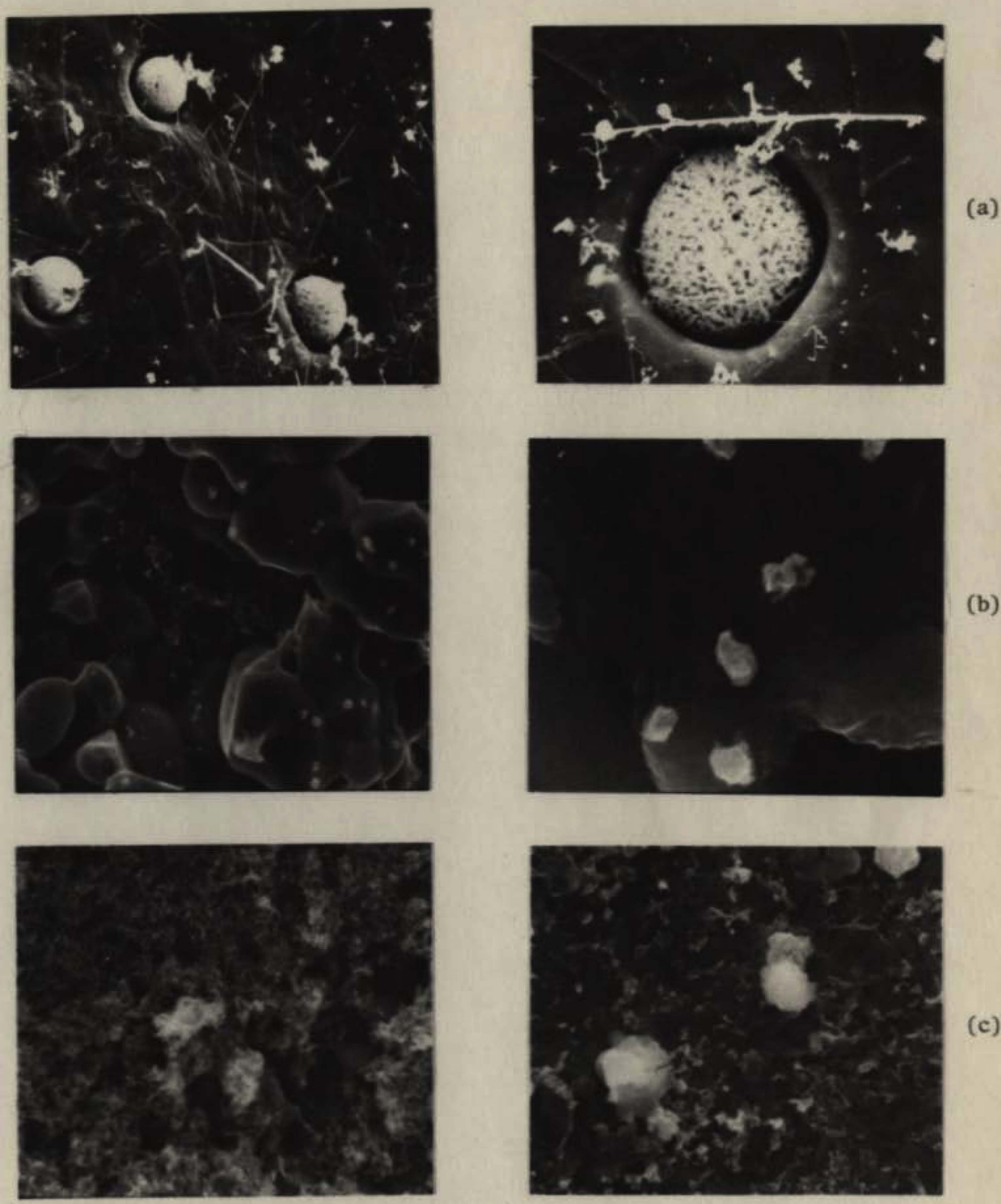

(a)

(b)

(c)

(X500) (X2000)

Fig. 4.13 Oxide inclusions in the Fe-V-O system
(a) FeV_2O_4, (b) V_2O_3 , (c) V_2O_3 + VO

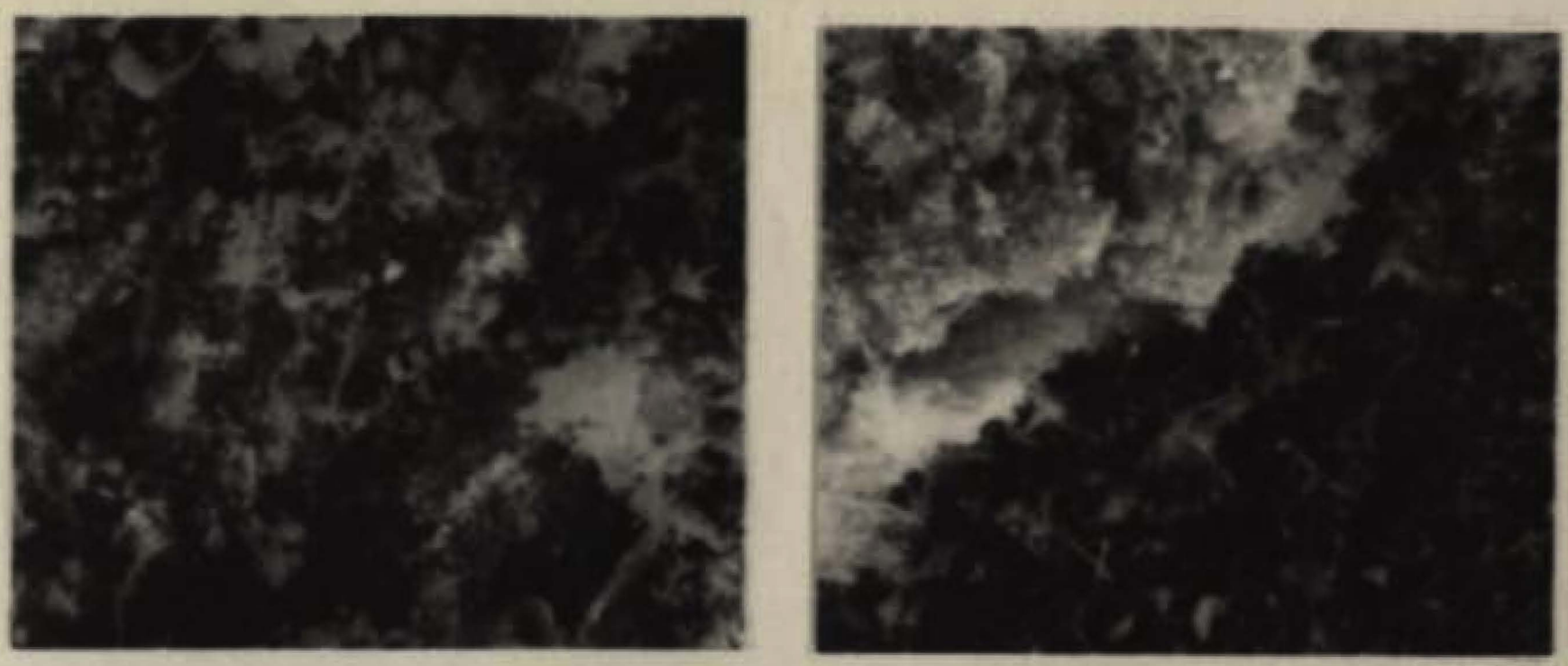

(a)

(b)

(X1000) (X2000)

Fig. 4.14 Oxide inclusions in the Fe-Cr-O system
(a) Cr_3O_4 (b) $FeCr_2O_4$

CHAPTER 5

DISCUSSION

5.1 Introduction

In this chapter the thermodynamic data obtained from this investigation has been compared with the values reported in the literature. Where the reported values have a form different from that of this work, the data has been recalculated and expressed in a form suitable for comparison.

In the application of galvanic cells for thermodynamic determinations, the cells have to satisfy certain stringent conditions. These conditions have been outlined and the experimental technique has been discussed in the light of these requirements. Further, any sources of error resulting from the deviation from these requirements have been discussed and compared with the sources of error present in other experimental techniques.

The thermodynamic data determined from the present experiments can be combined with other known data to obtain the free energies of formation of deoxidation products. Such calculations have been made for the Fe-V-O and Fe-Cr-O systems and compared with reported values from the literature. The results of the third law analysis have been compared with the standard enthalpy change for reaction 4.12 at $298^{o}K$ based on thermochemical data.

Finally the nature of the inclusions extracted from the ingots is

discussed. The shape and the structure of the deoxidation products are used to draw conclusions about their physical state at the reaction temperature and the mechanism for the formation of agglomerates of the oxides.

5.2 Effect of Electrolyte Reliability

It was pointed out in section 2.13 that in order to correlate the measured EMF of the cell with the activity of oxygen at the electrodes, the solid electrolyte should behave as an ionic conductor for the ions under consideration. Further, since the electronic conductivity in the solid electrolyte is a function of the partial pressure of oxygen and temperature, the solid electrolyte should be an ionic conductor at the temperatures and oxygen partial pressures of interest in deoxidation thermodynamics.

Calcia stabilized zirconia has been used extensively as a solid electrolyte. The electrolytic domain for calcia stabilized zirconia at steelmaking temperatures is reported to be outside the range of interest in steelmaking systems.[66,67] However, the determinations of Baker and West[66] and Patterson et al.[67] are either extrapolations from low temperature determinations or have employed air as a reference electrode. It has been pointed out by Fruehan[71] that determinations using gaseous electrodes at high temperatures could be in significant error due to gas diffusion through the pores and cracks in the electrolyte. This would result in more conservative estimates of the limits of the electrolyte domain. In his experiments, Fruehan has tested the results obtained with two electrolytes - calcia stabilized zirconia and yttria doped thoria - and found no significant

or systematic difference between the two electrolytes. Further, as can be seen from Table 2.9, the experimental determinations of the lower limit of the electrolytic domain for CSZ range from 10^{-8} atm, by extrapolation of the data of Baker and West,[66] to 3 x 10^{-13} atm according to Fruehan. Further, Fruehan has reported investigations on a number of systems using CSZ as the solid electrolyte and his data are in good agreement with that from other investigations.[84,85]

It was observed that CSZ can operate as a solid electrolyte at steelmaking oxygen potentials even down to the partial pressure of oxygen in equilibrium with chromium and chromic oxide, 8.4 x 10^{-13} atm at 1600°C. This can be inferred from the observation that the standard free energy changes associated with the reactions:

$$Fe_{(\ell)} + V_2O_{3(s)} + \underline{O}_{1w/o} \rightleftarrows FeV_2O_{4(s)} \qquad (5.1)$$

obtained from this work and for

$$Fe_{(\ell)} + Al_2O_{3(s)} + \underline{O}_{1w/o} \rightleftarrows FeAl_2O_{4(s)} \qquad (5.2)$$

obtained from the work of Stournaras,[86] are in good agreement with determinations made using other techniques.

The critical properties of the electrolyte were found to be purity, density and permeability. The significance of these three qualities are now discussed.

a) Purity. It was observed that whenever the solid electrolyte contained impurities such as silica and alumina, it performed poorly as a solid electrolyte. In a number of experiments it was found that the

crucible softened at high temperatures and would not contain the iron melt. A micrographic examination showed grain boundary silicate precipitates. Such crucibles also showed evidence of significant reaction with the melt. Worrell[59] has pointed out the significance of the purity of the electrolyte and this becomes even more critical when the electrolyte has to be employed as a shaped component. A number of determinations of the electrolytic domain have employed CSZ tubes and electrolyte purity affects these determinations significantly.

b) Density and Permeability. It was observed that crucibles whose density exceeded about 95% of the theoretical value, performed well under steelmaking conditions. Crucibles with lower densities did not hold the melt at high temperatures or retain their shape. Further, since the lower density was probably caused by porosity and microcracks, the cells could not meet any of the reversibility tests.

Generally lower density crucibles were not impervious. This became clear in the leak tests, for such crucibles could not hold a vacuum of 10^{-6} torr. Since a gas phase is in contact with the electrolytes, porosity and resulting gas transfer between the electrode compartments could result in non-standard operation of the cell. Hence,as pointed out in section 3.2.3, the crucibles had to be thoroughly tested prior to use.

The operation of the solid electrolytes was found to depend on the time for which the crucible was at the reaction temperatures. The cells generally performed satisfactorily for about 75 minutes unless some other phenomena affected the cell. This relatively short life could be due to formation of microcracks resulting from residual stresses produced

by sintering a shaped ceramic. In the experimental scheme, the plateaus corresponding to reactions 5.1 and 5.2 occurred last and the data calculated from this plateau is in good agreement with the literature. The consistency of these plateaus, in terms of reversibility tests and the thermodynamic data calculated from the plateau EMF's, was taken as a measure of the satisfactory performance of the electrolyte.

5.3 Effect of Ambiguity of the Cell Reaction

In order to obtain any significant information based on EMF measurements from electrochemical cells, it is imperative that the cell reaction be clearly and unambiguously defined. The electrochemical cell employed in these experiments can be represented as

$$\underset{(s)}{Mo} \;|\; \underset{(s)}{Cr,\ Cr_2O_3} \;\|\; \underset{\text{zirconia}}{\text{calcia stabilized}} \;\|\; \underset{(\ell)}{Fe\text{-}M\text{-}O} \;|\; \underset{\text{Cermet}}{Mo\text{-}ZrO_2} \qquad (5.3)$$

and, following the discussion in section 4.1, the virtual cell reaction can be written as:

$$3O_{\text{—1w/o}} + 2Cr_{(s)} \rightleftarrows Cr_2O_{3(s)} \qquad (5.4)$$

where the oxygen dissolved in iron is in equilibrium with the deoxidizer, 'M' added to the melt and one or more deoxidation products.

Any reaction that affects the concentration of any of the components of reaction 5.4 will result in a 'mixed' potential. Further, a mixed potential could also result from chemical reaction between the electrolyte and the electrodes.

At the reference electrode, the mixed potential could be caused by the oxidation of chromium to any oxide other than chromic oxide. While such oxides will certainly be formed from theoretical considerations, their quantities should be insignificant in comparison with Cr_2O_3 in order to avoid the formation of a mixed potential. The reactions leading to the formation of other known oxides of chromium can be expressed as

$$3Cr_{(s)} + 4\underline{O}_{1w/o} \rightleftarrows Cr_3O_{4(s)} \tag{5.5}$$

and $$Cr_{(s)} + \underline{O}_{1w/o} \rightleftarrows CrO_{(s)} \tag{5.6}$$

Higher oxides of chromium are not stable at the temperatures of interest in steelmaking.[44]

However, the standard free energy changes determined from these experiments agree very well with experiments using Mo/MoO_2 as the reference electrode by Jacob and Alcock[55] and hence mixed potential from this source is considered insignificant.

Another chemical reaction that is likely to occur in the reference electrode compartment involves the molybdenum lead:

$$2Cr_2O_{3(s)} + 3Mo_{(s)} \rightleftarrows 3MoO_2 + 4Cr \tag{5.7}$$

However, the molybdenum wire showed no signs of attack nor was there any evidence of black molybdenum oxide. Hence it was assumed that no significant mixed potential existed in the reference electrode.

In the melt compartment of the cell, a mixed potential could arise if the oxygen in the melt was in equilibrium with any element or oxide other than the deoxidizer or its oxides. Thus the main sources of

mixed potential would be contamination of the melt or deoxidation products, and reaction with the solid electrolyte crucible.

One of the features of the experimental technique employed is that the melt is contained in a calcia stabilized zirconia crucible. Calcia and zirconia are two of the most stable oxides under steelmaking conditions and hence it is very unlikely that a reaction of the type

$$ZrO_{2(s)} \rightleftarrows \underline{Zr}_{1w/o} + 2\underline{O}_{1w/o} \qquad (5.8)$$

would occur to any significant extent. The electrolyte crucible showed no evidence of reaction with the melt either in terms of attack or discoloration. The cermet was made of Mo/ZrO_2 for the same reasons. The only other oxide which came in contact with the melt and which was not a part of the system under study was alumina. This is also very stable at steelmaking temperatures and the alumina tube showed no evidence of deterioration.

The solid electrolytes were attacked during oxidation, after spinel formation was complete. However, the experiments were generally terminated before this stage and in any case no thermodynamic data was derived at this level of oxidation.

The oxygen activity in the melt could be affected by the dissolution of the contact (cermet) material in the melt which could set up a mixed potential. However, it was pointed out in section 3.3 that there was almost no dissolution of the cermet.

5.4 Effect of Polarisation

Another major source of deviation of the EMF from the thermodynamic value corresponding to the cell reaction is polarization. Polarization is of special importance in cells having a solid state reference electrode.

In galvanic cells using solid oxide electrolytes polarization could occur due to internal short circuiting or current leakage. In such cases oxygen could be transported from one electrode to the other down the chemical potential gradient. Thus, if the mass transport processes at the anode of the cell are not rapid, the oxygen potential at the electrolyte/electrode interface could change, resulting in an error in the cell EMF.

Where the metal/metal oxide reference electrode is the anode such a transport could form a film of oxide at the electrolyte surface. The oxygen potential at the reference electrode would rise above the equilibrium value resulting in a reduced EMF. However, such a phenomenon was not observed with the Cr/Cr_2O_3 reference electrode. This was further confirmed by the fact that the surface of the electrode in contact with the electrolyte showed no change in conductivity before and after experiments. Fortunately the high experimental temperatures involved make the diffusion processes quite rapid and facilitate equilibration at the electrode.

The degree of mixing of the Cr and Cr_2O_3 powders and their relative proportions in the mixture could alter polarization behaviour. As mentioned in section 3.2 various mixing ratios were tested and were found to have no effect on the cell EMF. The mixing ratio used in most of the experiments consisted of equal volumes of powders of similar sizes, in order to get the maximum contact between the metal and metal oxide particles.

In every experiment the cells were subjected to a reversibility test at the EMF plateaus. The test has been described in section 4.2, and the fact that the EMF returned to the same stable value after being disturbed in either direction by an externally imposed EMF, can be taken as a good indication of reversibility. If the cell had been polarized the EMF would have returned to a different value after a reversibility test.

Mo/MoO_2 has been used as a reference electrode by Jacob and Alcock[55] though mainly at lower temperatures. However, they have used it at 1600°C and report that it was found to be very stable and reversible. A Mo/MoO_2 reference electrode was tested in this work. The equilibrium partial pressure between Mo and MoO_2 is 7.1×10^{-8} at 1600°C and this electrode acts as a cathode to the melt. In a number of experiments it was observed that there was a significant transfer of oxygen to the melt and the outside of the CSZ crucible was coated by a thick adherent layer of molybdenum metal. Figure 5.1 shows a CSZ crucible after only 10 minutes at high temperature using a Mo/MoO_2 reference electrode. This resulted in failure to meet the reversibility tests. Hence Cr/Cr_2O_3 was used as the reference electrode in these experiments.

Polarization could also be caused by chemical reactions with the electrolyte since these reactions could alter the partial pressure of oxygen at the electrode/electrolyte interface. With a $Cr\text{-}Cr_2O_3$ electrode such an effect was not observed either at the reference electrode or the iron electrode.

At the iron electrode too, concentration polarization could occur

if there were an oxygen concentration gradient between the oxidizing gas/metal interface and the metal/electrolyte interface. This was checked by measuring the EMF while the melt was stirred with the cermet. No significant or systematic difference was observed in the measured EMF.

Current drawn from the cell during EMF measurements could result in polarization. The EMF was measured with an electrometer having an input impedance of 10^{14} ohms and with a potentiometer which ensured that the current drawn from the cell was extremely small.

Finally, Heyne and Beckmans[61] have pointed out that if the solid electrolytes exhibit a significant electronic conductivity, polarization could take place even without an external load on the cell. However, since the electrolyte performed satisfactorily in the experiments, polarization due to leakage currents is considered to be insignificant.

5.5 Effect of Inaccuracy in Measurements

In order for the thermodynamic data calculated from the measured EMF to be reliable, the various parameters in each experiment must be measured accurately. Following the discussion in section 4.1 the relation between log h_0, EMF and temperature can be written as

$$\log h_0 = 4.52 - \frac{13300-10.08E(mV)}{T} \qquad (5.9)$$

Hence the accurate measurement of the EMF and the reaction temperature is critical.

In order for the measured EMF to represent the free energy change

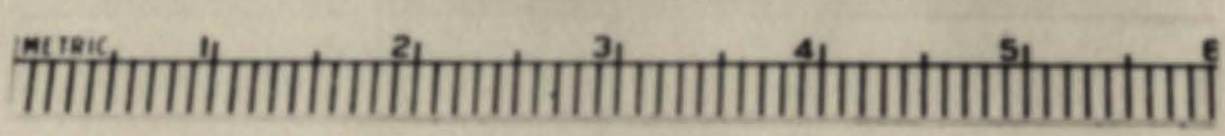

Fig. 5.1 C.S.Z. crucible coated with molybdenum metal (when Mo/MoO_2 was used as the reference electrode).

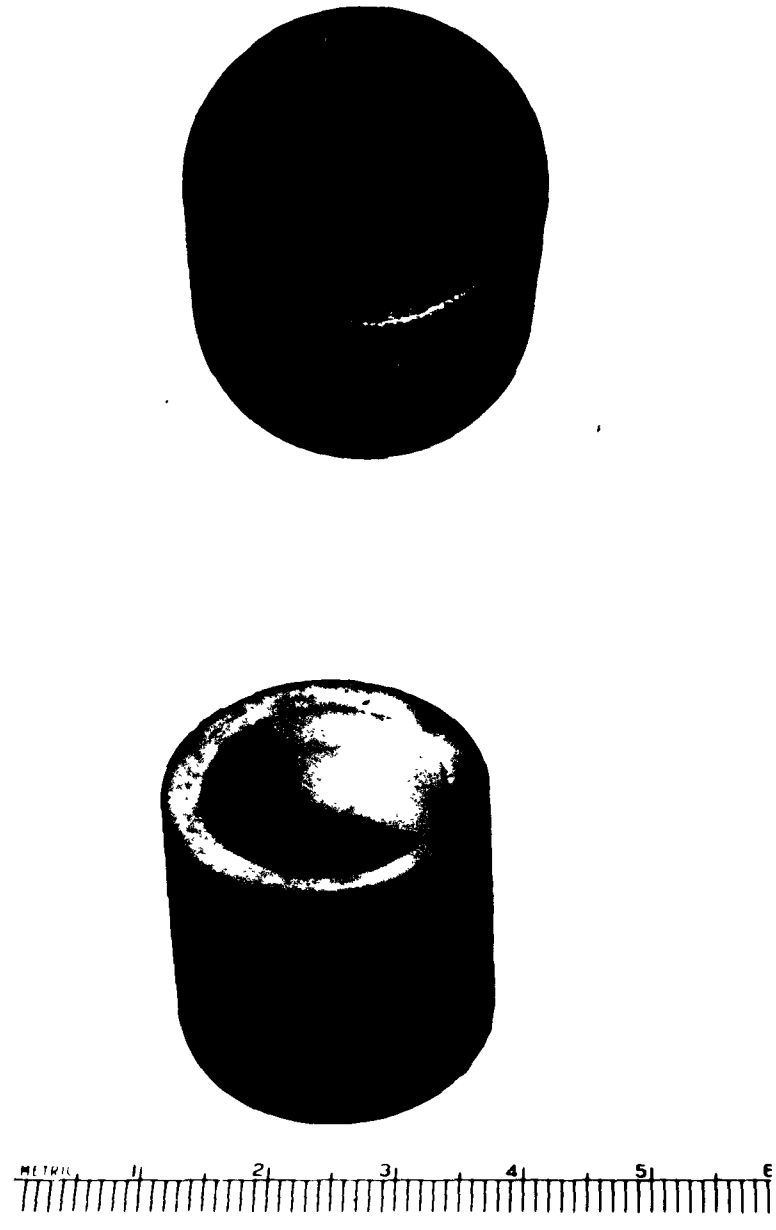

Fig. 5.1 C.S.Z. crucible coated with molybdenum metal (when Mo/MoO_2 was used as the reference electrode).

corresponding to the cell reaction exactly, it should be measured under 'open circuit' conditions - without drawing any current from the cell. This condition is almost attained with the electrometer since the current drawn is quite small ($<2 \times 10^{-16}$ amps). The potentiometer does measure the open circuit EMF at the null point but a small current is drawn while it is off balance. This results in a deviation, though very small, from the reversible cell EMF. The details of the EMF measurement have been described in section 3.6.

Further, it was observed that the 'plateau' EMF fluctuated over a range of ±2 mV. This introduced an uncertainty in the exact value of the plateau. The overall accuracy of the plateau EMF measurement is estimated to be ±3 mV, assuming that other effects such as polarization and induction were not significant. It has been outlined in section 3.7 that a great deal of care was taken to ensure that the entire cell was at a uniform temperature. However, the temperature did fluctuate within $\pm 2^{o}C$ during an experiment. Further, although the temperature measured was corrected for the deviation from a standard thermocouple (section 3.7), the actual temperature is accurate to only $\pm 3^{o}$ from the measured value. The overall uncertainty in temperature measurement is estimated at $\pm 5^{o}C$.

In addition to the inaccuracies in measurement, an error is also introduced due to the error in the standard free energy of formation of Cr_2O_3. This error is reported as ±300 cals. The total uncertainty in the calculated values of free energy changes due to the inaccuracies in measurement and the error at the reference electrode, is estimated at ±300 cals in the present work.

5.6 Sources of Error in Equilibration Techniques

The experimental techniques generally used in the study of deoxidation thermodynamics have been described in section 2.3. The common sources of error in experimental techniques, not involving solid electrolytes, will be discussed now.

The most important source of error is in the analysis for oxygen and deoxidizer elements. At low residual oxygen and deoxidizer contents in steel the accurate analysis of the elements is extremely difficult. This is particularly true for strong deoxidizers or where small amounts of residual oxygen are in equilibrium with small amounts of deoxidizer. Further, it is extremely difficult to get a 'clean' melt sample for analysis since fine suspensions of the deoxidation product are invariably present throughout the melt. The chemical analysis step in deoxidation studies is not required in the galvanic cell technique of the present work.

Chemical analysis of the melts, yields the weight percent concentration of the element in the iron samples. However, the equilibrium constants are based on the activities of the elements. Hence it is necessary to correct the analyzed concentration by empirically determined interaction parameters whose accuracy depends once again on chemical analysis. The value of the interaction parameter for vanadium on oxygen, e_O^V, as reported in the literature ranges from -0.14 to -0.3 and the corresponding value of e_O^{Cr} varies from -0.03 to -0.065.[3] In contrast, the EMF of an oxygen concentration galvanic cell is a direct measure of the activity of oxygen in iron at the experimental temperature.

The second major source of error lies in the attainment of 'equilibrium'.

Since there is no direct measure of the processes occurring at high temperatures in a melt, it is difficult to ascertain whether an equilibrium has been reached. This is also true of techniques where the galvanic cell is used in the form of a probe to measure oxygen activity. The technique used in these experiments provides a method for continuous monitoring of the melt and the melt does not have to 'equilibrate' as such. The EMF plateaus correspond to a time during which a deoxidation product transforms and this transformation has an associated equilibrium oxygen activity in the melt.

Finally, equilibration techniques cannot indicate high temperature reactions. Thus, it is not possible to study the thermodynamics of deoxidation products which are stable only at high temperatures. The facility of monitoring the activity of oxygen continuously makes it possible to determine the number of deoxidation products formed and the corresponding oxygen activities.

5.7 Thermodynamic Stability of Iron Vanadite as a Deoxidation Product

Studies of the Fe-V-O system have already been reviewed in section 2.5. However, the data as reported by the various authors is not always suitable for comparison with the results obtained in these experiments. The data obtained from section 2.5 can be manipulated to obtain the standard free energy change for the reaction

$$Fe_{(\ell)} + V_2O_{3(s)} + \underline{O}_{1w/o} \rightleftarrows FeV_2O_{4(s)} \qquad (5.10)$$

From the data for the equilibrium constants reviewed in section 2.5

and table 2.1 the activity of oxygen of iron in equilibrium with both the deoxidation products V_2O_3 and FeV_2O_4 - the oxygen activity at the transition point from V_2O_3 to FeV_2O_4 - can be calculated as follows:

$$K_{FeV_2O_4} = h_V^2 \, h_O^4 \tag{5.11}$$

$$K_{V_2O_3} = h_V^2 \, h_O^3 \tag{5.12}$$

$$h_{O_{V_2O_3/FeV_2O_4}} = \frac{K_{FeV_2O_4}}{K_{V_2O_3}} \tag{5.13}$$

This value of $h_{O_{V_2O_3/FeV_2O_4}}$ corresponds to the value of h_O obtained from the upper plateau of Fig. 4.1 in this work. This oxygen activity can also be calculated as a function of temperature from the data for log K_T reported in Table 2.1 and can be expressed as

$$\log h_{O_{FeV_2O_4/V_2O_3}}(T) = \log K_{FeV_2O_4}(T) - \log K_{V_2O_3}(T) \tag{5.14}$$

From the value of $\log h_{O_{FeV_2O_4/V_2O_3}}(T)$ thus obtained, the value of $\Delta G^o_{10}(T)$ can be calculated. The values of $\Delta G^o_{10}(T)$ and $\log h_{O_{V_2O_3/FeV_2O_4}}(T)$ calculated from various sources at 1600°C and 1575°C are listed in Table 5.1 and a plot of ΔG^o_{10} versus T is shown in Fig. 5.2.

It can be seen that the agreement between the results obtained in the present work and those of Dastur and Chipman,[4] Narita and Koyama,[6] Kojima et al.[8] and Jacob and Alcock[55] are in excellent agreement at 1600°C.

The results of Kontopoulos[78] and Turkdogan[1] disagree by about 1 kcal at 1600°C and those of Vahed[77] by about 5 kcal.

The results reported by Turkdogan[1] are from an interpretation of Fruehan's[85] work. Both Fruehan and Kontopoulos employed CSZ probes in their experiments. It has been pointed out by den Hertog and Slangen,[87] that with such probes the EMF measured is affected to a great extent by the dissolution of silica in the melt thereby setting up a mixed potential. Further, their experimental technique comprised of determining the oxygen activity in iron in equilibrium with one deoxidation product. From these values a plot of log h_O against log h_V was drawn and the transition point obtained by extending the "best fitting" lines from the regions of stability of V_2O_3 and FeV_2O_4. The combination of the two sources of error could easily account for the deviation from the results obtained in this work.

The results of Vahed[77] are in substantial error due solely to the fact that the EMF obtained from his galvanic cells correspond to the reaction

$$2VO_{(s)} + \underline{O}_{1w/o} \rightleftarrows V_2O_{3(s)} \qquad (5.14)$$

Vahed did not confirm the deoxidation products obtained from his melts by X-ray analysis and it will be shown in section 5.8 that his data is in good agreement with the present study when applied to reaction 5.14.

At 1575°C the results from this work and from Jacob and Alcock[55] are in good agreement considering that these authors also report an error of ±300 cals in their data. The results of Narita,[6] however, are in considerable disagreement and in fact show a trend opposite to that of other studies. Jacob and Alcock[55] have pointed out that a negative temperature

dependence of the oxygen potential is not in accord with the statistical thermodynamics of gases and condensed phases. The main contribution to the entropy change for reaction 5.10 arises from the combination of oxygen in solution in a liquid phase to form a solid crystalline product.

The values of ΔG^{o}_{10} are plotted against temperature in figure 5.2. Although a line is drawn through the results obtained in this work no interpretation is presented in terms of a second law analysis.

The Henrian activity of vanadium at the transition point from V_2O_3 to FeV_2O_4 can be calculated using equation 5.12. The values reported by various authors have been listed in Table 2.1. Using the value for $K_{V_2O_3}$ ($1600^{o}C$) as reported by Dastur and Chipman[4] the Henrian activity of vanadium obtained from this work is 0.17, which is in good agreement with all values reported in Table 2.1.

5.8 Thermodynamic Stability of VO as a Deoxidation Product

Equilibrium data for the formation of a VO phase at high vanadium concentrations in iron, have been reviewed in section 2.5 and Tables 2.1 - 2.4. Once again the data reported in Tables 2.1 and 2.4 can be processed to obtain the standard free energy change for the reaction

$$2VO_{(s)} + \underline{O}_{1w/o} \rightleftarrows V_2O_{3(s)} \qquad (5.15)$$

The Henrian activity of oxygen at the transition point of the stable oxide phase can be calculated by combining the relations for the equilibrium constants

$$K_{V_2O_3} = h_V^2 \, h_O^3 \qquad (5.12)$$

Table 5.1

Standard Free Energy Changes and Transition Oxygen Activities for the Reaction

$$Fe_{(\ell)} + V_2O_{3(s)} + \underline{O}_{1w/o} \rightleftarrows FeV_2O_{4(s)} \qquad (5.10)$$

	1600°C		1575°C	
Reference	$-\Delta G^{o}_{10}$	$-\log h_O$	$-\Delta G^{o}_{10}$	$-\log h_O$
Present study	12000	1.40	12700	1.50
Dastur & Chipman	12000	1.40	-	-
Narita & Koyama	11900	1.39	11878	1.405
Kojima et al.	12290	1.43		
Kontopoulos	13000	1.51	13150	1.55
Jacob & Alcock	12000	1.40	12400	1.46
Vahed	16860	1.97		
Turkdogan	13900	1.62		

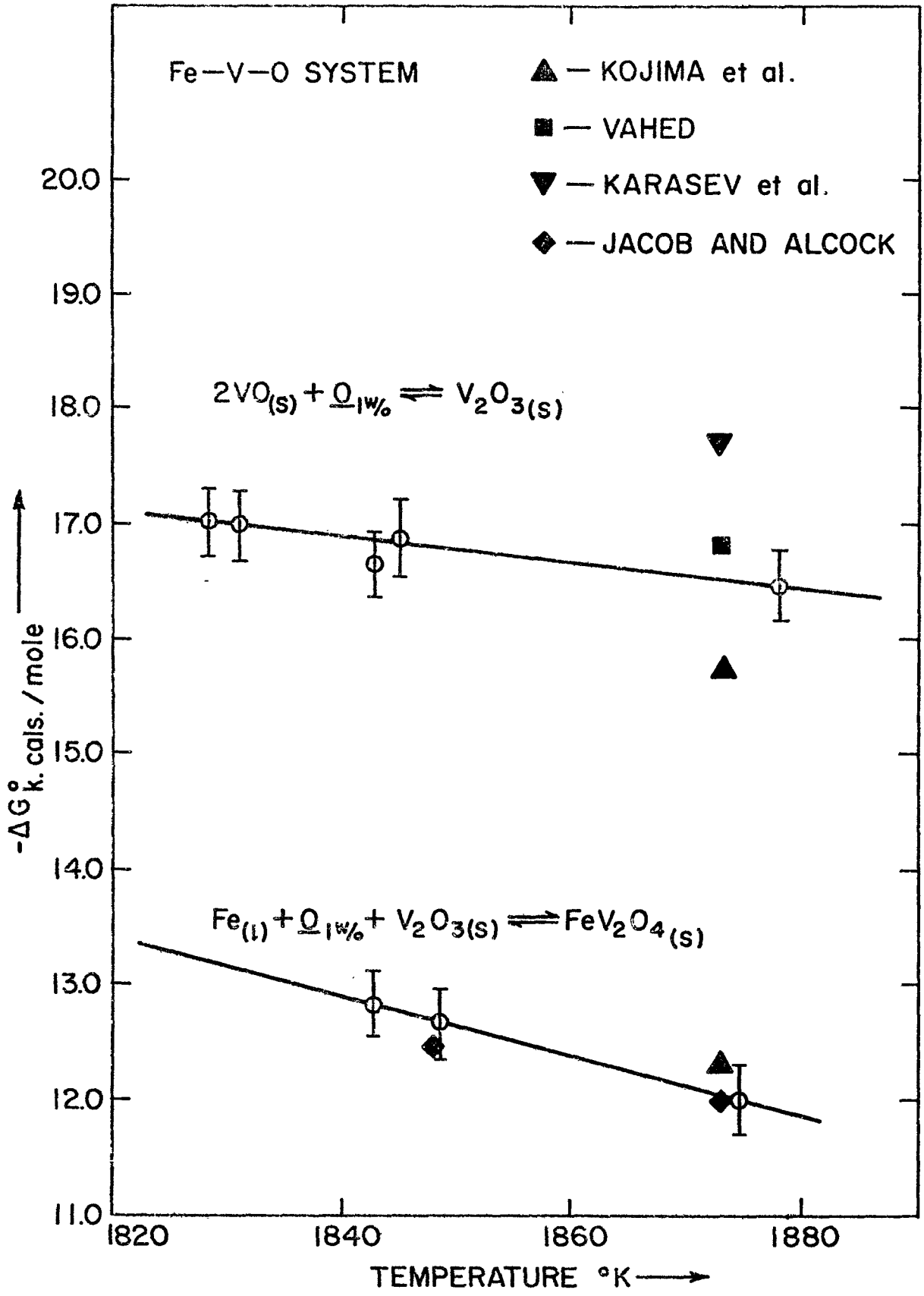

Fig. 5.2 Plot of ΔG° vs T in the Fe-V-O system

and $$K_{VO} = h_V h_O \tag{5.16}$$

to obtain

$$h_{O_{VO/V_2O_3}} = \frac{K_{V_2O_3}}{(K_{VO})^2} \tag{5.17}$$

The value of $\log h_{O_{VO/V_2O_3}}(T)$ can be calculated from the tabulated data for $\log K_T$ in Table 2.1, using the relation:

$$\log h_{O_{VO/V_2O_3}}(T) = \log K_{V_2O_3}(T) - 2 \log K_{VO}(T) \tag{5.18}$$

The values of ΔG^o_{15} and $h_{O_{VO/V_2O_3}}$ obtained from the present study are compared with those derived from data in Table 2.1, and Table 5.2.

It can be seen from Table 5.2 that the results from the present study are in reasonable agreement with those of Vahed.[77] However, Vahed's experiments had two main sources of error. He oxidized the melt to a high oxygen activity by adding Fe_2O_3 and made his measurements while the melt was being reduced. Iron oxides added to the melt can react with and affect the behaviour of the solid electrolyte. Vahed used a molybdenum wire as a contact to the liquid metal and the dissolution of molybdenum in iron could affect the thermodynamics of the deoxidation reaction under study. Though his results agree with the present work quite well at 1550°C and 1600°C, his data is quite erratic and shows a considerable scatter.

The results obtained from the work of Kojima et al.[8] at 1600°C show a higher oxygen activity at the transition point from VO to V_2O_3, than

Table 5.2

Free Energy Change for the Reaction

$$2VO_{(s)} + \underline{O}_{1w/o} \rightleftarrows V_2O_{3(s)}$$

Temp. ^oC	log h_O	$-\Delta G^o$(cals)	Reference
1570	-1.968	16,550	
1558	-2.03	17,081	This work
1570	-1.97	16,610	
1605	-1.92	16,410	
1550	-2.05	17,108	Vahed
1600	-1.96	16,795	
1650	-1.69	14,790	
1600	-1.83	15,700	Kojima, Inouye, Ohi
1550	-2.72	24,100	
1570	-2.82	23,810	Narita et al.
1600	-2.89	23,360	
1600	-2.06	17,693	Karasev et al.

the results of the present study. This could be accounted for by the fact that he determined the oxygen and vanadium activities by chemical analysis. Thus the measured oxygen represents the weight percent concentration of the total oxygen - including suspended deoxidation products.

The disagreement with Narita's[6] work is quite substantial - about 7 kcal at 1600°C. Narita et al.[7] used very large concentrations of vanadium in their melts and hence it is quite likely that their data represents a non-equilibrium condition which could account for the low oxygen potentials. At large concentrations of the deoxidizer, the deoxidation product could form a film on the surface of the melt making it very difficult for the reaction to reach equilibrium. Further, it has been pointed out in section 2.7 that Narita's results, in the regions where V_2O_3 and FeV_2O_4 are the equilibrium products, are thermodynamically inconsistent. Since the calculations for ΔG^o_{15} are based on those results, the value of ΔG^o_{15} is bound to reflect that inconsistency.

The results of Karasev[(5)] appear to be in good agreement with this study. However, it can be seen from Table 2.1 that his equilibrium constants for both V_2O_3 and VO are an order of magnitude higher than those reported by other investigators and probably reflect sampling from an unclean melt. He has reported the stable deoxidation product as V_2O_2 though he could not identify it by X-ray techniques. This is due to the fact that he obtained a slope of -1 for a plot of log h_O against log h_V and then postulated the formation of V_2O_2. This oxide has not been reported in the literature and the results of Karasev have to be treated as corresponding to the formation of VO.

Table 5.3

Activity of Vanadium at the Transition Point from VO to V_2O_3 at $1600^{o}C$

Source	h_V
Present study	1.01
Kojima et al.	0.9
Narita et al.	12.6
Karasev	9.4
Vahed	1.2

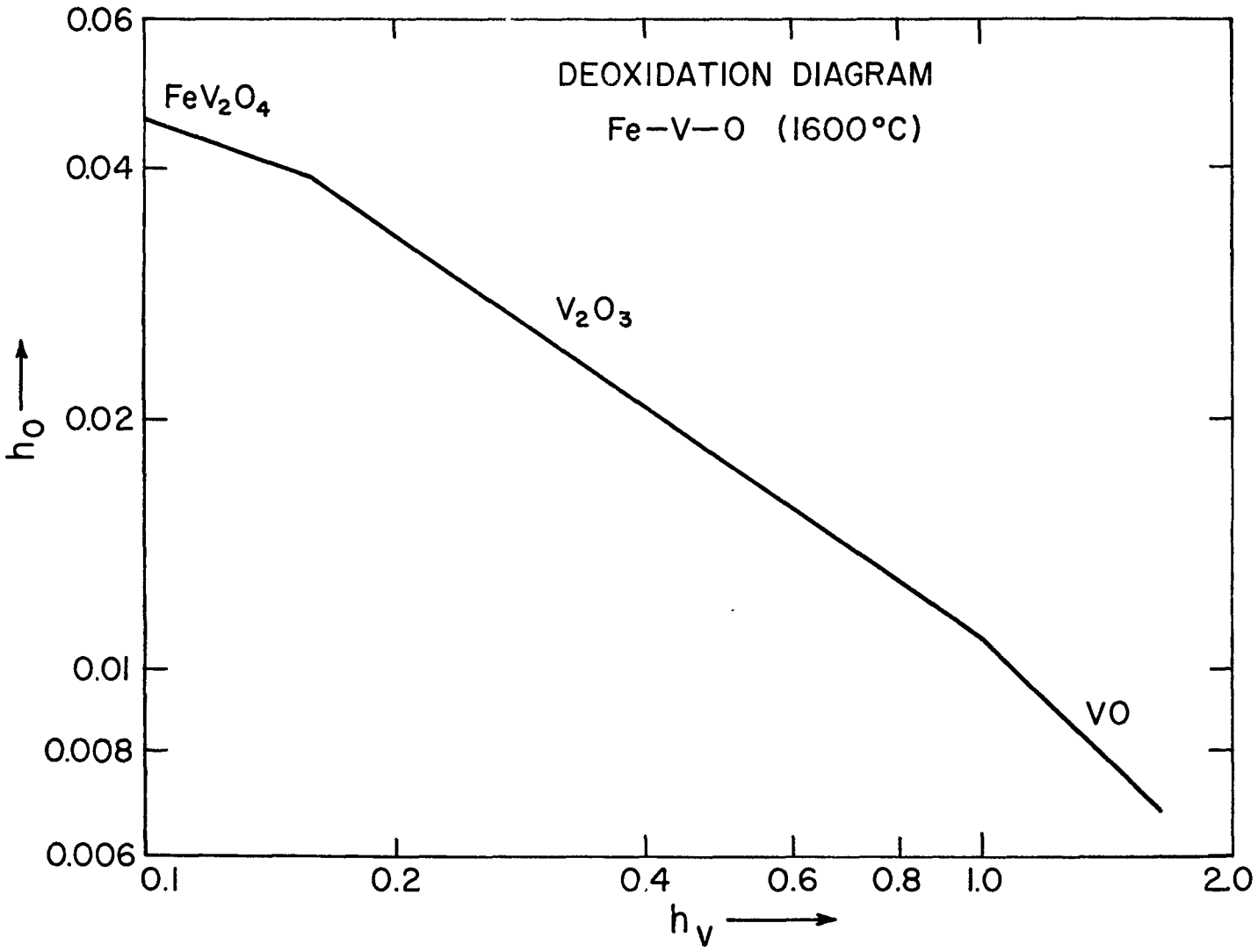

Fig. 5.3 Deoxidation diagram for the Fe-V-O system at 1600°C

The value of h_V at the transition point from VO to V_2O_3 at 1600°C can be calculated from $h_{O_{VO/V_2O_3}}$ and equation 5.12. The value of $K_{V_2O_3}$ used to calculate this h_V from the value of $h_{O_{VO/V_2O_3}}$ obtained from this work is taken from the data of Chipman and Dastur.[4] The values of h_V from various sources are compared in Table 5.3.

It is clear from Table 5.3 that the results of Narita et al.[7] represent a non-equilibrium condition for the vanadium content used in their work (4-10 wt%) is less than that required to form VO based on their values of K_{12} and K_{16}. A deoxidation diagram (log h_O versus log h_V) for the Fe-V-O system at 1600°C is plotted in Fig. 5.3.

5.9 Third Law Analysis

The 'Third Law' method of analysis of thermodynamic data for a reaction involves the conversion of free energy data at different temperatures, to give a common value of ΔH^o_{298}, using values of the Gibbs energy function calculated from heat capacity data for the products and reactants. This method has the following advantages:

1. Each experimental point is treated individually - even a single observation can be thus analyzed.

2. It can detect individual bad points in a set of experimental observations as points which lie outside the normal scatter of values around an average ΔH^o_{298}.

3. It can reveal non-equilibrium or erroneous trends if the calculated ΔH^o_{298} show some temperature dependence assuming that the available Gibbs energy functions are relatively accurate.

The results of the third law analysis of the data for the reaction

$$2VO_{(s)} + \frac{1}{2}O_{2(g)} \rightarrow V_2O_{3(s)} \qquad (5.19)$$

are shown in Table 4.11. It can be seen that the values of ΔH^o_{298} for reaction 5.19 are not temperature dependent, the average value being -80,900 cals/mole of V_2O_3.

There have been no direct determinations of ΔH^o_{298} for reaction 5.19. Hence it has to be calculated by combining the standard heats of formation of VO and V_2O_3 at 298°K. These values have been reviewed in section 2.6 and Table 2.4.

The value of ΔH^o_{298} for V_2O_3 generally accepted is -296 ± 6 kcal/mole. However, in a recent study Charlu and Kleppa[18] redetermined this value by a high temperature microcalorimetric method. In view of the accuracy of the technique they suggest that the value of ΔH^o_{298} for V_2O_3 should be -291 ± 0.9 kcal/mole, in agreement with the results of Mah and Kelley[17] and Rossini.[16]

In the case of ΔH^o_f for VO the value generally accepted is -98 ± 5 kcal/mole. However, the values determined by other workers[14,17] are as high as -105.5 ± 5 kcal. Using these four values of ΔH^o_f, the value of ΔH^o_{298} for reaction 5.19 have been calculated and reported in Table 5.4.

It can be seen that the agreement with the value determined from this work ranges from excellent to very bad. This could be accounted for by two main reasons:

1. The large uncertainty of ΔH^o_f values for VO and V_2O_3. Generally this uncertainty is of the order of ±5 kcal/mole.

Table 5.4

Standard Enthalpy Change for Reaction 5.19 Calculated from the literature

Source (Ref. No.)	ΔH^{o}_{298} (VO)	Source (Ref. No.)	$\Delta H^{o}_{298}(V_2O_3)$ kcal/mole	ΔH^{o}_{298}(5.19) kcal/mole
44	-98	44	-296	-100
44	-98	18	-291	-95
14	-105.5	44	-296	-85
14	-105.5	18	-291	-80

Note: reaction 5.19 $2VO_{(s)} + \frac{1}{2}O_{2(g)} \rightleftarrows V_2O_{3\,(s)}$

2. VO is a non stoichiometric compound with a composition range from $VO_{0.89}$ to $VO_{1.2}$. The stoichiometry of VO studied by the various authors is not clear from the literature. In the present work the stoichiometry of VO is fixed by the constraint that it has to be simultaneously in equilibrium with V_2O_3 and a certain oxygen activity in the melt.

Since stoichiometry is probably not a source of error in the case of V_2O_3, ΔH^o_{298} for V_2O_3 was combined with ΔH^o_{298} for reaction 5.19, obtained from this work, to calculate the value of ΔH^o_{298} for 'VO' of a stoichiometry determined by the experimental constraints. Choosing the value of ΔH^o_{298} (V_2O_3) of Charlu and Kleppa,[18] the value of ΔH^o_{298} (VO) thus obtained is -105.5 ± 5 kcal/mole.

5.10 Deoxidation Thermodynamics of the Fe-Cr-O System

The general principle of the experimental technique can be described as follows. A melt of iron and a deoxidizer element containing very little oxygen is oxidized by passing an oxidizing gas mixture over the surface. Monitoring the oxygen activity of the melt continuously makes it possible to determine the number of transformations undergone by the stable deoxidation product and the activities of oxygen at which transformations occur. In subsequent experiments the melt is quenched from various stages of oxidation and the deoxidation product, stable in that region, is determined by X-ray analysis. Once the deoxidation products are determined, the transformation reactions corresponding to each arrest in the EMF can be written, and the standard free energy changes for the reactions can be calculated.

However, the success of the technique depends on three main factors, assuming that the galvanic cell is working satisfactorily. They are:

1. The deoxidation products should be stable at high and low temperatures. Thus if an oxide is stable only at high temperatures, the identification of the product by X-ray diffraction would yield erroneous results.

2. An adequate amount of the deoxidation product should be formed in order to get a good sample for X-ray analysis.

3. Good standard diffraction patterns should be available for comparison.

In the iron-chromium-oxygen system, the observation that melts having a chromium content as small as 1.8% show two arrests in the EMF versus time curve, indicates that the deoxidation product transforms twice.

The stable deoxidation product above the upper plateau in the EMF was readily identified as iron chromite. The deoxidation product obtained from the region between the two plateaus gave a diffraction pattern which agrees reasonably well with the patterns for the 'distorted spinels' as reported by Hilty et al.[27] Due to the limitations in the size of the crucible and the chromium content of the melt with which the experiments could be successfully performed, the amount of deoxidation product that could be obtained was quite small. Hence the pattern obtained was not very sharp and the intensities of the lines could be compared only optically. Further, due to the long exposures required to obtain a pattern, the low angle lines were obscured by the background. In Debye-Scherrer cameras that do not employ a focussing crystal there also exists a significant absorption correction. In view of these considerations an agreement within $\pm 0.03 A^{o}$ in the 'd' spacings obtained on the diffraction pattern is taken

as reasonable. Hence the deoxidation product stable between the two plateaus is assumed to be a distorted spinel.

However, in order to get an arrest in the change of oxygen activity of the melt the 'distorted spinel' has to have a definite composition. If the 'distorted spinel' is merely a solid solution between Cr_3O_4 and $FeCr_2O_4$, for example, then the exchange between chromium and iron in the spinel could take place continuously, without any EMF arrest. Hilty et al. do not report a definite composition for the spinel but that would be inconsistent with the EMF plateau obtained in these experiments.

Sakao and Sano[29] have reported the formation of a spinel, which they reported as $Fe_2Cr_7O_{12}$, as the stable phase between $FeCr_2O_4$ and Cr_3O_4. $Fe_2Cr_7O_{12}$ can also be represented as a solid solution between $FeCr_2O_4$ and Cr_3O_4 in a fixed ratio of 2:1. However, the authors do not report any diffraction pattern for their oxide phases. Since no other composition of the 'distorted spinel' has been reported and an adequate sample for precise lattice parameter determinations could not be obtained by the present technique, $Fe_2Cr_7O_{12}$ was taken as the stable product in the region between the two plateaus.

Hilty et al. report that the distorted spinel could dissociate during cooling to form Cr_2O_3 and Cr. However, no evidence of chromium was observed in the diffraction pattern obtained from these samples. Based on these conclusions about the deoxidation products at the upper plateau, the reaction corresponding to this plateau can be written as:

$$3Fe_{(\ell)} + 2Fe_2Cr_7O_{12(s)} + 4O_{-1w/o} \rightleftarrows 7FeCr_2O_{4(s)} \qquad (5.20)$$

The deoxidation product stable below the lower plateau of the EMF vs time curve was taken as Cr_3O_4, though it could not be positively identified. This is based on the following reasons:

1. The amount of deoxidation product formed is very small. Whenever experiments with large chromium contents were carried out, oxidation of the melt and control of the experiment was found to be very difficult.

2. Hilty et al. have reported that Cr_3O_4 decomposes on cooling, to form Cr_2O_3 and Cr

$$Cr_3O_{4(s)} \rightleftarrows Cr_2O_{3(s)} + Cr_{(s)} \qquad (5.21)$$

and the diffraction pattern obtained for the oxide gave a number of lines which could be attributed to chromium (Table 4.10 and Appendix 1). While it can be seen from the diffraction patterns of iron and chromium (Appendix 1) that the strongest lines correspond to almost identical 'd' spacings, the pattern obtained is taken to correspond to chromium because, as reported in section 3.10, extreme care was taken to remove iron from the X-ray sample.

3. Though the X-ray pattern obtained from the samples did not correspond to Cr_2O_3, this may be due to the fact that the total amount of sample was very small and a sharp pattern could not be obtained.

4. It appears logical that the deoxidation product stable in a region beyond a solid solution of Cr_3O_4 and $FeCr_2O_4$ would be Cr_3O_4.

Hence the deoxidation product stable below the lower plateau is assumed to be Cr_3O_4.

The reaction corresponding to the lower plateau can then be written as

$$6Fe_{(\ell)} + 7Cr_3O_{4(s)} + 8O_{-1w/o} \rightleftarrows 3Fe_2Cr_7O_{12(s)} \qquad (5.22)$$

It was observed that only a small amount of deoxidation product was formed at the lower plateau in melts with a chromium content of just over 1.8%. This was noticed during the course of the experiments and on examination of the cooled ingot. Thus, assuming that 1.8% Cr is the smallest amount of chromium required to form Cr_3O_4, the equilibrium constant for the following reaction can be calculated

$$Fe_2Cr_7O_{12(s)} \rightleftarrows 2Fe_{(\ell)} + 7\underline{Cr}_{1w/o} + 12\underline{O}_{1w/o} \qquad (5.23)$$

$$K_{23} = h_{Cr}^{7}\, h_{O}^{12} \qquad (5.24)$$

The value of K_{23} can be calculated using a value for h_{Cr} of 1.8 and the value of h_O obtained from the EMF at the lower plateau. The value of K_{23} thus obtained, is 2.4×10^{-22} at 1600°C, compared with the value of 1.1×10^{-16} obtained by Sakao and Sano.[29] However, they report the critical chromium content for the formation of Cr_3O_4 as 9%. The observation that two plateaus are obtained even at 1.8% Cr in the melt contradicts the observations of Sakao and Sano.

Sakao and Sano determined this limit by an equilibration technique described in section 2.8. Following the discussion in section 5.6, their technique is expected to give high estimates of the critical chromium content. Further, in view of the large values of the exponents of chromium and oxygen activities in equation 5.24 a small error in analysis would result in large errors in the value of K_{23}.

Since $Fe_2Cr_7O_{12}$ is also in equilibrium with $FeCr_2O_4$ the same equilibrium constant, with the value of h_O taken from the upper plateau, gives an estimate of the critical chromium content in the melt before $Fe_2Cr_7O_{12}$ can be formed.

From the results obtained in these experiments, this limit at 1600°C is 0.31% Cr. A deoxidation diagram of log h_O vs log h_{Cr} at 1600°C as estimated from these experiments is presented in Fig. 5.4 and a plot of ΔG^o vs T in Fig. 5.5.

Other deoxidation products could be formed at lower activities of oxygen and larger chromium contents. However, no attempts were made to investigate the formation of these oxides as it is not certain if the electrolyte would perform satisfactorily at the corresponding, low, oxygen potentials.

The deoxidation scheme presented in this analysis agrees with that of Hilty et al.[27] and Sakao and Sano[29] in terms of the nature of deoxidation products. However, it can be seen from Table 2.6 that the limits of the stability of the deoxidation products as reported by these authors are in considerable disagreement with the limits estimated from the present study. This could be caused by the fact that they had no method of monitoring the reactions as they occurred at the high temperature and also because chemical analysis would give values of oxygen and chromium contents higher than the actual values, for reasons outlined in section 5.6.

The deoxidation scheme generally reported in the literature gives $FeCr_2O_4$ and Cr_2O_3 as the only two deoxidation products.[24,25] However, it has been pointed out by Jacob and Alcock[55] that Fe, $FeCr_2O_4$ and Cr_2O_3 do not co-exist in equilibrium. If $FeCr_2O_4$ and Cr_2O_3 were the only two deoxidation products formed they would have to co-exist at the chromium and oxygen activities corresponding to the transition point.

It can be seen from Table 2.6 that the reported values of the

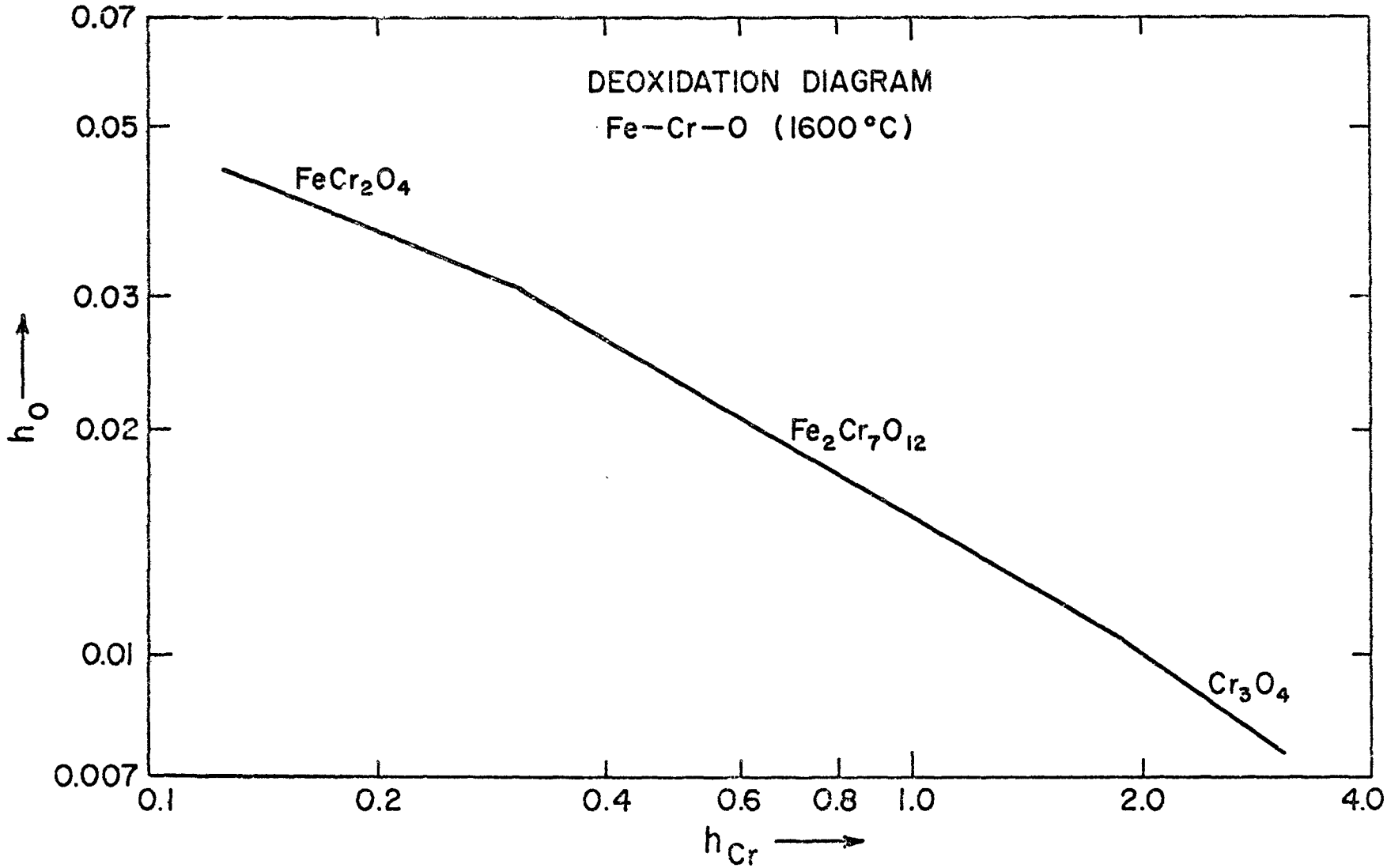

Fig. 5.4 Deoxidation diagrams for the Fe-Cr-O system at 1600°C

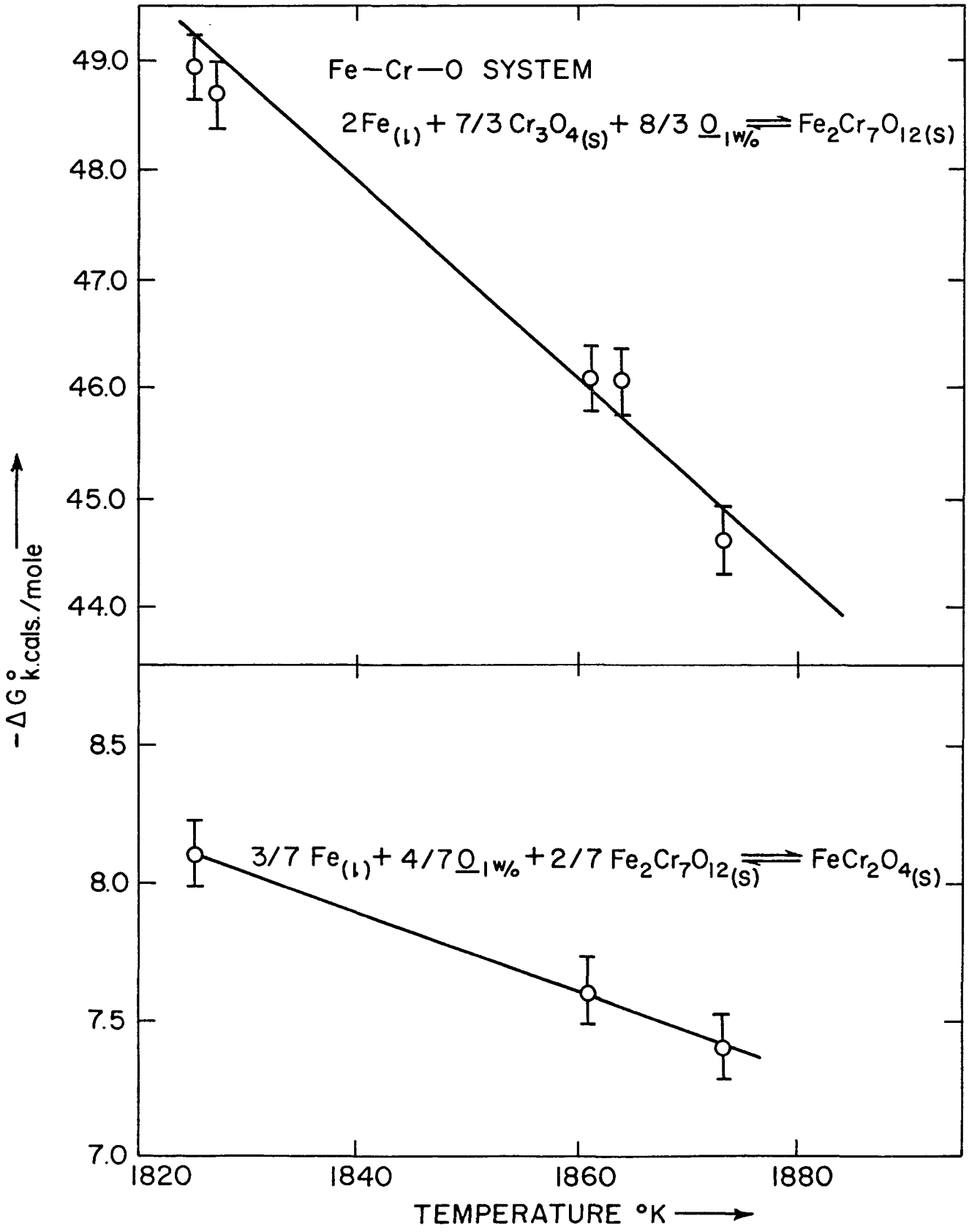

Fig. 5.5 Plot of ΔG° vs T in the Fe-Cr-O system

chromium content at the transition point are inconsistent. Further, the equilibrium constants reported for the reaction

$$FeCr_2O_{4(s)} \rightleftarrows Fe_{(\ell)} + 2\underline{Cr}_{1w/o} + 4\underline{O}_{1w/o} \tag{5.25}$$

$$K_{24} = h_{Cr}^2 \, h_O^4 \tag{5.26}$$

are in good agreement. Thus the oxygen activities at the transition points reported in Table 2.6 are also inconsistent, ranging from 0.3 from the results of Nakamara et al.[31] to 0.017 from the earlier results of Chen and Chipman.[24]

When the observations of the present study are interpreted following this deoxidation scheme, the results prove to be inconsistent. The deoxidation reaction for the formation of Cr_2O_3 can be written as

$$Cr_2O_{3(s)} \rightleftarrows 2\underline{Cr}_{1w/o} + 3\underline{O}_{1w/o} \tag{5.27}$$

with an equilibrium constant

$$K_{27} = h_{Cr}^2 h_O^3 \tag{5.28}$$

The value of K_{27} can be calculated from the determinations of the standard free energy of formation of Cr_2O_3 by combining it with the standard free energy changes for the reactions

$$Cr_{(s)} \rightleftarrows \underline{Cr}_{1w/o} \tag{5.28}$$

and

$$1/2 \; O_2 \rightleftarrows \underline{O}_{1w/o} \tag{5.29}$$

Using the value of ΔG_f^o (Cr_2O_3) determined by Pehlke et al.[83] and values for

ΔG^{o}_{28} and ΔG^{o}_{29} discussed in sections 2.10 and 2.6, respectively, a value of K_{27} of 1.2×10^{-4} at $1600^{o}C$ is obtained.

In the present study Cr_2O_3 would have to be the stable phase in the region between the two plateaus. Thus the value of K_{25} can be used to determine the equilibrium chromium concentration at both transformation points. Using the values of h_O obtained from the plateaus in the present study the values of h_{Cr} at the upper and lower plateaus at $1600^{o}C$ are 2 and 10.1 respectively. This is inconsistent with the observation that two plateaus were obtained even with 1.8% Cr in the melt. Further, X-ray analysis shows that the product obtained from the region between the two plateaus is not Cr_2O_3.

Another scheme of deoxidation products which could be suggested is - chromite above the upper plateau, Cr_3O_4 between the plateaus and CrO below the lower plateau. This scheme is not acceptable for the following reasons:

1. It appears inconsistent that Cr_3O_4 - a spinel - would transform to $FeCr_2O_4$, another spinel, in a one step process, especially since the reaction is essentially one where chromium atoms in the spinel are replaced by iron atoms.

2. Following the discussion in section 2.2, if log h_O is plotted against log h_{Cr}, for the formation of various deoxidation products, the chromium concentration at the transition point for $FeCr_2O_4$ to Cr_3O_4 would be higher than that for $FeCr_2O_4$ to Cr_2O_3.

3. The scheme would suggest CrO as a stable product at relatively low chromium contents. This is inconsistent with the observation that CrO

is formed under conditions of very high chromium contents and very low oxygen activities in silica saturated systems.

Hence, following the discussions of Hilty et al.,[27] Sakao and Sano[29] and Jacob and Alcock[55] the deoxidation scheme discussed above ($FeCr_2O_4$, $Fe_2Cr_7O_{12}$, Cr_3O_4) is the only one consistent with the present observations. A further, definite confirmation was not possible in this work due to the limitations of the experimental technique.

5.11 Physical Characteristics of Deoxidation Products

The micrographs of the oxide inclusions obtained from the ingots are shown in Figs. 4.13 and 4.14. In all cases the inclusions are seen to be either individual crystals or aggregates of small crystallites. This indicates that they were formed as solid products at the experimental temperatures. Hence it can be assumed that the various oxides of the deoxidant do not have extensive mutual solubility. The deoxidation products are bound to contain some oxides of iron but can be adequately represented by the deoxidation schemes discussed earlier.

Oxides of the type V_2O_3, VO and Cr_3O_4 can be seen to form massive aggregates which do not have any particular shape. However, the spinel inclusions generally form 'globular' agglomerates of small crystallites.

Turkdogan[92] has discussed various models for the formation and growth of oxides in liquid iron. He has concluded that oxides form by nucleation and grow by diffusion of oxygen to the deoxidant when the latter is added to the melt.

However, the globular agglomerates of crystallites suggest that small oxide crystallites are formed throughout the melt. Due to the high

interfacial energy between the iron and the oxides, they are rejected by the iron and are forced to agglomerate, much like very fine particles of coal suspended in water. This could explain why the oxide inclusions are generally found to be larger than what would be expected, if their size was controlled by diffusion, during a deoxidation process.

5.12 Significance of the Present Work

In studies of deoxidation thermodynamics, solid electrolytes have generally been used in the form of oxygen probes to make single measurements. The chronopotentiometric technique developed in this investigation can be used to determine deoxidation diagrams of the type shown in Figs. 5.3 and 5.4 for simple and complex deoxidation systems.

In steelmaking practice, control of the deoxidation processes is crucial for the following reasons:

1. The case of removal of deoxidation products from liquid steel by assimilation in a slag cover depends on the type of oxide formed. Simple oxides are more readily absorbed than the spinel type of deoxidation product.

2. Deoxidation products not assimiiated in the slag remain as inclusions in the steel after casting. The mechanical behaviour of these inclusions during subsequent processing of the steel is governed by the types of oxide and their morphology. Further, the nature of the oxide inclusions also affects the corrosion resistance of the steel. Hence in steelmaking practice it may be desirable to suppress the formation of a particular deoxidation product.

3. In the production of high strength low alloy (HSLA) steels elements like V and Ti are added in very small quantities ($\simeq 0.3\%$) to obtain

carbide and nitride precipitates which improve the mechanical properties of steel. In order to form the carbide or nitride precipitates the vanadium has to be in solution in iron and not tied up as oxides. Since oxidation of the vanadium cannot be completely prevented, amounts slightly in excess of that required for the formation of carbides and nitrides has to be added to the steel. Similarly in the production of low alloy steels and stainless steels losses of chromium due to oxidation have to be accounted for while alloying additions are made.

Deoxidation diagrams, such as the ones determined in this investigation, can be used in the control of deoxidation processes in steelmaking. Thus in the Fe-V-O system, if spinel formation is to be prevented, the activity of oxygen will have to be lowered below the transition point from FeV_2O_4 to V_2O_3 (Fig. 5.3), by other means, before vanadium can be added. These diagrams can also be used to estimate the amount of vanadium or chromium lost during processing of the steel in order to ensure that the desired amount of residual vanadium for the formation of carbides and nitrides or chromium for alloying is still available in the steel.

The nature of oxide inclusions formed in steel is of great interest, especially in complex deoxidation. The technique employed in this study to monitor the oxygen activity in liquid steel can be used to obtain controlled samples of the deoxidation product, which can then be cooled, at any desired rate, for physical examination and chemical analysis.

In the Fe-Cr-O system, samples of the deoxidation product obtained from known stages of oxidation showed that Cr_2O_3 is not formed as a deoxidation product at steelmaking temperatures. Since determinations of the solution

thermodynamics of the Fe-Cr-O system reported in the literature assume Cr_2O_5 to be a deoxidation product, reinterpretation of the experimental results is necessary. The data for the transition point from $FeCr_2O_4$ to Cr_2O_5 as reported in the literature are inconsistent, ranging from 3 to 7% Cr. Some of this discrepancy can be explained by the erroneous assumption that Cr_2O_3 is a deoxidation product.

The deoxidation scheme presented for the Fe-Cr-O system in Fig. 5.4 needs further confirmation. The exact composition of the distorted spinel and the formation of Cr_3O_4 as a deoxidation product could not be unambiguously confirmed in the present work. These need to be determined by precise X-ray diffraction and spectrochemical techniques in order to confirm the deoxidation scheme. The values of oxygen and chromium activities at the transition points in the deoxidation diagram are consistent with steelmaking practice since Cr is found to be only slightly less powerful than V as a deoxidizer.

CHAPTER 6

SUMMARY AND CONCLUSIONS

1. Deoxidation thermodynamics of liquid iron is generally studied by equilibration techniques which involve high temperature reactions followed by analysis at room temperature. Hence it is not possible to make any direct formulations of the processes occurring at the high temperature. A technique to monitor the reactions at the elevated temperature can lead to a better understanding of the deoxidation process.

2. A high temperature electrochemical cell:

$$Mo_{(s)}, Cr\text{-}Cr_2O_{3(s)} \mid \begin{matrix}\text{calcia stabilized}\\ \text{zirconia}\\ \text{solid electrolyte}\end{matrix} \mid Fe\text{-}M\text{-}O_{(\ell)}, \quad \begin{matrix}Mo/ZrO_2\\ \text{Cermet}_{(s)}\end{matrix}$$

has been employed to study the deoxidation thermodynamics of liquid Fe-V-O and Fe-Cr-O systems in the temperature range 1550-1600^{o}C.

3. A new cell design was developed in order to monitor the oxygen activity of the liquid melt continuously. The cell was tested in a number of ways and was found to behave reversibly. The free energy change for the reaction:

$$Fe_{(\ell)} + \underline{O}_{1w/o} + V_2O_{3(s)} \rightleftarrows FeV_2O_{4(s)}$$

determined with this technique is in excellent agreement with data reported

in the literature, confirming the accuracy and the reliability of the technique.

4. A process was developed to form and sinter a molybdenum-zirconia cermet at the end of a long molybdenum wire lead. The cermet contact virtually eliminated molybdenum dissolution in iron and provided an excellent electrical contact to the molten metal.

5. The new experimental technique offers the following advantages:

a) It enables continuous monitoring of oxygen activity in liquid iron.

b) It enables the study of deoxidation reactions at high temperatures without imposing external constraints on the system.

c) It provides a direct indication of the processes occurring at high temperatures.

6. The technique was used to characterize the thermodynamics of VO as a deoxidation product. The Henrian activity of oxygen and vanadium in liquid iron where V_2O_3 transforms to VO was found to be 0.012 and 1 respectively at 1600°C.

7. The standard free energy change for the reaction

$$2VO_{(s)} + \underline{O}_{1w/o} \rightleftarrows V_2O_{3(s)} \qquad (6.1)$$

obtained is -16410 cals. at 1600°C. This reaction was studied in the temperature range 1550 to 1600°C but due to the small experimental temperature range a second law equation for the free energy change is not presented.

8. The stability ranges of the deoxidation products in the Fe-V-O system are:

Oxide	Stability Range	Temperature
FeV_2O_4	wt.%V<0.17	1600°C
V_2O_3	0.17 to 1.0%	1600°C
VO	wt.%V>1.0	1600°C

9. The standard heat of formation at 298°K (ΔH^o_{298}) of VO calculated from the present data by the 'Third Law' method is -80,900 cals/mole. This corresponds to the stoichiometry of VO determined by the constraint that it has to be in equilibrium with V_2O_3 and a fixed oxygen potential in liquid iron.

10. Investigations in the liquid Fe-Cr-O system showed that when a melt with an initial chromium content of 1.8% was oxidized, the deoxidation product transformed twice, i.e. three different oxides were formed.

11. Based on the identification of oxides, obtained from a known stage of oxidation, by X-ray diffraction it was found that Cr_2O_3 was not formed as a stable deoxidation product in the Fe-Cr-O system. Thermodynamic calculations predicting that Cr_2O_3 will be unstable at chromium contents of <3% at 1000°C confirm this observation.

12. The deoxidation products formed and their stability ranges are suggested as follows:

Oxide	Stability Range	Temperature
$FeCr_2O_4$	up to 0.3% Cr	1600°C
distorted spinel	0.3% to 1.8% Cr	1600°C
Cr_3O_4	above 1.8% Cr	1600°C

13. From the measured oxygen activities, the free energy changes associated with the transformation of the deoxidation products have been calculated in the temperature range 1550 to 1600^{o}C.

14. Micrographic examination of the deoxidation products shows that they can form as individual crystals, colonies of small crystallites or as globular aggregates of small crystallites. These 'globules' can be formed by the following mechanism:

a) Small crystallites are formed throughout the melt.

b) They are forced to agglomerate through rejection by the liquid iron.

15. The technique can be used to study the behaviour of oxygen in a number of systems such as:

1. Iron based systems with one or more deoxidizers.
2. Non-ferrous systems like liquid copper and nickel and their alloys.
3. Oxide mixtures where both the oxides are essentially stoichiometric.

References

1. Turkdogan, E.T., J.I.S.I., 210, p. 21, 1972.

2. Bodsworth, C. and Bell, H.B., "Physical Chemistry of Iron and Steel Manufacture", 2nd Edition, Longman, London, 1972.

3. Jacquemont, A., Gattellier, C. and Olette M., IRSID report No. 109.3, Deoxidation Equilibrium in Liquid Iron, January 1975.

4. Chipman, J. and Dastur, M.N., Trans. AIME 191, p. 111, 1951.

5. Karassev, R.A., Polyakov, A.J. and Samarin, A.M., Izv. Ak. Nauk. SSSR, O.T.N. 12, p. 1794, 1952.

6. Narita, K. and Koyama, S., Trans. I.S.I. Japan 9, p. 53, 1969.

7. Narita, K., Koyama, S. and Kawaguchi, F., Tetsu to Hagane 56, p. 366, 1970.

8. Kojima, Y., Inouye, M. and Ohi, J.I., Arch. Eisenh. 40, p. 657, 1969.

9. Jacob, K.T. and Alcock, C.B., private communications.

10. Kunnmann, W., Rogers, D.B. and Wold, A., J. Phys. Chem. Solids 24, p. 1535, 1963.

11. Wakihara, M. and Katsura, T., Bull. Chem. Soc. of Japan 44, p. 3043, 1971.

12. Kay, D.A.R. and Kontopoulos, A., Intl. Symp. on Metallurgical Chemistry, Univ. of Sheffield, England, 1971.

13. Kobayashi, M., Scientific Reports, Tohoku Imp. Univ., Japan 22, p. 1240 1933.

14. Allen, N.P., Kubaschewski, O. and Von Goldbeck, O., J. Electrochem. Soc. 98, p. 417, 1951.

15. Brewer, L., Chem. Rev. 52, p. 1, 1953.

16. Rossini, R.D., Wagman, D.D., Evans, W.H., Levine, S. and Jaffe, I., "Selected Values of Chemical Thermodynamic Properties", NBS (U.S.) Circ. 500, 1952.

17. Mah, A.D. and Kelley, K.K., "Heats and Free Energies of Formation of Oxides of Vanadium", U.S. Bur. of Mines Rep. Invest. 5858, 1961.

18. Charlu, T.V. and Kleppa, O.J., High Temp. Science 5, p. 260, 1973.

19. Floridis, T.P. and Chipman, J., Trans. AIME 212, p. 549, 1958.

20. Sticher, J. and Schmalzried, H., "Zur Geometrischen Darstellung Thermodynamischer Zustandsgrossen in Mehrstoffsystemen auf Eisenbasis", Clausthal, Germany, 1975.

21. Pelton, A., Univ. of Montreal, private communications.

22. Barin, I. and Knacke, O., "Thermochemical Properties of Inorganic Substances", Springer-Verlag (Pub), Berlin, 1973.

23. Chipman, J., Basic Open Hearth Steelmaking, G. Derge (Ed.), AIME, p. 640, 1964.

24. Chen, H.M. and Chipman, J., Trans. ASM 38, p. 71, 1947.

25. Lintschewski, B.W. and Samarin, A.M., Stahl und Eisen 174, p. 1780, 1954.

26. Turkdogan, E.T., JISI 178, p. 278, 1954.

27. Hilty, D.C., Forgeng, W.D. and Folkman, R.L., J. of Metals 7, p. 253, 1955.

28. Chipman, J., JISI 180, p. 97, 1955.

29. Sakao, H. and Sano, K., J. Jap. Inst. Met. 26, p. 236, 1962.

30. Adachi, A. and Iwamoto, N., Trans. I.S.I. Japan 16, p. 188, 1966.

31. Nakamura, Y., Ohno, T. and Segawa, K., Proc. ICSTS, Suppl. Trans. I.S.I. Japan 21, p. 456, 1971.

32. Zapffe, C.A., Trans. ASM 38, p. 114, 1947 (written discussion of reference 24).

33. McCoy, C.W. and Philbrook, W.O., TMS-AIME 212, p. 226, 1958.

34. Robinson, J.W. and Pehlke, R.D., Met. Trans. 5, p. 1041, 1974.

35. Zapffe, C.A., J. Am. Ceramic Soc. 27, p. 293, 1944.

36. Healy, G.W. and Schottmiller, J.C., TMS-AIME 230, p. 420, 1964.

37. Katsura, T. and Muan, A., TMS-AIME 230, p. 77, 1964.

38. Novokhatski, I.A. and Lenev, L.M., Russ. Journal of Inorg. Chem. 11, p. 1078, 1966.

39. Rezukhina, T.N., Leistskii, V.A. and Istomin, B.A., Elektrokhimiya 11, p. 467, 1965.

40. Tretjakow, J.D. and Schmalzried, H., Berichte der Bunsengesellschaft, 69, p. 396, 1965.

41. Jeannin, Y., Mannerskantz, C. and Richardson, F.D., TMS-AIME 227, p. 300, 1963.

42. Pugliese, L.A. and Fitterer, G.R., Met. Trans. 1, p. 1997, 1970.

43. Coughlin, J.P., "Heats and Free Energies of Formation of Inorganic Oxides", U.S. Bureau of Mines, Bulletin 542-68, 1954.

44. Wicks, C.E. and Block, F.E., "Thermodynamic Properties of 65 Elements", U.S. Bureau of Mines, Bulletin 605, 1963.

45. Maier, C.G., "Sponge Chromium", U.S. Bureau of Mines, Bulletin 436, 1942.

46. Buzek, Z., Chemical Metallurgy of Iron and Steel, I.S.I. London (Pub), p. 173, 1973.

47. Littlewood, R., Can. Met. Quart. 5, p. 1, 1966.

48. Kiukkola, K. and Wagner, C., J. Electrochem. Soc. 104, p. 374, 1957.

49. Fischer, W.A. and Janke, D., Arch Eisenh. 40, p. 707, 1969.

50. Korousic, B., Rudarsko Metalurski Zbonnik, p. 395, 1969.

51. Kiukkola, K. and Wagner, C., J. Electrochem. Soc. 104, p. 307, 1957.

52. Korousic, B., Rudarsko-Metalurski Zbonnik, p. 47, 1970.

53. Jeffes, J.H.E. and Sridhar, R., "Electromotive Force Measurements in High Temperature Systems", C.B. Alcock (Ed.), Am. Elsevier (Pub.), 1968.

54. Shores, D.A. and Rapp, R.A., J. Electrochem. Soc. 119, p. 300, 1972.

55. Jacob, K.T. and Alcock, C.B., Met. Trans. 'B', 6B, p. 215, 1975.

56. Etsell, T.H. and Flengas, S.N. Chem. Rev. 70, p. 339, 1970.

57. Rapp, R.A. and Shores, D.A., "Physicochemical Measurements in Metals Research", Vol. IV, Part II, R.A. Rapp (Ed.), Wiley Interscience (Pub.), New York, 1970.

58. Schmalzried, H. and Pelton, A.D., Ann. Rev. of Mat. Science 2, p. 143, 1972.

59. Worrell, W.L., Bull. American Ceramic Soc. 53, p. 425,1974.

60. Friedman, L.M., Oberg, K.E., Boorstein, W.M. and Rapp, R.A., Met. Trans. 4, p. 75, 1973.

61. Heyne, L. and Beckmans, N.M., Proc. British Ceramic Soc. 19, p. 229, 1971

62. Schmalzried, H., Z. Electrochem. 66, p. 572, 1962.

63. Patterson, J.W., J. of Electrochem. Soc. 118, p. 1033, 1971.

64. Steele, D.C.H. and Alcock, C.B., TMS-AIME 233, p. 1359, 1965.

65. Tretyakov, J.D. and Muan, A., J. Electrochem. Soc. 116, p. 331, 1969.

66. Baker, R. and West, J.M., JISI 204, p. 212, 1966.

67. Patterson, J.W., Bogren, E.C. and Rapp, R.A., J. Electrochem. Soc. 114, p. 752, 1967.

68. Fischer, W.A. and Janke, D., Arch. Eisenh. 39, p. 89, 1968.

69. Schmalzried, H., Z. Physik. Chem. N.F. 38, p. 87, 1963.

70. Fitterer, G.R., J. of Metals 18, p. 961, 1966.

71. Turkdogan, E.T. and Fruehan, R.J., Can. Met. Quart. 11, p. 371, 1972.

72. Pargeter, J.K., Can. Met. Quart. 6, p. 21, 1967.

73. Schwerdtferger, K., TMS-AIME 239, p. 1276, 1967.

74. Diaz, C.M. and Richardson, F.D., Trans. Inst. of Min. and Met., p. 196, 1967.

75. Brabie, V. and Eketorp, S., Jarnets Metallurgi, Royal Inst. of Tech., Stockholm, Sweden, 1975.

76. Jacquemont, A., Gattelier, C. and Olette, M., C.R. Acad. Sci. Paris 277, Ser. C, p. 271, 1973.

77. Vahed, A., "Solid Electrolytes and Deoxidation", M.Eng. Thesis, McMaster University, Hamilton, Canada, 1973.

78. Kontopoulos, A., "Thermodynamics of the Fe-V-O System", Ph.D. Thesis, McMaster University, Hamilton, Canada, 1971.

79. Iwase, M. and Mori, T., Kyoto University, private communications.

80. Belford, T.N. and Alcock, C.B., Trans. Faraday Soc. 64, p. 822, 1964.

81. Wanibe, Y., Yamauchi, Y., Kawai, K. and Sakao, H., Trans. I.S.I.J. 12, p. 472, 1972.

82. Jacob, K.T. and Alcock, C.B., University of Toronto, private communications.

83. Pehlke, R.D., Mazandrany, F.N. and Radzilowski, R.H., Geochim. and Cosmochim. Acta 39, p. 833, 1975.

84. Fruehan, R.J., TMS-AIME 245, p. 1215, 1969.

85. Fruehan, R.J., Met. Trans. 1, p. 2083, 1970.

86. Stournaras, C., Ph.D. Thesis, McMaster University, Hamilton, Canada, 1977.

87. Den Hertog, H.W. and Slangen, B., Ironmaking and Steelmaking, p. 64, 1976.

88. Fruehan, R.J., Martonik, L.J. and Turkdogan, E.T., TMS-AIME 233, p. 1501, 1969.

89. JANAF Thermochemical Tables, 2nd Edition, D.R. Stull and H. Prophet (Ed.), U.S. Dept. Comm. 1971.

90. J.C.P.D.S. Tables, Joint Committee on Powder Diffraction Standards, L.G. Berry (Ed.) Pennsylvania, 1972.

91. Pastorek, R.L. and Rapp, R.A., TMS-AIME 245, p. 1711, 1969.

92. Turkdogan, E.T., "Sulfide Inclusions in Steel", J.J. de Barbadillo and E. Snape (Ed.), ASM Publication, p. 1, 1975.

Appendix 1

Standard* X-Ray Diffraction Patterns for Selected Chemicals

FeV_2O_4		V_2O_3		VO	
dA^o	I/I_o	dA^o	I/I_o	dA^o	I/I_o
4.79	35	3.65	60	2.38	30
2.93	60	2.70	80	2.06	80
2.50	100	2.47	60	1.45	100
2.39	04	2.32	02	1.24	60
2.07	80	2.18	20	1.19	60
1.90	04	2.03	02	1.03	50
1.69	30	1.83	25	0.94	50
1.60	90	1.69	100	0.92	70
1.47	95	1.61	02		
1.40	06	1.57	3		
1.31	10	1.47	25		
1.27	25	1.43	30		
1.25	18	1.33	10		
1.20	08	1.24	04		
1.16	04	1.22	02		
		1.19	02		
		1.17	06		
		1.13	03		
		1.09	06		
		1.06	06		

*Source: Joint Committee on Powder Diffraction Standards[90]

Appendix 1

Standard* X-Ray Diffraction Patterns for Selected Compounds

Chromite		Distorted spinel		Cr_3O_4	
d, A^o	I/I_o	d, A^o	I/I_o	d, A^o	I/I_o
4.80	30	4.85	40	4.78	40
2.93	60	2.98	40	3.05	30
2.50	100	2.92	60	2.86	40
2.40	10	2.52	100	2.58	100
2.075	80	2.48	50	2.39	20
1.695	10	2.40	40	2.34	10
1.595	90	2.10	40	2.16	60
1.468	100	2.05	30	1.90	20
1.401	30	1.71	20	1.725	30
1.315	10	1.68	10	1.655	90
1.266	30	1.62	50	1.590	20
-	-	1.60	50	1.525	60
-	-	1.58	20	1.432	80
-	-	1.483	40	1.348	10
-	-	1.460	60	1.287	30
-	-	1.325	10	1.280	50
-	-	1.274	30	1.217	10
-	-	1.265	10	-	-

*Source - Chromite and Cr_3O_4 - JCPDS[90]

Distorted Spinel - Hilty et al.[27]

Appendix 1

Standard* X-Ray Diffraction Patterns for Selected Chemicals

Cr_2O_3		Cr	
d, A^o	I/I_0	d, A^o	I/I_0
3.6	40	2.04	100
2.64	100	1.44	16
2.46	60	1.18	30
2.17	30	1.02	18
1.80	30	0.91	20
1.662	80		
1.456	30		
1.422	50		

*Source - Joint Committee on Powder Diffraction Standards(90)